Antarctica's sedimentary basins and their influence on ice sheet dynamics

A.R.A. Aitken[1,2], L. Li[1], B. Kulessa[3,4], D. Schroeder[5,6], T.A. Jordan[7], J. Whittaker[8], S. Anandakrishnan[9], E.J. Dawson[5], D. A. Wiens[10], O. Eisen[11,12], M.J. Siegert[13]

1. School of Earth Sciences, The University of Western Australia, Perth, Western Australia, Australia
2. Australian Centre of Excellence for Antarctic Science, The University of Western Australia, Perth, Western Australia, Australia
3. School of Biosciences, Geography and Physics, Swansea University, Wales, UK
4. School of Geography, Planning and Spatial Sciences, The University of Tasmania, Hobart Tasmania, Australia
5. Department of Geophysics, Stanford University, Stanford, California, USA
6. Department of Electrical Engineering, Stanford University, Stanford, California, USA
7. British Antarctic Survey, Cambridgeshire, UK
8. The Institute of Marine and Antarctic Science, The University of Tasmania, Hobart, Tasmania, Australia
9. College of Earth and Mineral Sciences, Pennsylvania State University, Pennsylvania, USA
10. Department of Earth & Planetary Sciences, Washington University, St. Louis, Missouri, USA
11. Glaciology, Alfred Wegener Institute, Helmholtz Centre for Polar and Marine Research, Bremerhaven, Germany
12. Department of Geosciences, University of Bremen, Bremen, Germany
13. Grantham Institute and Department of Earth Science and Engineering, Imperial College London, London, UK

Corresponding author: Alan Aitken (alan.aitken@uwa.edu.au)

Key Points

- Recent advances in detection and characterization of subglacial sedimentary basins are reviewed
- A new map of Antarctica's sedimentary basins is presented and implications for glacial processes are discussed
- Some future directions in Antarctic subglacial sedimentary basins research are explored

Abstract

Building a knowledge of Antarctica's sedimentary basins develops our understanding of the coupled evolution of tectonics, ice, ocean, and climate. In comparison to non-basin regions, sedimentary basins have distinct subglacial properties that impact ice sheet dynamics and may influence future ice sheet change. Despite this importance, our knowledge of Antarctic sedimentary basins is restricted. Remoteness, the harsh surface environment, the overlying ice sheet, fringing ice shelves and sea ice all make fieldwork challenging. Nonetheless, in the past decade the geophysics community has made great progress in internationally coordinated data collection and compilation. Parallel advances in data processing and analysis also support a new level of insight into Antarctica's subglacial environment. Here, we summarize recent progress in understanding Antarctica's sedimentary basins. We review advances in the technical capability of radar, potential fields, seismic and electromagnetic techniques to detect and characterize basins beneath ice. In addition, we review advances in integrated multi-data interpretation including emerging machine learning approaches. These new capabilities permit a new continent-wide mapping of Antarctica's sedimentary basins and their characteristics, aiding definition of the tectonic development of the continent. Crucially, Antarctica's sedimentary basins interact with the overlying ice sheet through key dynamic feedbacks that have the potential to contribute to rapid ice sheet change. Looking ahead, future research directions include increasing data coverage within logistical constraints, and resolving major knowledge gaps, including insufficient sampling of the ice sheet bed and poor definition of subglacial basin structure and stratigraphy. Translating the knowledge of sedimentary basin processes into ice sheet modelling studies is critical to underpin better capacity to predict future change.

Plain Language Summary

Antarctica is the keystone to the former supercontinent Gondwana and, because of its unique isolated location at the South Pole, it has important consequences for understanding changing global climate and ocean change. In several ways, sedimentary basins beneath the ice sheet interact with the ice sheet above and can potentially contribute to rapid ice sheet changes that impact global sea level and climate. These sedimentary basins have not all been systematically mapped due to the challenge of studying them beneath thick ice. In this work we review technical progress towards the understanding of sedimentary basins in the subglacial environment, and we map out the sedimentary basins beneath Antarctica's ice. We explore how improved knowledge of Antarctica's basins helps to (1) understand important tectonic events in the continent, (2) unravel the evolution of the landscape and the ice sheet, and (3) contribute to improved predictions of future ice sheet change. Remaining challenges to further advance Antarctic sedimentary basins research are identified and some future directions for study are discussed.

1   Introduction

Sedimentary basins are widely preserved on all Earth's continents and provide distinct environments for physical, chemical and biological processes [*Evenick*, 2021]. Antarctica is no exception and possesses several major sedimentary basins and many smaller ones distributed across the continent. Seasonally ice-free marine regions, including the Ross, Weddell, and Amundsen seas, and much of the East Antarctic continental margin are relatively well surveyed (Fig 1). However, the unique challenge of ice-covered inland Antarctica, with very limited and spatially clustered outcrop (Fig 1), a kilometers-thick ice sheet and severe environmental and logistical challenges has meant that the distribution and nature of sedimentary basins is poorly known inland. On the continental shelf, ice shelves and perennial sea-ice limit access to both marine and terrestrial techniques. Sedimentary basins are important not just for the understanding of Antarctic geology, but also because they provide key boundary conditions for glacial processes, with major impacts on the dynamics of the overlying ice sheet [*Bell et al.*, 1998; *Gooch et al.*, 2016; *Kulessa et al.*, 2019; *Li et al.*, 2022; *Person et al.*, 2012; *Siegert et al.*, 2018; *Studinger et al.*, 2001; *Tankersley et al.*, 2022; *Zhang et al.*, 2018].

The discovery of sedimentary basins in Antarctica has been a continuing theme since the earliest Antarctic expeditions [*Anderson*, 1965]. The earliest expeditions captured both the existence of extensive sedimentary rocks in outcrop [*Ferrar*, 1907; *Mawson*, 1940] and speculated on the presence of major sedimentary basins in the marine regions, especially the Ross, Weddell and Scotia Seas [*Mawson*, 1928]. A more comprehensive record emerged in the second half of the 20th Century, in particular the period following the 1957/8 International Geophysical Year (IGY) [*Naylor et al.*, 2008], when geophysical mapping of subglacial geology became a consistent feature of Antarctic exploration [*Bailey et al.*, 1964; *Bentley et al.*, 1960; *Evans and Robin*, 1966]. Key techniques such as radio echo sounding (RES), since the 1960s [*Bingham and Siegert*, 2007a; *Schroeder et al.*, 2020; *Turchetti et al.*, 2008], active and passive seismic, since the 1950s and 1990s respectively [*Anandakrishnan et al.*, 2000; *Bentley et al.*, 1960; *Lawrence et al.*, 2006; *Robin*, 1958] and airborne magnetic and gravity surveys, since the 1960s and 1990s respectively [*Behrendt et al.*, 1966; *Bell et al.*, 1999b] were developed and adapted to Antarctic requirements. This led to the first continent-scale compilations, including for ice thickness and bed elevation BedMap [*Lythe and Vaughan*, 2001], for magnetic data ADMAP [*Golynsky et al.*, 2001; *Golynsky et al.*, 2006] and for gravity ADGRAV [*Bell et al.*, 1999a].

The 21st Century has seen continued development and refinement of these approaches, and of course the broadening of coverage over the continent, and the last decade has seen the development of much more detailed and comprehensive compilations [*Frémand et al.*, 2022b; *Fretwell et al.*, 2013; *Golynsky et al.*, 2018; *Scheinert et al.*, 2016]. New techniques for compilation have emerged including the integration of satellite gravity and magnetic data [*Ebbing et al.*, 2018; *Ebbing et al.*, 2021; *Scheinert et al.*, 2016], the inclusion of mass-conservation techniques [*Morlighem et al.*, 2020] and geostatistical approaches [*MacKie et al.*, 2021].
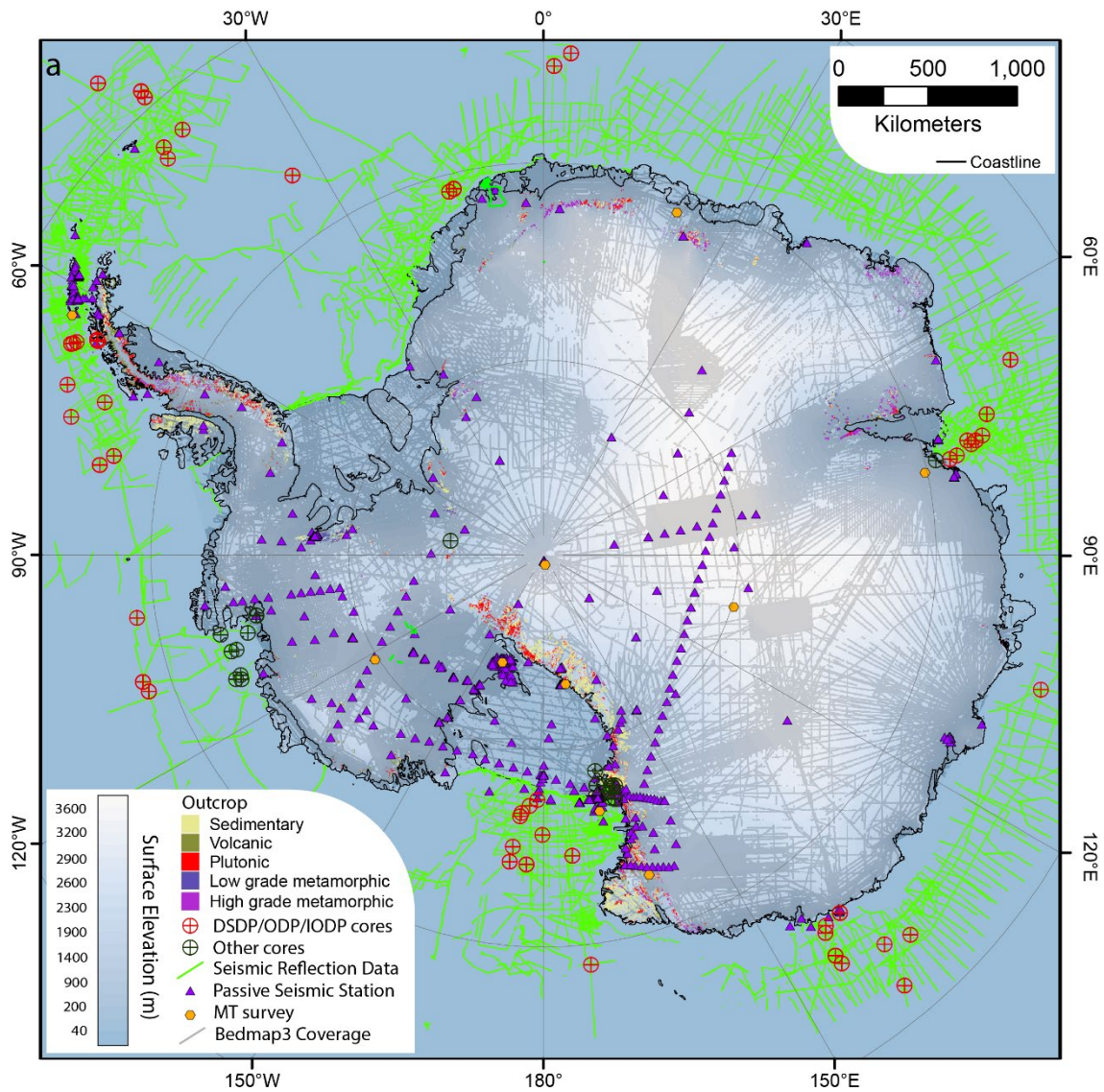
99
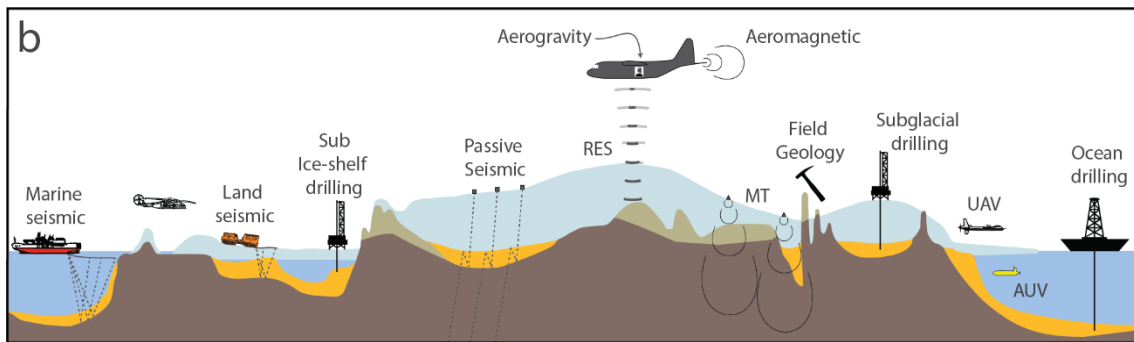
100

101 *Figure 1: a) Map of data coverage in Antarctica indicating outcropping regions, drill core sites, passive*

102 *seismic and MT stations, active seismic reflection lines offshore and limited onshore data. Bedmap3 data*

103 *coverage mostly is derived from airborne RES data [Frémand et al., 2022b], but not all surveys measured*

104 *gravity or magnetic data. b) Approaches to detection and characterization of sedimentary basins, including*

105 *direct characterization of rocks, and indirect characterization from geophysical data. MT – magnetotelluric,*

108 These advances in the coverage and quality of key geophysical datasets, coupled with the development of

109 new data processing and analysis techniques, mean it is now feasible to map with some confidence the

110 sedimentary basins of the Antarctic continent [*Li et al.*, 2022]. In this review, we explore the state of the art

111 with respect to defining the subglacial sedimentary basins of Antarctica, and we summarize the extent and

112 nature of these across the continent. The evolving tectonic setting of basin formation since Pangea is

113 discussed. We explore the interactions of sedimentary basins with glacial processes and consider possible

114 implications for ice sheet dynamics. Finally, we look ahead to the next set of challenges in defining the

115 extent, characteristics and importance of sedimentary basins in Antarctica.

116 2   Defining Subglacial Sedimentary Basins

117 2.1   What is a sedimentary basin?

118 A sedimentary basin is defined by the development of accommodation-space into which sediments have

119 been deposited. This definition needs several concepts to align: First, the development of a topographic

120 depression or shallow-sloped platform is required; second, there must be a source of sediment derived from

121 mechanical erosion, or from chemical or biological processes; third the deposition and accumulation of

122 sediments must occur and fourth, these must be preserved to the present day. The most common situation

123 on continents is that sediments eroded from highlands are deposited and preserved in a topographic

124 depression, forming a sedimentary basin [*Allen et al.*, 2015].

125 Sedimentary and metasedimentary rocks are commonly interpreted to represent their sedimentary basin,

126 potentially defining such properties as extent and thickness of fill and the depositional environment. Later

127 uplift, erosion, deformation, intrusion by magmatic rocks, or other events may make definition of the

128 original depositional basin hard to achieve. Furthermore, in metamorphic rocks, physical properties may

129 become dominated by crystal structures rather than fluid-filled pore networks, and this affects both the

130 geophysical expression [*Enkin et al.*, 2020] and the nature of their interaction with glacial processes

131 [*Krabbendam and Glasser*, 2011]. For these reasons we exclude from this study exposed metasedimentary

132 rocks of greenschist facies or above. Also, we exclude exposures of recent sediment deposits such as

133 moraines except where these form part of a basin sequence, as the extents of these cannot be reliably

134 defined at a large scale.

135 For this paper we define two major classes of sedimentary basin. We define a type 1 basin to exist where a

136 substantial amount of basin-fill, including sediments and sedimentary rocks, is preserved in the original

137 depositional basin, with no evidence for substantial uplift, major deformation or metamorphism. A certain

138 degree of compaction, diagenesis and deformation are expected in all basins. In contrast, we define type 2

139 basins to exist where exposures or other evidence indicate the presence of sedimentary rocks but not
140 preserved in their original depositional basin.

2.2 Recent progress in characterization of subglacial sedimentary basins

142 Globally, the analysis of sedimentary basins is commonly achieved through extensive use of outcrops, where
143 available, supported by drill core and high resolution active seismic reflection studies allowing detailed basin
144 characterization. In Antarctica these key data are available only in selected areas (Fig 1), and in the general
145 case, the major challenge is to define and characterize basins in the subglacial environment, for which
146 specialized techniques are needed.

2.2.1 Direct geological characterization

148 Direct access to rocks through outcrop, detrital samples or drill core is fundamental to sedimentary basin
149 analysis, permitting a full assessment of sedimentary characteristics and enabling application of detrital
150 geochronology, thermochronology and other key analysis techniques. In marine and some sub-ice shelf
151 settings of Antarctica (Fig 1), drilling programs with linked seismic surveys have revealed many key features
152 of sedimentary basins on the continental shelf, in particular in the Ross Sea, Prydz Bay and Amundsen Sea
153 [*Gohl et al.*, 2017; *Marschalek et al.*, 2021; *McKay et al.*, 2016; *Whitehead et al.*, 2006]. Ice shelf and sea-ice
154 cover is a major limitation for offshore studies, leading to a substantial data gap on the inner continental
155 shelf. Developing offshore exploration technologies including Autonomous Underwater Vehicles [*Batchelor
156 et al.*, 2020; *Davies et al.*, 2017; *Dowdeswell et al.*, 2008], seafloor drilling [*Gohl et al.*, 2017] and sub-ice shelf
157 drilling [*Gong et al.*, 2019] are enabling these data gaps to be filled.

158 For onshore regions, Antarctica possesses high-quality sedimentary rock outcrops in numerous areas, and
159 these can provide the core-knowledge for basin studies in those regions. The collation of Antarctic geological
160 data has progressed, with continent-scale compilations of key data [*Cox et al.*, 2019; *Sanchez et al.*, 2021].
161 While much knowledge has been gained by these approaches, a severe limitation is the tendency for
162 outcrop to occur only on major highlands, isolated nunataks and coastal islands, leaving unsampled the low-
163 lying regions that contain the bulk of sedimentary rocks. This leads to some undesirable bias towards older
164 and/or uplifted sedimentary rocks and, therefore, the utility of outcrop-based data to infer subglacial
165 geology is limited. Outcrop data is also focused in spaced clusters (Fig 1), often with a high degree of internal
166 complexity, meaning that interpolation between these clusters carries high uncertainty.

167 Detrital samples from much younger sediments can mitigate exposure bias [*Maritati et al.*, 2019; *Mulder et
168 al.*, 2019; *Thomson et al.*, 2013], but the lack of a precisely known source location for these samples renders
169 their use to characterize inland basins highly uncertain. Plainly, for a more representative sampling of the
170 Antarctic bedrock, drilling is necessary. As with offshore drilling, onshore sub-ice drilling techniques are
171 developing [*Gong et al.*, 2019; *Goodge et al.*, 2021; *Hodgson et al.*, 2016; *Kuhl et al.*, 2021; *Talalay et al.*,

172 2021] and have seen operation in several locations (Fig 1), with an intent to expand towards more
173 systematic coverage in the future. Notably, the alignment of these records with major ice-coring initiatives
174 has strong potential to inform glacial evolution on multiple timescales.

2.2.2 Indirect characterization

176 Despite the benefits of these direct methods, a systematic coverage of Antarctica requires indirect
177 characterization from geophysical data to survey the regions where no direct information exists. The major
178 techniques include ground and/or ship-based techniques including active and passive seismic methods and
179 magnetotellurics, as well as airborne techniques including gravity and magnetic methods and radio-echo
180 sounding (RES).

2.2.2.1 Radio-echo sounding

182 RES is an efficient geophysical method to characterize the morphology and nature of the ice sheet bed. In
183 the context of basin studies, RES data can define both the large-scale morphology of topographic
184 depressions, but also the detailed character of the bed, as defined by along-track roughness. While radar
185 data can give a robust characterization of the bed at fine resolutions, hundreds of meters or less, the
186 technique cannot directly indicate a sedimentary origin, nor is it able to define the thickness or properties of
187 the sedimentary cover.

188 RES systems have been used for more than five decades to determine the thickness of ice sheets in an
189 effective way [*Schroeder et al.*, 2020]. Over that period, more than 1.5 million line-kilometers of RES data
190 have been collected with airborne surveys predominating in recent times [*Frémand et al.*, 2022b; *Morlighem*
191 *et al.*, 2020]. By subtracting the radar-defined ice thickness from surface elevation data, bed topography can
192 be determined. Surface elevation may be obtained from the RES data itself, from other sensors (e.g. LIDAR)
193 on the same platform, or from remote sensing products (e.g. DEMs from satellite studies). The final product
194 is bed elevation profiles of the ice-bed interface that are interpolated to produce gridded bed topography
195 products. Interpolation may be done in numerous ways, including direct spline-based interpolation [*Fretwell*
196 *et al.*, 2013] or geostatistical interpolation [*MacKie et al.*, 2021]; with the inclusion of ice sheet flow data,
197 mass-conservation approaches may be used also [*Morlighem et al.*, 2020].

198 For the nadir-facing acquisition geometry of RES, specular and quasi-specular returns from the surface and
199 bed are typically the most prominent features in a radar trace [*Haynes et al.*, 2018], which allows for
200 straightforward interpretation of along profile ice thickness and bed topography. Although the earliest
201 systems were incoherent [*Schroeder et al.*, 2019] the development of coherent systems [*Gogineni et al.*,
202 1998] and synthetic aperture radar processing with range migration [*Heliere et al.*, 2007; *Peters et al.*, 2007]
203 improved the azimuth resolution of radargrams and the resulting extracted thickness profiles as well as
204 improving clutter mitigation in regions of high topographic relief and layover. More recently, swath

205   [*Holschuh et al.*, 2020], tomographic [*Paden et al.*, 2010], and array-based [*Young et al.*, 2018] systems as

206   well as the availability of ultra-wideband systems [*Arnold et al.*, 2020; *Hale et al.*, 2016] have further

207   improved the geometric resolution of RES observations, with range resolution in the tens of centimeters and

208   along-track resolution in the tens of meters [*Kjær et al.*, 2018].

209   The roughness of the bed encodes information on the morphologic and geologic character of the subglacial

210   interface [*Jordan et al.*, 2010a; *Rippin et al.*, 2014; *Siegert et al.*, 2005]. This roughness can be estimated

211   directly from thickness profiles [*Bingham and Siegert*, 2007b] and – with assumptions on the fractal

212   character of the bed – extrapolated to finer scales [*Jordan et al.*, 2017b]. Where perpendicular crossovers

213   are available, the anisotropy of this bed roughness can also be estimated [*Cooper et al.*, 2019; *Eisen et al.*,

214   2020]. In addition to its resolvable along-profile signature, finer-scale (i.e. wavelength-scale) roughness is

215   also encoded in the bed echo character including its abruptness [*Jordan et al.*, 2017b], specularity [*Schroeder*

216   *et al.*, 2015; *Young et al.*, 2016], and amplitude distribution [*Grima et al.*, 2019]. Notably, these fine-scale

217   relative metrics are insensitive to (even large) absolute errors in ice thickness (e.g. from firn correction or

218   surface registration). Finally, the radiometric signature of bed echoes can also encode information on bed

219   materials [*Christianson et al.*, 2016; *Tulaczyk and Foley*, 2020] and thermal state [*Chu et al.*, 2018]. These

220   signatures are often difficult to unambiguously interpret at the glacier to ice sheet scale [*Matsuoka*, 2011],

221   without multi-frequency [*Broome and Schroeder*, 2022] or multi-static observations [*Bienert et al.*, 2022] or

222   polarimetric [*Corr et al.*, 2007; *Dall et al.*, 2010; *Frémand et al.*, 2022a; *Scanlan et al.*, 2022] observations.

223   These approaches can characterize and constrain the wavelength-scale roughness (tens of centimeters or

224   smaller) and sub-Fresnel-zone geometry [*Haynes et al.*, 2018; *Jordan et al.*, 2017b] (meters to tens of

225   meters) of the bed, orders of magnitude finer-scale constraints than along-profile approaches [*Bingham and*

226   *Siegert*, 2009].

227   *2.2.2.2   Gravity and magnetic data*

228   These passive techniques measure the intensity and in some cases the direction of the Earth's naturally

229   occurring gravity and magnetic fields. Magnetic and gravity data do not require large power-sources, nor a

230   coupling to the Earth's surface, and airborne surveys have been widely deployed across Antarctica, most

231   commonly in combination with RES surveys from the same platform (Fig 1).

232   Gravity data are sensitive to the summed effects of mantle and crustal masses, including sedimentary rocks.

233   Due to their porosity, sedimentary rocks typically have lower density than the crystalline basement, causing

234   relative gravity lows over sedimentary basins [*Aitken et al.*, 2016a; *Bell et al.*, 1998; *Frederick et al.*, 2016].

235   Airborne gravity data collections systems include several major types of gravity meter, the conventional

236   stabilized-platform air-sea gravimeter [*Bell et al.*, 1999b] and derivations of this technology [*Studinger et al.*,

237   2008]. More recently, so-called "strapdown" systems have been used, which are based on inertial navigation

238   sensors including triads of high specification accelerometers and gyroscopes rigidly attached to the aircraft

239 [*Jordan and Becker*, 2018]. In either approach the observed accelerations are dominated by aircraft

240 accelerations, and a well constrained gravity solution is dependent on an accurate recording of the aircraft

241 location and elevation and careful removal from the recorded signal of aircraft accelerations and motion as

242 well as temporal gravity variations such as tides. Accurate navigational systems such as differential GNSS are

243 therefore essential to achieve the best quality data.

244 Older spring-based meters were restricted to straight and level flight, constraining operational logistics, and

245 limiting the ability to collect other data types at the same time. This sensitivity to aircraft dynamics meant

246 accuracies of 3-5 mGal were typical [*Jordan et al.*, 2010b]. In recent times advances in sensor technology and

247 processing methods have allowed collection of gravity data during more dynamic draped flights and an

248 overall improvement in data quality, with accuracies of 1-2 mGal now typical [*Jordan and Becker*, 2018;

249 *Studinger et al.*, 2008]. Despite these improvements, gravity data processing imposes a low pass filter on the

250 data, typically 70 seconds or more, that leads to spatial resolution in the order of 5-10 km, depending on

251 aircraft velocity. This may be between 60 and 140 m/s for the fixed-wing platforms used in Antarctica. A

252 recent innovation is the adoption of helicopter-borne operations, which promises further improvement in

253 spatial resolution [*Jensen and Forsberg*, 2018; *Wei et al.*, 2020]. Future application of strapdown gravity on

254 slower-flying Unmanned Aerial Vehicle (UAV) platforms also holds the promise of higher resolution and

255 potentially lower cost gravity surveys. An additional limit on the wavelengths resolved by gravity surveys is

256 the ice sheet thickness, which means observations are often made several kilometers from the bed

257 interface, limiting the minimum resolvable wavelength. These factors limit the capacity for detection of

258 abrupt spatial changes in gravity, such as may be associated with glacial landforms and fault-bounded

259 sedimentary basins. Despite these residual limitations, the improved accuracy of gravity sensor technology

260 allows modern airborne gravity data to be applied with confidence at scales of 5 kilometers and above.

261 The observed gravity field is a summation of several components including topography and crustal thickness,

262 as well as sedimentary mass deficits, therefore, to understand sedimentary basins these other factors must

263 be accounted for. Ice, ocean and bed topography is corrected for using the Bouguer correction or an

264 equivalent, which models and subtracts the effect of known topography and bathymetry, assuming

265 reference densities for rock, ice and water [*Hirt et al.*, 2016; *Scheinert et al.*, 2016]. In Antarctica, the thick

266 ice sheet load in the continental interior also generates a Moho down warp causing distinct negative

267 Bouguer anomalies that do not reflect crustal geology, and it is desirable to correct for this. Because

268 topographic loads may be balanced by the Moho or other masses in the deep crust or uppermost mantle, for

269 the isostatic residual anomaly, the condition is imposed that surface loads are balanced by variable crustal

270 thickness, either locally in the Airy case, or via an elastic or visco-elastic flexure [*Paxman et al.*, 2017]. Airy

271 isostasy models are easy to apply and provide a consistent convention for interpretation, but are prone to

272 overcorrection, whereas carefully applied flexural models may provide superior removal of isostatic effects

273   [*Jordan et al.*, 2013a; *Paxman et al.*, 2017]. Negative isostatic-residual gravity anomalies often indicate

274   sedimentary basins, although low-density basement rocks, such as granitic intrusions, can also give rise to

275   negative anomalies, requiring differentiation with other data [*Jordan et al.*, 2010b].

276   Despite the intricacies of processing and interpretation, sedimentary basin structure can potentially be

277   defined from gravity data for wavelengths >10 km, and for sedimentary rock thicknesses greater than ~500

278   m, although larger and thicker basins are resolved with more confidence. Gravity-derived thicknesses are

279   ambiguous, varying linearly with density contrast, and an inability to separate clearly the basin source from

280   other possible sources is a limiting factor to be overcome during interpretation.

281   For magnetic data, oxidation of magnetite to hematite during weathering means that sedimentary rocks in

282   general have low magnetization relative to crystalline basement [*Enkin et al.*, 2020]. While low-

283   magnetization rocks do not generate a magnetic anomaly, their presence increases the distance between a

284   basement source and the aircraft sensor — this distance also includes the thickness of water and ice and the

285   height of the aircraft above the surface. Increased source-sensor separation causes anomalies to have

286   reduced amplitude and increased wavelength and sedimentary basins are thus characterized by reduced

287   magnetic anomaly gradients [*Reid*, 1980; *Reid et al.*, 1990]. Analysis of the anomaly gradients using depth to

288   magnetic source estimation techniques is often applied to define sedimentary basin thickness and

289   distribution [*Aitken et al.*, 2014; *Ferraccioli et al.*, 2009a; *Tankersley et al.*, 2022].

290   Airborne magnetic data are collected from magnetometers that, most commonly, are attached to aircraft by

291   a tail-boom, at wingtips, or in some cases towed. Fixed-wing surveys dominate [*Aitken et al.*, 2020; *Jordan*

292   *and Becker*, 2018; *Tinto et al.*, 2019] modern data collection but helicopter surveys are also used in specific

293   settings [*Damaske et al.*, 2003; *Ferraccioli and Bozzo*, 2003; *Ferraccioli et al.*, 2009b; *Gohl et al.*, 2013a;

294   *Wilson et al.*, 2007]. In contrast to gravity surveys, instrument precision is not a major source of error, and

295   improvements in practice have focused on managing the highly unusual magnetic environment of

296   Antarctica, being close to the magnetic pole, and so especially vulnerable to space weather and intense

297   diurnal variations. In addition, the need for longer-range surveys and multi-year campaigns demands

298   additional care in data processing. The most recent approaches consider more fully the complexities of the

299   four-dimensional magnetic field [e.g. *Aitken et al.*, 2020], however the Antarctic geomagnetic environment

300   and logistical constraints remain substantial limitations on dataset accuracy relative to aeromagnetic data on

301   other continents.

302   A limitation of both gravity and magnetic approaches is the inability for airborne surveys to accurately

303   recover field components at wavelengths longer than the scale of the survey [*Scheinert et al.*, 2016]. For this,

304   the expansion of satellite-based gravity, gravity gradiometry and magnetic data, including the GRACE, GOCE

305   and SWARM missions has provided a crucial new understanding of the long-wavelength structure of the

306 continent [*Ebbing et al.*, 2018; *Ebbing et al.*, 2021; *Pappa et al.*, 2019a; *Pappa et al.*, 2019b], these also

307 underpinning more accurate compilations [*Ebbing et al.*, 2021; *Golynsky et al.*, 2018; *Hirt et al.*, 2016]. The

308 GOCE mission in particular has allowed new understandings of crustal structure, including efforts to define

309 sedimentary basins [*Capponi et al.*, 2022; *Haeger and Kaban*, 2019].

310 Overall, the ability to define sedimentary basins through gravity and magnetic approaches has improved

311 substantially in recent years, with particularly more accurate gravity recovery at shorter wavelengths, and

312 the incorporation of satellite magnetic and gravity data at longer wavelengths. These improvements mean

313 that, where airborne data exist, the identification of subglacial sedimentary basins is possible for basins with

314 thicknesses greater than ~500m and with spatial resolutions of 10 kilometers or possibly less. These data are

315 associated with physical non-uniqueness and, given other unknowns they do not unambiguously define the

316 geometry or physical properties of the basin fill. Unless these are otherwise constrained, these uncertainties

317 limit their use for a quantitative 3D understanding of basin morphology.

318 ### 2.2.2.3   Active and Passive Seismic

319 Seismic techniques record elastic waves in the ground, either from natural or non-specific anthropogenic

320 origins (e.g. earthquakes, ambient noise) or artificial sources of a controlled anthropogenic nature (e.g.

321 explosives, airguns, vibrators). Use of the former (passive seismic) typically involves continuous observations

322 from three-component seismometer arrays, while the latter (active seismic) typically uses shorter-term,

323 triggered observations with (usually single component) geophones, although hybrid approaches are also

324 used. Seismometers or geophones must be deployed in or on the ground for on-ice surveys, or in the water

325 for marine surveys. Of these methods active seismic approaches provide the more comprehensive image of

326 basin architecture.

327 Despite this, the application of active seismic techniques in Antarctica has several drawbacks. Active source

328 marine surveys can cover hundreds of kilometers per day in open water, although around Antarctica, the

329 presence of icebergs may disrupt surveying. By contrast, on-ice surveys that use explosive sources and

330 individual geophones as receivers can cover a few km per day in Antarctic conditions [*Anandakrishnan et al.*,

331 1998; *Johnston et al.*, 2008; *Peters et al.*, 2006]. The use of the vibroseis method over snow with a towed

332 streamer allows the collection of tens of kilometers per day. By this approach it has become possible to

333 obtain larger-scale surveys with several hundred kilometers per field season [*Eisen et al.*, 2015; *Smith et al.*,

334 2020]. Nevertheless, on-ice active seismic data are currently limited in spatial extent (Fig 1).

335 Unlike radio waves used in RES, seismic waves can penetrate subglacial environments such as water,

336 sedimentary strata, and the basement beneath, providing crucial information necessary to understand

337 glacial dynamics. In addition, due to the simpler timing requirements (relative to RES) sources and receivers

338 can be separated, allowing for bi-stactic or multi-static configurations that can exploit angle-dependent

339   information from reflections. Several seismic approaches have been employed to detect and define

340   sedimentary basins in Antarctica. The tomographic approach determines the bulk velocity and thickness of a

341   geologic unit underneath the ice. As the seismic wave speed in sedimentary basins is significantly lower than

342   in crystalline basement, the thickness and properties of such a unit can be estimated, especially with long-

343   baseline (wide-angle) reflection and refracted wave seismic surveys [*Blankenship et al.*, 1986; *Leitchenkov et*

344   *al.*, 2016; *Trey et al.*, 1999].

345   Seismic waves will reflect and refract at unit horizons where the acoustic impedance (defined as the product

346   of seismic velocity and density) changes. The seismic wave speed and density of sedimentary basin fill is

347   usually lower than that of crystalline basement, resulting in a generally lower acoustic impedance for

348   sedimentary basins. Furthermore, as the acoustic impedance of ice is well known, the reflection from the

349   subglacial interface can be used to determine the properties of that layer. Acoustic impedance

350   measurements along profiles can be used to discriminate between regions of hard bedrock from sediments

351   or water at the bed. Of particular significance is the ability to discriminate different structures associated

352   with tills and tillites that have a direct link to subglacial processes at the bed [*Anandakrishnan et al.*, 1998;

353   *Horgan et al.*, 2021; *Muto et al.*, 2016; *Muto et al.*, 2019b; *Peters et al.*, 2006; *Smith et al.*, 2013].

354   Reflection seismic methods can be used to map the stratigraphy of the geological units underlying the ice

355   sheet and ice shelf. The active seismic technique is especially important for resolving sub-ice shelf

356   bathymetry and basins [*Rosier et al.*, 2018; *Smith et al.*, 2020], as unlike radio waves the seismic waves can

357   penetrate into strata beneath electrically conductive seawater. These data can be used to constrain gravity-

358   based approaches [*Eisermann et al.*, 2020; *Muto et al.*, 2016]. The identification of a geologic stratigraphy

359   indicates that a subglacial unit is of probable sedimentary origin, and the details of its structure can be

360   interpreted to understand the depositional environment, and age relationships with faults and volcanic

361   edifices [e.g. *Horgan et al.*, 2005; *Johnston et al.*, 2008; *Kristoffersen et al.*, 2014].

362   As reflection seismic surveys have high spatial resolution, they provide a very good estimate of the ice

363   thickness and thus bed topography. In comparison to RES methods, ice-internal structure is not well

364   resolved, but seismic techniques are better able to characterize subglacial properties. Seismic profiles can be

365   analyzed in the same way as RES profiles for bed roughness, however, as they very often record over a larger

366   offset (source-to-receiver distance) spread than RES methods, they are less prone to the influence of side

367   reflections and smoothing given that adequate processing is applied in the form of migration.

368   Our ability to detect and discriminate sedimentary basins in seismic data is improving. Because seismic data

369   quality increases with the square root of the number of observations, data acquisition speed is key. Over the

370   last decade, progress in borehole drilling techniques (e.g. the rapid air movement drill system [Gibson et al.,

371   2020]), geophone design and deployment (e.g. Georods [Voigt et al., 2013]), and a combination of highly

372 efficient source-receiver systems (e.g. vibroseis-snowstream combination [Eisen et al., 2015]) all contributed

373 to increasing the seismic data coverage and thus our ability to detect sub-ice properties. Nevertheless, as

374 active seismic surveys are logistically still demanding, studies have been either only locally constrained or

375 require considerable resources to cover regional distances.

376 Passive seismic methods for detecting and studying sedimentary basins can estimate the seismic velocity

377 structure of the upper few kilometers of the crust using seismograph arrays deployed for periods of time

378 ranging from months to years. These techniques use naturally occurring seismicity within the ice sheet or

379 from earthquakes around the world, as well as seismic 'noise' from ambient sources such as ocean waves.

380 These surveys are relatively simpler than active source surveys as they don't require the source technology

381 (drills and explosive or a vibroseis truck). Passive seismic techniques can map sedimentary basin thickness on

382 a regional scale with a few seismic stations. Thus, passive techniques offer coverage of remote parts of

383 Antarctica, but at lower resolution than is possible for active seismic methods. One common method to

384 estimate the thickness of sedimentary basins is the so-called receiver function method. The P-wave (or S-

385 wave) from a remote earthquake and converted phases at basin boundaries can be used to estimate basin

386 properties with high sensitivity to acoustic impedance contrasts at structural interfaces located beneath the

387 recording station. Another method is to use the background, so-called ambient noise recorded at two

388 stations to estimate an equivalent to a seismic wave between those two stations. Ambient noise studies can

389 resolve broader lateral changes in seismic velocity structure. Joint application of these methods has become

390 common, providing the ability to resolve sedimentary basins.

391 Receiver function analysis provides images of structural interfaces below a seismic station using processing

392 that enhances seismic waves converted from S to P or P to S at structural interfaces [*Ammon*, 1991]. The

393 depth to the sediment-bedrock interface and thus the sediment thickness is determined from the time delay

394 of the converted phase, after adjusting for ice thickness [*Anandakrishnan and Winberry*, 2004; *Chaput et al.*,

395 2014]. The use of higher frequencies compared to typical receiver function analysis (4 Hz vs < 1 Hz) allows

396 detection of sediment thicknesses of a few hundred meters and also can provide some approximate

397 constraints on the velocity of the sediment layer [*Dunham et al.*, 2020]. While low-velocity relative to

398 igneous or metamorphic basement, consolidated sedimentary rocks may not provide sufficient density and

399 velocity contrast to be discernible in receiver functions.

400 Ambient noise analysis uses short-period seismic surface waves obtained from the ambient noise field

401 derived from non-specific sources, in particular ocean waves. By correlating records from two seismic

402 stations, the shallow structure beneath the ice sheet along the interstation path can be constrained [*Pyle et*

403 *al.*, 2010; *Shen et al.*, 2018]. The correlation yields the Green's Function for wave propagation between the

404 stations, from which the phase and group velocity and ultimately the shear-wave velocity structure is

405 obtained. If the distribution of seismic stations is dense enough, sediment and sedimentary rock thicknesses

can be mapped throughout the region from phase and group velocity tomography maps, so results are not restricted to the locations of seismographs. The use of both Rayleigh and Love waves provides better results, since Love waves have superior resolution at shallow depths [*Zhou et al.*, 2022]. Constraints on shallow structure from ambient noise Rayleigh waves can be improved by also measuring the ratio of horizontal to vertical displacement [*Lin et al.*, 2012; *Pourpoint et al.*, 2019]. Joint inversion of several of these datasets using a Bayesian formalism, including receiver functions, surface wave group and phase velocities, and horizontal to vertical ratios, can improve resolution of sedimentary material beneath the ice sheet [*Dunham et al.*, 2020; *Pourpoint et al.*, 2019].

Sedimentary basin thicknesses have been estimated using passive seismic techniques throughout West and Central Antarctica. *Pourpoint et al.* [2019] found thicknesses ranging from 0.1 to 1.5 km beneath seismic stations near the Thwaites Glacier drainage area, with the thickest sediment in the deep topography of the Byrd Basin and Thwaites Glacier bed. *Dunham et al.* [2020] found sediment thicknesses ranging from 0.1 to 0.9 km beneath seismographs in the West Antarctic Rift System (WARS) and Ellsworth Mountains region. *Zhou et al.* [2022] mapped sedimentary basin thicknesses throughout West and Central Antarctica with ambient noise surface wave methods. They found 4-5 km thick basins beneath the Ross Ice Shelf but in other regions of the study area maximum thicknesses were at most about 1.5 km, except in small regions where spatial resolution is lacking. They interpreted the lack of thick sedimentary basins, as found for intracratonic basins in other continents, as indicating that basins in this region of Antarctica may have been sediment starved throughout most of their post-Gondwana geological history, although erosion may also have been significant.

2.2.2.4 Electromagnetic and magnetotelluric

Electromagnetic techniques also include active and passive techniques. Due to their limited depth penetration, airborne approaches are not widely applicable to subglacial geology, although can be applied in ice-free regions [*Foley et al.*, 2015]. Ground based electric and electromagnetic techniques saw limited use in the past, however the most broadly applied approach in recent times is passive magnetotellurics [*Hill*, 2020]. The magnetotelluric technique provides the capacity to image deep within the Earth and is generally applicable to detect and to image sedimentary basins through their electrical properties, which are commonly related to water content, salinity and temperature. Assuming that subglacial sediments and sedimentary rocks are water-saturated, the key expected controls on bulk resistivity values are the connected porosity of the pore space and the salinity of the waters within them, defined empirically [see *Glover*, 2016].

Although a relatively old technique, the magnetotelluric method has been increasingly applied due in large part to improved ability to generate robust model solutions with high performance computing and improved sensor technologies. Magnetotelluric applications to crustal and upper mantle imaging in the polar regions

440   are reviewed in *Hill* [2020]. Building on most recent relevant work [*Gustafson et al.*, 2022; *Key and Siegfried*,

441   2017; *Kulessa et al.*, 2019; *Siegert et al.*, 2018] we focus here on examining the potential scope and

442   limitations of magnetotelluric imaging of the hydrogeological and thermal properties of subglacial

443   sedimentary basins.

444   The source fields of the magnetotelluric technique are inherently wideband, ranging from ~10^{-5} Hz to 10^4 Hz,

445   generated when electrical storms and interactions between the solar wind and the ionosphere produce

446   fluctuations in Earth's magnetic field. These fluctuations then induce correspondingly wideband telluric

447   currents in ice sheets and the underlying crust and mantle. Signal period is a proxy for depth, with longer-

448   period signals representing structure deeper in the Earth. Under favorable circumstances and depending on

449   the bandwidth and collection procedure of the survey, temporally coincident measurements of magnetic

450   and electric potential fields allow the bulk electrical resistivity distributions to be estimated from the near

451   surface at the highest frequencies, to depths of ~ 400 km at the lowest frequencies. Data collection is

452   typically focused in the high frequencies for near-surface studies (AMT 10^0 Hz to 10^4 Hz), across a central

453   broad band (BBMT 10^{-3} Hz to 10^2 Hz) for general crust and mantle studies, and long-period MT (LPMT 10^{-1} Hz

454   to 10^{-4} Hz) for mantle-focused studies. For the investigation of subglacial sedimentary basins beneath the

455   Antarctic Ice Sheet the higher-frequency band of the magnetotelluric spectrum is of most interest. On the

456   one hand this is attractive in that high-quality magnetotelluric data can be acquired with day-long station

457   occupations if wind speeds are low (<< 10 m s^{-1}), as compared with station occupations of a week or more

458   required for upper mantle studies.

459   Many challenges arise in ice sheet settings related to potential violations of fundamental source field

460   assumptions owing to the proximity to the geomagnetic south pole, high contact resistances of electrodes

461   buried in firn, and spin drift of charged snow particles generating strong broadband electrical noise [see *Hill*,

462   2020]. The last is a particular challenge in the imaging of subglacial sediment basins because the broadband

463   frequencies exploited in doing so are particularly susceptible to noise contamination by drifting snow. A

464   second specific challenge arises when firn is absent and ice is exposed at the surface instead, forming a

465   major barrier to the deployment of electrodes and magnetometers and associated wiring. This could be a

466   problem especially in coastal regions where seasonal melting and refreezing is widespread.

467   Notwithstanding these challenges, a growing number of Antarctic measurement campaigns have

468   demonstrated that high-quality magnetotelluric data can be acquired with careful survey planning and using

469   bespoke electrode pre-amplifiers [*Hill*, 2020]. Subglacial sediment basins are particularly well suited for

470   magnetotelluric exploration because they are expected to be several orders of magnitude less resistive

471   (order of $10^{-1} - 10^1$ Ωm) than both the underlying crystalline crust (typically > 10^2 Ωm) and the overlying ice.

472   Cold Antarctic ice has typical bulk resistivities of ~ $10^4 - 10^6$ Ωm but these can exceed 10^8 Ωm for temperate

473   clean-ice glaciers [*Kulessa*, 2007].

474 Magnetotelluric imaging of subglacial sedimentary basins remains poorly documented, however, with only a

475 few studies in Antarctica. Although not yet widely applied, magnetotelluric surveying can reveal high-quality

476 images of subglacial sediment basins and has unique potential for detecting and defining liquid groundwater

477 within them [*Gustafson et al.*, 2022]. The use of seismic data to constrain magnetotelluric inversions has not

478 yet been attempted with cutting edge joint inversion schemes but will very likely result in even higher-

479 quality images in the future [*Key and Siegfried*, 2017; *Kulessa et al.*, 2019; *Siegert et al.*, 2018].

480 There are two major complications for interpretation, however, in that Archie's law contains a cementation

481 exponent that has never been calibrated for subglacial sediments; even more significantly, Archie's law is not

482 applicable where sediments have noticeable clay mineral contents requiring a significantly adapted

483 formulation [*Kulessa et al.*, 2006]. This is likely a particular problem for coastal subglacial sedimentary basins

484 where contents of marine clays are not normally negligible.

485 Finally, it is expected that a significant geothermal gradient will exist between the base and top of subglacial

486 sedimentary basins, especially where they have a vertical extent of several kilometers and also are buried

487 beneath several kilometers of cold ice. [*Kulessa et al.*, 2019] demonstrated with a conceptual model that

488 such temperature gradients will likely result in a multi-fold increase in bulk resistivity between the base and

489 top of subglacial sediment basins, largely due to a temperature-controlled decrease in ionic mobility in

490 sediment pore waters. This inference suggests that bulk resistivity models can be used to infer temperature

491 changes in subglacial sedimentary basins and implied geothermal heat flux into the ice sheet base, a key

492 unknown in ice sheet modelling, especially in high-heat flux settings.

493 Overall, magnetotelluric measurements are powerful tools to explore subglacial sedimentary basins, the

494 associated groundwater and geothermal heat fluxes, and their interactions with the ice sheet base. In most

495 Antarctic situations, porosity, pore-fluid salinity, clay mineral contents and temperature changes will

496 combine to control bulk resistivity magnitudes, a complication that may be further compounded for coastal

497 sediment basins. These ambiguities require external constraint to develop a quantitative interpretation of

498 sedimentary properties from bulk resistivities.

2.2.3   Integrated Studies

499

500 As we have seen above, each of the listed methods has the capacity to define the existence of sedimentary

501 basins beneath ice, and in many cases also particular characteristics such as thickness, internal geometry,

502 seismic velocity, density, electrical conductivity. These characteristics each may resolve different aspects of

503 the basin, and furthermore, each technique has different uncertainties and so the methods are

504 complementary. In particular, the inherent ambiguities in most data available can lead to major errors when

505 any single technique is used. For example, outcrops may be selected for erosion resistance through

506 landscape forming processes while low-roughness topography may be caused by glacial erosion [*Jamieson et*

507 *al.*, 2014] and low gravity anomalies and/or smooth magnetic gradients may be caused by low-density or
508 non-magnetic basement rocks.

509 Integrated studies that use multiple datasets are necessary to properly resolve these ambiguities [*Grikurov*
510 *et al.*, 2003]. For airborne geophysical surveys, the combination of RES, gravity and magnetic data has
511 proved powerful, and this is especially enhanced where suitable ground observations are also collected.
512 Major recent, ongoing, and upcoming data collection programs have sought to synergize multidisciplinary
513 data collection and modelling [*MacGregor et al.*, 2021; *Scambos et al.*, 2017]. The co-interpretation of
514 multiple complex and sparse geoscience datasets has a high task-complexity, that may lead to difficulty
515 making reliable judgements [*Swink and Speier*, 1999]. As a human-led process which relies on interpreter
516 skill, the background, knowledge and biases of the investigator can have substantial impacts on results
517 [*Wilson et al.*, 2019]. Although clearly not without uncertainty, multi-data analyses provide the potential to
518 manage subjectivity in interpretation and support the ability to make sound judgements [*Aitken et al.*, 2018].

519 A consistent data-based mapping at continental scale is challenged by highly variable data quality, resolution
520 and availability as well as the challenge of combining multiple datasets into a consistent map that accounts
521 for all data. To define basal boundary conditions, we may seek initially to define the presence or absence of
522 sedimentary cover, which is a prerequisite to understanding its thickness, age, and other properties.
523 Geostatistical and machine learning techniques provide relatively unbiased and data-based approaches to
524 understanding this in a probabilistic sense. *Li et al.* [2022] apply the random forest approach with multiple
525 data types to map for all Antarctica the likelihood of sedimentary basins at the bed. *MacKie et al.* [2021]
526 apply a trained logistic regression model to simulated topographic roughness model to infer geological bed
527 type associated with the presence of sediments. Such techniques are highly valuable with respect to their
528 consistent response to data, provided those data are not too variable in their properties (resolution,
529 accuracy etc), but they are not able always to accommodate irregularly sampled or sparse data, while non-
530 numerical data can also be problematic to include. In this work we use the results of such techniques with a
531 wide range of prior findings and datasets (Fig. 2) to develop a new understanding of sedimentary basins
532 beneath the Antarctic Ice Sheet.

3 Antarctica's Sedimentary Basins

3.1 Methods & Validation

535 The sedimentary basin distribution is mapped continent wide using a flexible basin classification approach
536 applied in a GIS. The map presented here (Figure 3) is manually classified based on a wide range of
537 continent-scale datasets and derivative products. To develop the map, an initial classification into basins and
538 non-basins was automatically derived from the machine learning derived likelihood map of Li et al. (2022),
539 using a threshold of 0.5. From this initial point (Fig 2a) the polygons for individual regions were scrutinized

540 and edited considering additional data including outcrop information, along-track roughness (Fig 2b) bed

541 elevation (Fig 2c) and its spatial variability (Fig 2d), gravity magnitudes (Fig 2e) and their spatial variability

542 (Fig 2f), aeromagnetic data (Fig 2g) and their spatial variability (Fig 2h) and sedimentary basin thickness

543 estimates from passive and active seismic datasets. The results and interpretations from many published

544 studies and maps were also accommodated in the mapping process.

545
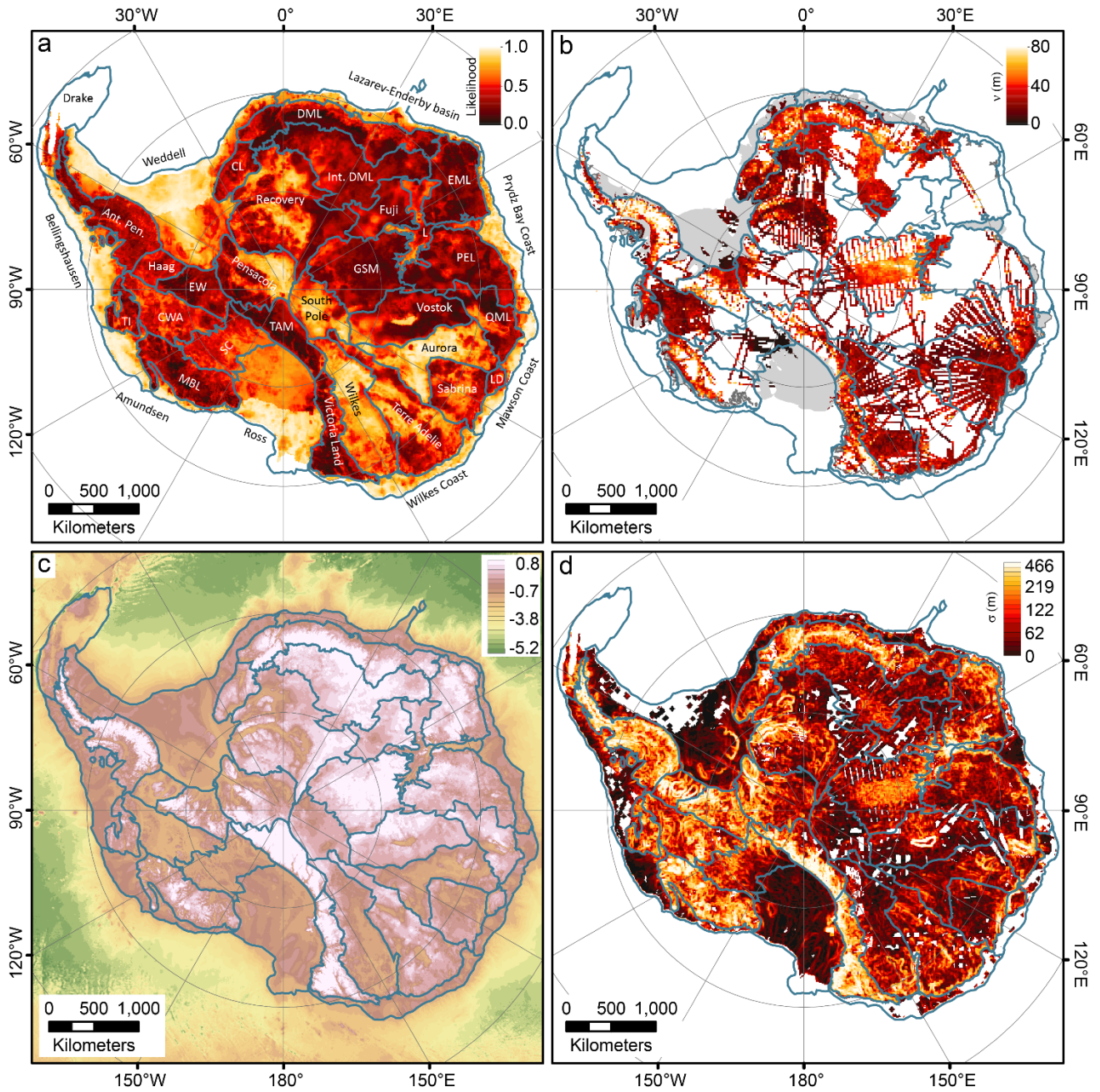
Figure 2: Key models and datasets for defining basin distribution in Antarctica including a) model of

sedimentary basin likelihood from machine learning [Li et al., 2022], b) along-track roughness using airborne

RES data compiled from Eisen et al. [2020] and other data. Along track roughness ν was calculated using a

spatial technique as in Eisen et al. [2020], c) a bed elevation model and d) its large-scale spatial variability

550 defined as standard deviation in a 30 km by 30 km window; both from BedMachine Antarctica [Morlighem,

551 2020]. Major sedimentary basin regions used for classification are outlined. CWA – Central West Antarctica,

552 EW – Ellsworth Whitmore, SC – Siple Coast, CL, TAM – Transantarctic Mountains, DML -Dronning Maud Land,

553 GSM – Gamburtsev Subglacial Mountains, EML- Enderby-Mac Robertson Land, PEL – Princess Elizabeth Land,

554 QML – Queen Mary Land, LD – Law Dome
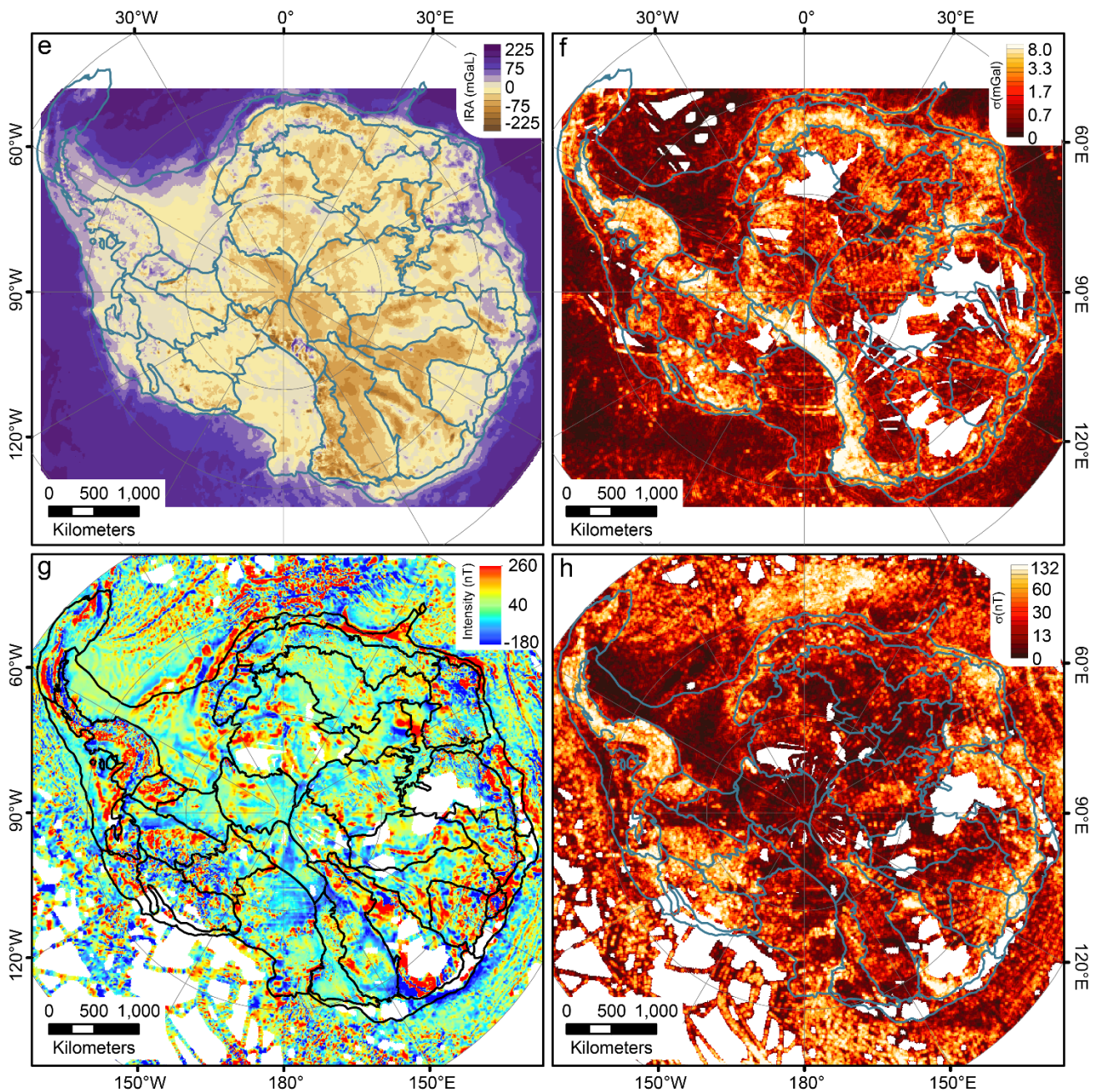
556 Figure 2 (continued): e) Airy isostatic residual gravity anomaly and f) spatial variability (standard deviation,

557 30 km window) of Bouguer gravity anomaly. Gravity data after AntGG [Scheinert et al., 2016] and additional

558 data [Forsberg et al., 2018; Kvas et al., 2021; Olesen et al., 2020; Paxman et al., 2019a; Sandwell et al., 2014;

559 Tinto et al., 2019; Young et al., 2017a] g) magnetic field intensity anomaly and h) its spatial variability.

560　*Magnetic data after ADMAP-2 [after Golynsky et al., 2018] and additional data [Ferraccioli et al., 2020;*

561　*Forsberg et al., 2018; Paxman et al., 2019a; Tinto et al., 2019; Young et al., 2017b].*

562　3.1.1　Geology classification
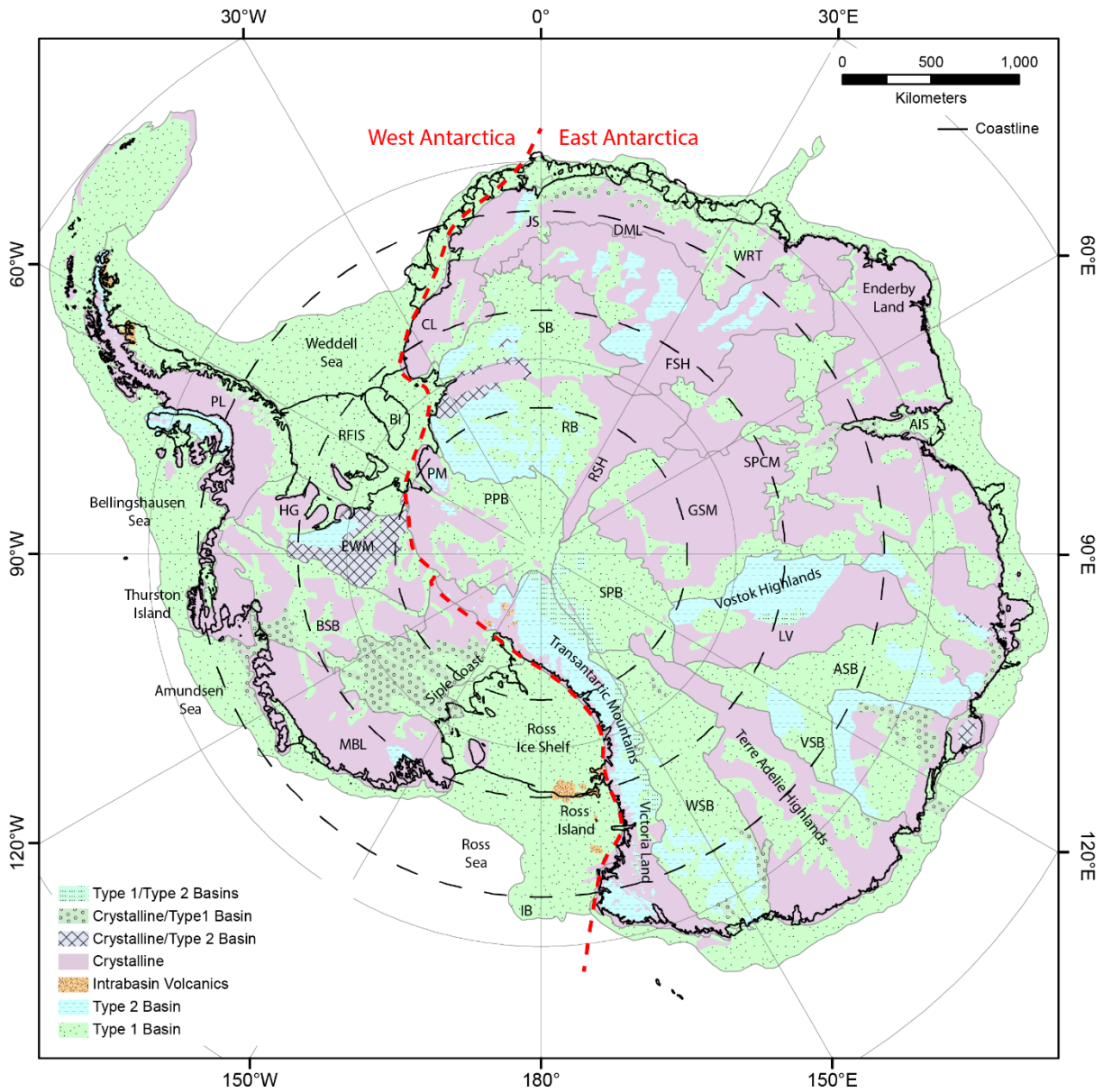
564　*Figure 3: Classification of geological bed type in Antarctica showing the main classes of type 1 and type 2*

565　*basins, intra-basin volcanics, and crystalline basement, as well as regions of mixed type classification. Major*

566　*sedimentary basin regions are outlined in grey. The coastline shows both the ice sheet grounding line and the*

567　*ice shelf edge. Dashed lines indicate locations of annular profiles (Fig. 6). PL – Palmer Land, RFIS – Ronne-*

568　*Filchner Ice Shelf, BI – Berkner Island, HG – Haag Block, EWM – Ellsworth Whitmore Mountains, PM –*

569　*Pensacola Mountains, BSB – Byrd Subglacial Basin, MBL – Marie Byrd Land IB – Iselin Bank, CL – Coats Land,*

570　*PPB – Pensacola-Pole Basin, RB – Recovery Basin, RSH – Recovery Subglacial Highlands, JS – Jutulstraumen,*

571　*DML -Dronning Maud Land, WRT -West Ragnhild Trough, FSH – Fuji Subglacial Highlands, AIS – Amery Ice*

Shelf, SPCM – Southern Prince Charles Mountains, GSM – Gamburtsev Subglacial Mountains, SPB – South

573 *Pole Basin, LV – Lake Vostok, ASB – Aurora Subglacial Basin, VSB – Vincennes Subglacial Basin, WSB – Wilkes*

574 *Subglacial Basin*

575 As discussed above, the principal distinction we wish to make here is between crystalline basement

576 dominated regions, and sedimentary basins. However, a binary classification is inadequate to cover the

577 range of circumstances that the geology presents. Retaining simplicity, we classify the bed type into four

578 main classes: crystalline basement, intra-basin volcanic, and type 1 and type 2 basins (Fig 3). Often, the data

579 contain characteristics of more than one of these types, due either to variable bed types present in small

580 areas, or due to transitional conditions from one type to another and so we also have three mixed-type

581 classes, although their distribution is relatively restricted compared to the major types (Fig 3).

582 The crystalline basement class indicates where the bed is interpreted to consist of igneous or metamorphic

583 rocks (including high-grade metasedimentary rocks), with either no sedimentary cover, or a thin veneer that

584 is below the detection thresholds of the datasets used. Typically, these regions possess the characteristics of

585 high elevation and high gravity with high variability in topography, gravity, and magnetic data. Along track

586 roughness tends to be high for this class. Type cases for this class include regions in the Transantarctic

587 Mountains, Dronning Maud Land, Marie Byrd Land and the Gamburtsev Subglacial Mountains.

588 The type 1 basin class represents regions where sedimentary basins are preserved in relatively unmodified

589 basins, with typical characteristics of low elevation and low gravity, and low variability in gravity and

590 magnetic data. Along-track roughness tends to be low. Commonly, basins of this type have sufficient

591 thickness for this to be modeled in gravity and aeromagnetic data and detected in seismic data (Fig 6). Type

592 cases for this class include the Ross and Weddell embayments, and the Wilkes, Aurora and Pensacola-Pole

593 Subglacial Basins.

594 The intra-basin volcanics class includes areas where volcanic rocks are interpreted to be emplaced within a

595 type 1 basin sequence, that is they are younger than the base of the basin and may interfinger with or

596 overlie sedimentary rocks. Typically, this class relies on outcrop data and aeromagnetic data to define the

597 extents of volcanic complexes where they are dominant. It is noted that basins may contain volcanic rocks

598 without them being evident in geophysical data and the extent of volcanic rocks is likely underestimated.

599 The type case for this class is the McMurdo Volcanic Complex in the Ross Sea.

600 Finally, we define the type 2 basin class where sedimentary rocks are known or inferred but the original

601 depositional basin is not preserved. These rocks tend to predate the formation of the present landscape, are

602 often uplifted to high elevations, may be intruded by younger igneous rocks, may be heavily eroded and

603 overall have geophysical characteristics more similar to crystalline basement than type 1 basins. The type

604 case for this class is the Beacon Supergroup, with its characteristic high elevation exposures through the

605 TAM and mesa-like topography as a consequence of widespread Jurassic dolerite intrusions. Type 1 basins

606 are prominent in the TAM and in the Ellsworth Whitmore mountains, with subglacial examples inferred in

607 Dronning Maud Land, and subglacial highlands in Vostok and Aurora regions (Fig 3).

Rank	Dataset	Variable
1	Topography	Elevation
2	Topography	Rebounded elevation
3	Gravity	Free air anomaly
4	Gravity	Bouguer anomaly
5	Topography	Rebounded elevation variation (30 km)
6	Gravity	Bouguer variation (30 km)
7	GOCE	Mean curvature
8	GOCE	Structure Index
9	Magnetic	Magnetic intensity variation (30 km)
10	Gravity	High-pass Airy IRA (1000km)
11	Magnetic	Magnetic total gradient
12	Gravity	High-pass Bouguer Anomaly (1000km)
13	Magnetic	Magnetic total anomaly
14	Gravity	Airy IRA
15	Magnetic	High-pass pseudogravity (1000 km)
16	Magnetic	Pseudogravity
17	Magnetic	Magnetic Intensity RTP

Rank	Dataset	Variable
1	Gravity	Airy IRA
2	GOCE	Structure Index
3	GOCE	Mean curvature
4	Gravity	Bouguer anomaly
5	Magnetic	Magnetic intensity variation (30 km)
6	Gravity	High-pass Bouguer Anomaly (1000km)
7	Gravity	Free Air Anomaly
8	Magnetic	Magnetic total gradient
9	Gravity	High-pass Airy IRA (1000km)
10	Topography	Rebounded elevation
11	Topography	Elevation
12	Gravity	Bouguer variation (30 km)
13	Magnetic	Magnetic total anomaly
14	Topography	Rebounded elevation variation (30 km)
15	Magnetic	Pseudogravity
16	Magnetic	High-pass pseudogravity (1000 km)
17	Magnetic	Magnetic Intensity RTP

| Rank	Dataset	Variable
1	Topography	Elevation
2	Topography	Rebounded elevation
3	Gravity	Bouguer anomaly
4	Gravity	Bouguer variation (30 km)
5	Topography	Rebounded elevation variation (30 km)
6	Gravity	Airy IRA
7	Gravity	High-pass Bouguer Anomaly (1000km)
8	Gravity	Free Air Anomaly
9	Magnetic	High-pass pseudogravity (1000 km)
10	Magnetic	Magnetic total anomaly
11	Magnetic	Magnetic total gradient
12	Magnetic	Magnetic intensity variation (30 km)
13	GOCE	Structure Index
14	Magnetic	Magnetic Intensity RTP
15	Gravity	High-pass Airy IRA (1000km)
16	Magnetic	Pseudogravity
17	GOCE	Mean curvature

608

609 *Figure 4: Relative effect sizes for selected datasets for a) crystalline basement vs type 1 basins, b) crystalline*

610 *basement vs type 2 basins, c) type 1 basins vs type 2 basins. For each, datasets are ordered by Cohen's effect*

611 *size indicating the ability of the dataset to discriminate those classes. The listing on the right highlights the*

612 *datasets in rank order. Effect sizes above 0.8 may be considered a large effect, and below 0.5 a small effect.*

3.1.1.1   Class Validation

614   For validation, we may review this geological bed type classification against the major numerical datasets

615   available to the interpretation. Summary statistics for each input dataset were calculated for each class using

616   a Zonal Statistics GIS tool. These statistics allow to define the distinctiveness of the class-level populations, in

617   terms of differences of means, factoring in standard deviation, and so illuminate the data that most strongly

618   differentiate between classes (Fig 4). In figure 4 we show, with orange and blue lines the extent to which the

619   zonal mean for the class differs from the mean for the entire region. Where these differ substantially,

620   especially in sign, that dataset can discriminate the two selected classes. Furthermore, we may directly

621   compare the population-level distinctiveness between classes, for which we derive Cohen's effect size (Fig

622   4). Values above 0.8 may be considered a large effect, indicating a strong discriminator while values below

623   0.5 may be considered a small effect, indicating a weak discriminator.

624   The primary classification we seek is the distinction between type 1 basins and crystalline basement. For

625   these two classes, large effect sizes are seen for topography elevation datasets, while medium effect sizes

626   are seen for free air and Bouguer gravity, topography and gravity variation and satellite gravity-gradient

627   components (Fig 4a). In contrast, the distinction between crystalline basement and type 2 basins is weaker,

628   with medium effect sizes seen for Airy IRA and satellite gravity-gradient components (Fig 4b).   The

629   distinction between type 1 and type 2 basins is strong, with large effect sizes for subglacial topography

630   elevation datasets, Bouguer gravity datasets and variability measures for these, and medium effect sizes for

631   Airy IRA and high pass filtered Bouguer gravity (Fig 4c). Finally, the in-basin volcanics class is sharply defined

632   relative to all other classes, these being most clearly differentiated with large or medium effect sizes for

633   magnetic data products as well as for variability in topography and gravity data.

634   The relationships highlighted above support the following as key criteria in classifying subglacial geology

635   class: type 1 basins are defined most by their low topography at large scales, accompanied by relatively high

636   Bouguer gravity, perhaps counter to expectations (note the opposite sign to topography in Fig 4a, 4c). With

637   respect to their classification from type 1 basins, type 2 basins show similar characteristics to the crystalline

638   basement class, but with a stronger effect from gravity data, reflecting characteristic gravity lows. Type 2

639   basins can be separated from crystalline bed by their low response in Bouguer and Airy IRA gravity

640   anomalies and satellite gravity gradiometry components. The magnetic dataset does not discriminate

641   strongly between these three classes but is strongly linked to the in-basin volcanics class, which is also

642   identified by high spatial variability in all datasets.

643
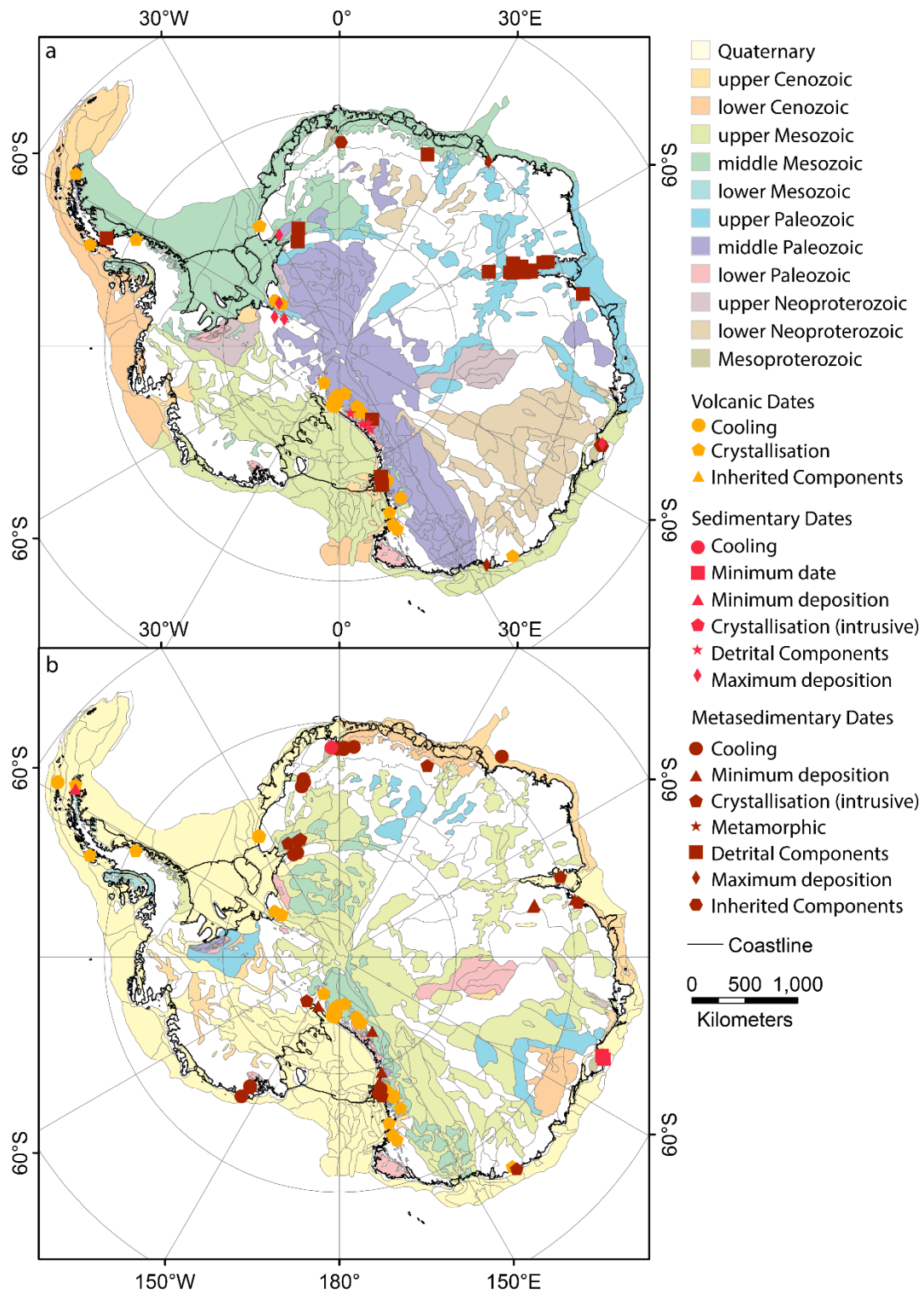
Figure 5: Interpreted ages for a) base of the basin sequence and b) top of the basin sequence. Locations of

selected age information for volcanic, sedimentary, and metasedimentary rocks are derived from PetroChron

Antarctica [Sanchez et al., 2021], and broadly indicate where basin ages are better constrained.

647

3.1.2 Age Classification

In addition to geological class we seek to define the age of the basins, which besides its importance for tectonic understanding, may correspond to very different conditions for the ice sheet for basins of different age. The interpreted age distribution indicates the evolving tectonic conditions of Antarctica and its landscape, although due to the general paucity of robust age-dating outside of outcropping regions, and also the very limited capacity for stratigraphic correlation beneath the ice, these interpretations are on necessarily broad timescales.

For each basin, we define an interpreted age for the base and the top of the basin sequence (Fig. 5). The base of basin age (Fig. 5a) represents a maximum bound on basin age, either from a known maximum age (e.g. from maximum deposition), or from the interpreted age of the underlying crust. The top of basin age (Fig. 5b) represents a minimum bound on basin age, either from a known minimum age (e.g. cooling age), from a capping or intruding unit or from geomorphological criteria including interpreted regions of glacial erosion and deposition.

3.1.3 Basin Thickness

Except for RES data, the data types in the preceding section can all be used to generate models of the thickness of sedimentary cover. It is possible to interpolate sedimentary thickness between existing data points, giving an estimate of the thickness of sedimentary cover across the continent [*Baranov et al.*, 2021]. However, the fundamental differences between basin-sensing techniques, their differing resolution and accuracy, and specific features of individual surveys and models leads to major uncertainty in defining basin thickness.

Figure 6 shows several sedimentary basin thickness models, including models derived from gravity [*Haeger and Kaban*, 2019], interpolation of seismic data [*Baranov et al.*, 2021], passive seismic models [*Zhou et al.*, 2022], seismic reflection data and magnetic depth to basement [*Tankersley et al.*, 2022] and marine seismic reflection data [*Hochmuth et al.*, 2020; *Lindeque et al.*, 2016b; *Straume et al.*, 2019]. While there is some commonality between these models, there are also many differences and only the seismic reflection models show strong consistency with each other.

Three major factors contribute to this discrepancy. First, the resolution of techniques differs and so distinctly separate features in one technique are likely to be merged in another. Consequently, thickness models will differ greatly in the presence of complexity (e.g. Ross Island in Fig. 6b). Second, the physical properties detected with each technique differ and furthermore, not all techniques have agreed criteria for the definition of the basin-basement interface. Finally, the different techniques have different capacity to image deep basin fill, and to accurately define the base of basins is often challenging, for example depth to magnetic basement commonly defines sills within the basin sequence, and there is often no solution

possible for the basement beneath. Ultimately, while a general agreement can be reached on the extent of
sedimentary basins, their thicknesses remain poorly constrained in Antarctica, except where seismic
reflection data have been collected.
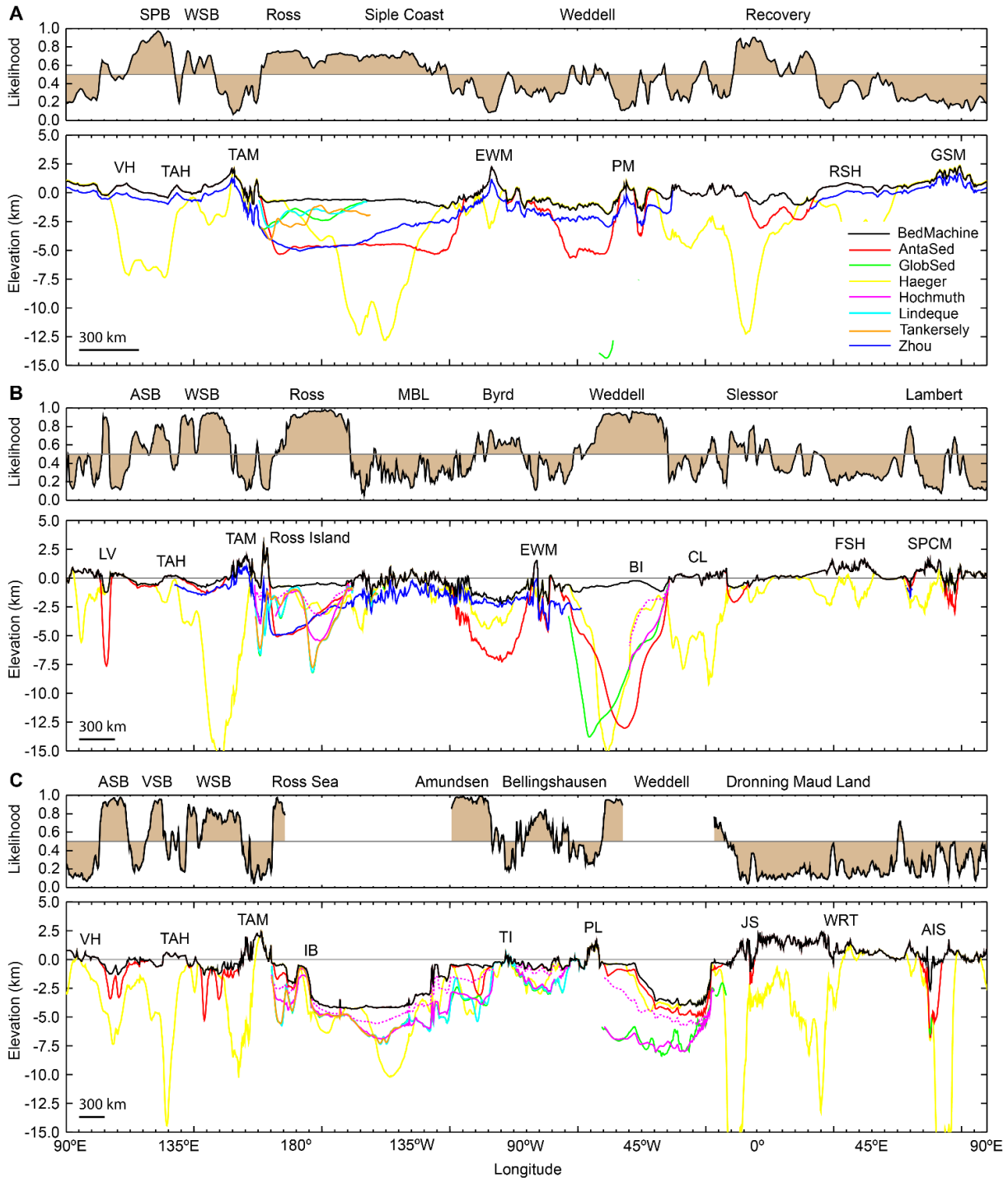
*Figure 6: Annular profiles at latitudes of a) 82.5°S b) 77.5°S and c) 72.5°S (see figure 3 for locations). For
each, the upper panel shows the basin likelihood model of [Li et al., 2022] and the lower panel bed
topography [Morlighem, 2020] and base-basin elevation for several basin thickness model [Baranov et al.,
2021; Haeger and Kaban, 2019; Hochmuth et al., 2020; Lindeque et al., 2016b; Straume et al., 2019;*

689   *Tankersley et al., 2022; Zhou et al., 2022]. SPB – South Pole Basin, WSB – Wilkes Subglacial Basin, VH -*

690   *Vostok Highlands, TAH – Terre Adelie Highlands TAM – Transantarctic Mountains, EWM – Ellsworth*

691   *Whitmore Mountains, PM – Pensacola Mountains, RSH – Recovery Subglacial Highlands, GSM – Gamburtsev*

692   *Subglacial Mountains, ASB – Aurora Subglacial Basin, MBL – Marie Byrd Land, LV – Lake Vostok, BI- Berkner*

693   *Island, CL – Coats Land, FSH – Fuji Subglacial Highland, SPCM – Southern Prince Charles Mountains, VSB –*

694   *Vincennes Subglacial Basin, IB – Iselin Bank, TI – Thurston Island, PL – Palmer Land, JS – Jutulstraumen, WRT -*

695   *West Ragnhild Trough, AIS – Amery Ice Shelf.*

3.2 West Antarctic Basins

697   West Antarctica, in a geomorphological division, includes the continental regions on the Pacific-facing side of

698   the chain of mountains extending from Northern Victoria Land through the Transantarctic and Pensacola

699   Mountains to Coats Land (Fig 3). This region possesses several major basin-dominated regions, in particular

700   the Ross, Amundsen and Weddell regions, and is characterized by the low-elevation topography associated

701   with these. West Antarctica's crust has a varied history but the majority has formed since the Cambrian as a

702   result of accretionary tectonics at Gondwana's paleo-Pacific margin [*Jordan et al.*, 2020]. It is noted that the

703   inferred boundary between the Paleozoic crust and the Proterozoic crust of East Antarctica, is not co-located

704   with the geomorphological boundary. Rather it traverses centrally through the Ross Embayment [*Tinto et al.*,

705   2019], and also has been affected by later translation of the Haag and Ellsworth-Whitmore and Marie-Byrd

706   Land blocks [*Jordan et al.*, 2020]. This basement hosts a series of basins of diverse origin extending from the

707   Cambrian to the Quaternary

3.2.1 The Ross Embayment and Siple Coast

709   This sector of West Antarctica is bounded by the Transantarctic Mountains to the west and the West

710   Antarctic Ice Sheet (WAIS) divide to the south with the basement-dominated Marie Byrd land to the east. In

711   Marie Byrd land, small type 1 basins are interpreted in glacial troughs (Fig. 7) but the major known basin

712   (type 2) is defined by the variably metamorphosed <520 Ma to >440 Ma Swanson Formation, dominated by

713   turbidites and flysch. These rocks represent a middle-Cambrian to Ordovician basin, with sediments derived

714   from the Ross Orogen and a variety of Proterozoic sources [*Yakymchuk et al.*, 2015]. These sediments were

715   deposited along the Gondwana margin, initially on the continental slope and rise in the Cambrian – lower

716   Ordovician but possibly later in a fore-arc/accretionary prism setting as a convergent margin setting

717   developed [*Jordan et al.*, 2020].

718   The Ross Sea is of the most well studied regions in Antarctica and the existence of major sedimentary basins

719   is well established, with their stratigraphy revealed in multi-channel seismic data as well as numerous drill

720   cores (Fig 1). These studies define a thick sequence of late Cretaceous to Quaternary sedimentary rocks

721 separated into several packages by regional unconformities [*Davey and Brancolini*, 1995; *Lindeque et al.*,

722 2016a; *Pérez et al.*, 2021].

723
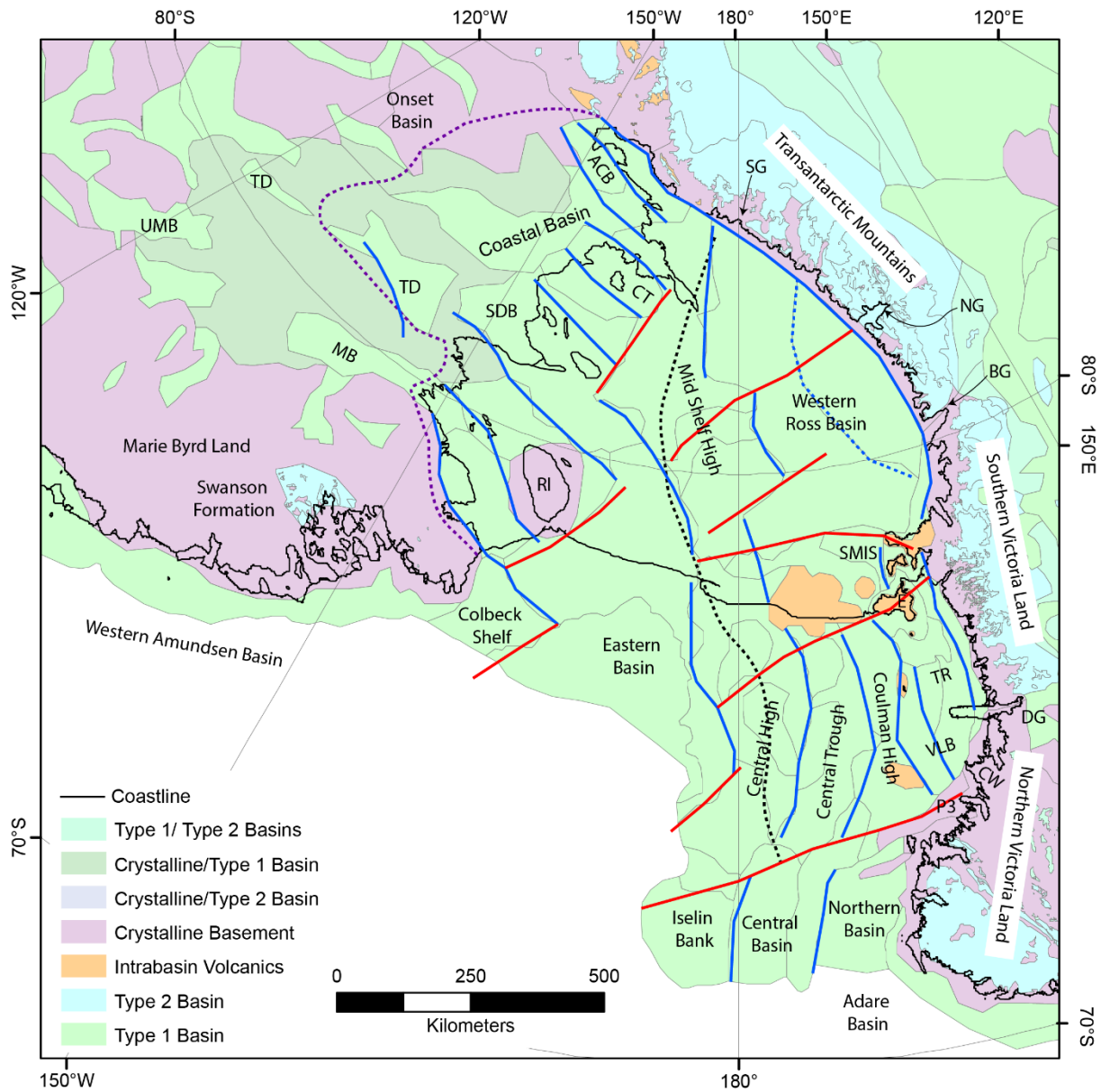
724 *Figure 7: Sedimentary basins of the Ross Sea and Siple Coast regions, showing basin regions and*

725 *reinterpreted basin structures, rift parallel (blue) and transverse (red). Basin faults are reinterpreted from*

726 *prior studies [Davey et al., 2021; Lindeque et al., 2016b; Pérez et al., 2021; Sauli et al., 2021; Studinger et al.,*

727 *2001; Tankersley et al., 2022; Wilson et al., 2012; Wilson, 1999]. Also shown are the interpreted East*

728 *Antarctica-West Antarctica basement boundary (black) [Tinto et al., 2019], and the seismically defined*

729 *extents of thick basin cover [Zhou et al., 2022] (purple). UMB – Upstream MacAyeal Basin, MB - MacAyeal*

730 *Basin, TD - Trunk D Basin, ACB – Amundsen Coast Basin, CT - Crary Trough, SDB - Siple Dome Basin, TR –*

731 *Terror Rift, VLB – Victoria Land Basin, P3 – Polar 3 Anomaly, RI – Roosevelt Island, SG – Shackleton Glacier,*

732 *SMIS – Southern McMurdo Ice Shelf, NG – Nimrod Glacier, BG – Byrd Glacier, CW – Cape Washington, DG –*
733 *David Glacier, E - Erebus*

734 The Ross Sea basin has four major depocenters, the Victoria Land Basin, the Central Trough, the Eastern
735 Basin and the Northern Basin [*Davey and Brancolini*, 1995] separated by basement highs with much less fill,
736 the Coulman High and Central High; only Roosevelt Island appears sediment free [*Wilson and Luyendyk*,
737 2006]. These basins initiated with rifting in the late Cretaceous, but with relatively little basin-fill deposited.
738 The first major sequence (RSS-1) is discontinuous and is observed in isolated grabens in the eastern to
739 central Ross Sea, and may represent this rifting event, with thermal subsidence perhaps extending into the
740 early Cenozoic [*Luyendyk et al.*, 2001]. A later phase of Eocene to Oligocene rifting is interpreted in the
741 Victoria Land Basin [*Fielding et al.*, 2008]. A basin-wide unconformity (RSU-6) indicates a period of erosion in
742 the Oligocene, occurring not later than 26 Ma in the Eastern Basin [*Kulhanek et al.*, 2019], potentially
743 associated with sea-level fall associated with large-scale glaciation in Antarctica. Correlation of RSU-6 into
744 the Victoria Land Basin has been problematic [cf. *Davey et al.*, 2000; *Fielding et al.*, 2008], but may align with
745 a mid-Oligocene unconformity that marks the end of the early rift stage of *Fielding et al.* [2008]. Subsequent
746 to this, basin deposition was episodic, but with relatively little extension, the glacial evolution of the
747 continent being the major driver of basin evolution in most of the Ross Sea [*Anderson et al.*, 2019; *De Santis*
748 *et al.*, 1999; *Kim et al.*, 2018; *Lindeque et al.*, 2016a; *Marschalek et al.*, 2021; *Pérez et al.*, 2021]

749 Upper Oligocene to Lower Miocene strata (RSS-2) are preserved in the major basins of the Ross Sea, but are
750 thin to absent on the basement highs [*Pérez et al.*, 2021]. These sediments are interpreted to be deposited
751 in a glacio-marine setting associated with a fluctuating ice sheet margin including glaciation of local
752 bathymetric highs [*De Santis et al.*, 1999]. Early to middle Miocene (18-15 Ma) sedimentary deposition (RSS-
753 3 & RSS-4) is interpreted in detail in *Pérez et al.* [2021]. In contrast to the thick and structurally segmented
754 packages of the lower sequence, this package overall is laterally continuous across the southern Ross Sea,
755 but with complex internal structure that is representative of changeable ice sheet dynamics, as documented
756 in several drill core records [*Levy et al.*, 2016; *Marschalek et al.*, 2021; *McKay et al.*, 2016]. A major mid-
757 Miocene erosional event (RSU-4), indicating the advance of a major ice sheet over the Ross Sea is
758 interpreted associated with the Mid-Miocene Climate Transition [*Bart*, 2003; *Pérez et al.*, 2021]. The post
759 mid-Miocene sedimentary basin record is similarly characterized by numerous and repeated ice sheet
760 advance and retreat cycles [*Anderson et al.*, 2019; *Bart et al.*, 2000; *Halberstadt et al.*, 2018; *McKay et al.*,
761 2012a; *McKay et al.*, 2012b; *Naish et al.*, 2009]. Consequently, sediment thicknesses are relatively low,
762 except in deeper water in the northeast where substantial progradation of the shelf edge is seen [*Hochmuth*
763 *and Gohl*, 2019; *Pérez et al.*, 2021], and in the west where the Terror Rift has substantially deepened the
764 bathymetry [*Sauli et al.*, 2021; *Wenman et al.*, 2020].

765   The Terror Rift has generated the ~ 4 km thick rhombic Discovery Graben, extending from Cape Washington

766   to, at least, Ross Island [*Sauli et al.*, 2021], with a seismically defined extension into the southern McMurdo

767   Ice Shelf [*Johnston et al.*, 2008], and possibly further south [*Tankersley et al.*, 2022]. Stratigraphic

768   considerations suggest that after Eocene- Oligocene rifting, a period of thermal subsidence persisted until

769   renewed extension from ~13 Ma drove the renewed tectonic development of accommodation space in the

770   Discovery Graben [*Fielding et al.*, 2008], however a more continuous evolution may be considered [*Granot*

771   *and Dyment*, 2018; *Sauli et al.*, 2021]. Within the western Ross Sea, the McMurdo Volcanic Complex

772   represents widespread and prominent volcanism, and some of these volcanoes are associated with flexural

773   basin development [e.g. *Horgan et al.*, 2005; *Wenman et al.*, 2020] generating repositories of Neogene

774   sedimentation and glacial development [*McKay et al.*, 2012a; *McKay et al.*, 2012b; *McKay et al.*, 2016; *Naish*

775   *et al.*, 2009].

776   The northwestern Ross Sea has a distinct Cenozoic evolution. The Northern Basin is directly associated with

777   the adjacent Adare Basin, which formed during seafloor spreading from 43 to 26 Ma, while the oceanic crust

778   beneath the Central Basin, north of the Central Trough, may have formed from 61 to 53 Ma [*Cande and*

779   *Stock*, 2004]. The Northern Basin is offset from the Victoria Land Basin by the Polar 3 magnetic anomaly,

780   inferred to represent an intrusion emplaced into a transcurrent fault zone. With the implication that this

781   fault zone extends further offshore to the Iselin Bank, *Davey et al.* [2021] present a three-stage

782   reconstruction of the northern Ross Sea involving: 10 to 26 Ma – Terror Rift opening and minor extension of

783   WARS [*Granot and Dyment*, 2018], 26 to 43 Ma – Opening of the Adare Basin and Northern Basin; 53 to 61

784   Ma – Opening of the Central Basin and northern Central Trough, accommodated by Polar-3 transfer and its

785   extension to the Iselin Rift [*Davey et al.*, 2021].

786   The extension of the basin forming events known from the southern Ross Sea beneath the Ross Ice Shelf is

787   highly likely, although the structure of these basins has not been fully demonstrated, due to the lack of

788   extensive seismic data and ambiguous gravity signals [*Karner et al.*, 2005]. Recent geophysical data have

789   begun to reveal the structure of this basin: Airborne geophysical surveying across the Ross Ice Shelf has

790   allowed the identification of several depocenters from depth to magnetic basement calibrated against the

791   southern Ross Sea [*Tankersley et al.*, 2022]. These show continuation of the Ross Sea systems into Eastern

792   and Western depocenters separated by a mid-shelf high connecting with the Central High. The Eastern

793   depocenter narrows inland to a distinct trough beneath Siple Dome. A smaller depocenter is located to the

794   east of Roosevelt Island. The western depocenter beneath the Ross Ice Shelf is broad with a weakly defined

795   ridge separating two sub-basins. In addition, recent passive seismic models map sedimentary thickness in

796   the region using ambient noise tomography, also revealing thick sedimentary basins beneath the Ross Ice

797   shelf and southern Ross Sea [*Zhou et al.*, 2022]. The structure of these is different to the magnetic studies,

798   likely reflecting the different spatial sensitivities of these techniques. Similarly, the mapping of *Li et al.* [2022]

799   indicates a high likelihood of major basins beneath the Ross Ice Shelf (Fig 2a). Despite these first

800   considerations being addressed, the absence of seismically constrained basin geometry and stratigraphy

801   limits the understanding of Cenozoic deposition and erosion patterns beneath the Ross Ice Shelf.

802   A further extension of the WARS into the Siple Coast region suggests a likely continuation of the basin-

803   forming processes; however, the Siple Coast has distinctly different characteristics to the Ross Embayment.

804   Although sedimentary cover is widely recognized in many geophysical surveys, sedimentary deposits are

805   apparently thinner (in general < 1 km) and not ubiquitous. Ambient noise tomography resolves a broad basin

806   region extending ~400 km inland from the coast [*Zhou et al.*, 2022]. Aeromagnetic data at the coast suggest

807   several ~75 km wide depocenters beneath Siple Dome aligned with the previously identified Trunk D Basin

808   [*Bell et al.*, 1998], the Crary Trough, and on the Amundsen Coast, respectively north and south of the Crary

809   Ice Rise [*Tankersley et al.*, 2022]. The southernmost of these has recently been defined using magnetotelluric

810   and passive seismic data [*Gustafson et al.*, 2022]. In the mapping of *Li et al.* [2022] the Siple Coast region

811   returns sedimentary bed likelihoods dominantly between 0.25 and 0.75 indicating the relatively ambiguous

812   nature of this region at large scales, however high likelihood basin regions are identified for the MacAyeal

813   Ice Stream, for the Siple Dome/Trunk D Basin, the Crary Trough and the Amundsen Coast. Inland, beyond the

814   limit of the broad basin-dominated region [*Zhou et al.*, 2022] a basement-dominated pattern is seen

815   however, four smaller basins are identified associated with the uppermost MacAyeal Ice Stream, Trunk D

816   [*Peters et al.*, 2006], the Onset Basin linking to the Crary Trough [*Bell et al.*, 1998; *Peters et al.*, 2006] and a

817   southern basin linking to the Amundsen Coast [*Studinger et al.*, 2001]. The rest of the region is here

818   classified as mixed type 1 basin/crystalline basement. The exact configuration of sedimentary cover is not

819   well resolved, but nonetheless there is likely to be sufficient sedimentary cover for basin-influenced

820   processes to occur widely.

821   The transition from the Ross Sea to the Siple Coast involves, in the west, several transitions in basin

822   architecture (Fig 7) – one located from the Polar-3 anomaly to Iselin Bank, which separates the Northern

823   Basin from the Victoria Land Basin and the Central Basin from the Central Trough [*Davey et al.*, 2021];

824   another located at the Discovery Accommodation Zone, separating the Victoria Land Basin and Central

825   Trough from the Western Ross Basin [*Wilson*, 1999], and a third located outboard of Shackleton Glacier

826   separating this broad basin from the narrower basins of the Amundsen Coast and Crary Trough [*Tankersley*

827   *et al.*, 2022]. The situation in the east is simpler, with the Eastern Basin separating at Roosevelt Island into

828   two narrower depocenters – one extending to Siple Dome, the other to MacAyeal Ice Stream [*Tankersley et*

829   *al.*, 2022; *Zhou et al.*, 2022]. In general, the tendency is for narrower and more defined depocenters

830   developing inland, indicating a probable combination of deeper exposure level inland due to repeated

831   glaciation events with reduced Cenozoic subsidence and sediment loading [*Paxman et al.*, 2019b; *Wilson et*

832   *al.*, 2012], and potentially stronger lithosphere under WAIS divide.

3.2.2 Interior West Antarctica

Interior West Antarctica includes a prominent low-lying region east of the WAIS divide including the Byrd Subglacial Basin and the Bentley Subglacial Trough (each extending > 2 km below sea level), the central West Antarctica region is bounded to three sides by high-standing regions, the Ellsworth Whitmore and Haag regions to the west, the Thurston Island region to the north and Marie-Byrd Land to the northeast. To the southwest, an indistinct transition leads to the Siple Coast.

The Ellsworth Whitmore Mountains preserve the oldest known sedimentary rocks in West Antarctica, with a ~ 13 km thick sequence of Cambrian to Permian sedimentary rocks [*Castillo et al.*, 2017; *Craddock et al.*, 2017]. The lowermost unit, the Heritage Group, comprises lower- to middle-Cambrian sedimentary rocks including a lower sequence of terrestrial volcaniclastic, shallow marine clastic sediments and limestones, an overlying sequence of transitional terrestrial to marine sedimentary rocks and overlying these Late-Middle to Late Cambrian carbonate-dominated rocks [*Curtis and Lomas*, 1999]. Thin transitional beds divide the Heritage Group from the Upper Cambrian to Devonian Crashsite Group, deposited in a fluvial to shallow-marine environment [*Curtis and Lomas*, 1999]. The glacial-derived Whiteout Conglomerate is interpreted to represent the early Permian Gondwanide glaciation at ca. 300 Ma [*Isbell et al.*, 2008] and is overlain by the Polarstar Formation including argillite, sandstone and coal measures, interpreted to represent post-glacial deposition in the Gondwana Basin [*Elliot et al.*, 2017]. Overall, this basin has been interpreted to represent a transition from a rift setting in the early Cambrian to a passive margin setting extending into the Permian [*Castillo et al.*, 2017; *Craddock et al.*, 2017]. Isolated exposures elsewhere in the Ellsworth-Whitmore Block [*Cox et al.*, 2019] also possess sedimentary rocks and we infer the unexposed region to be of mixed type class, preserving the Paleozoic basin intruded by younger granite suites.

Seismic observations suggest that the central West Antarctica region is not occupied by a major broad sedimentary basin [*Zhou et al.*, 2022], but sedimentary rocks likely exist in association with low lying regions [*Li et al.*, 2022]. The low-elevation areas possess markedly smooth beds, and in many cases low isostatic residual gravity anomalies indicating relatively young sedimentary rocks are present [*Jordan et al.*, 2010b]. Three basins are interpreted in this region, each with different glacial catchments: The Pine Island Rift Basin underlies the upper Pine Island Glacier catchment [*Jordan et al.*, 2010b]; The Byrd Subglacial basin underlies the upper portion of the Thwaites Glacier catchment [*Studinger et al.*, 2001]; and the Bentley Subglacial Trough flanks the Ellsworth Whitmore block, connecting to the Ferrigno Rift Basin [*Bingham et al.*, 2012]. The thickness of sedimentary rocks in these is variable but locally may be up to 2 km thick. The geometry of these basins indicates several phases of extension, with ~E-W oriented basins overprinted by later extension generating ~NE-SW aligned basins (Fig 8). The former set may relate to structures in the southern Weddell Sea while the latter are aligned with WARS rift axis and the Siple Coast basins.
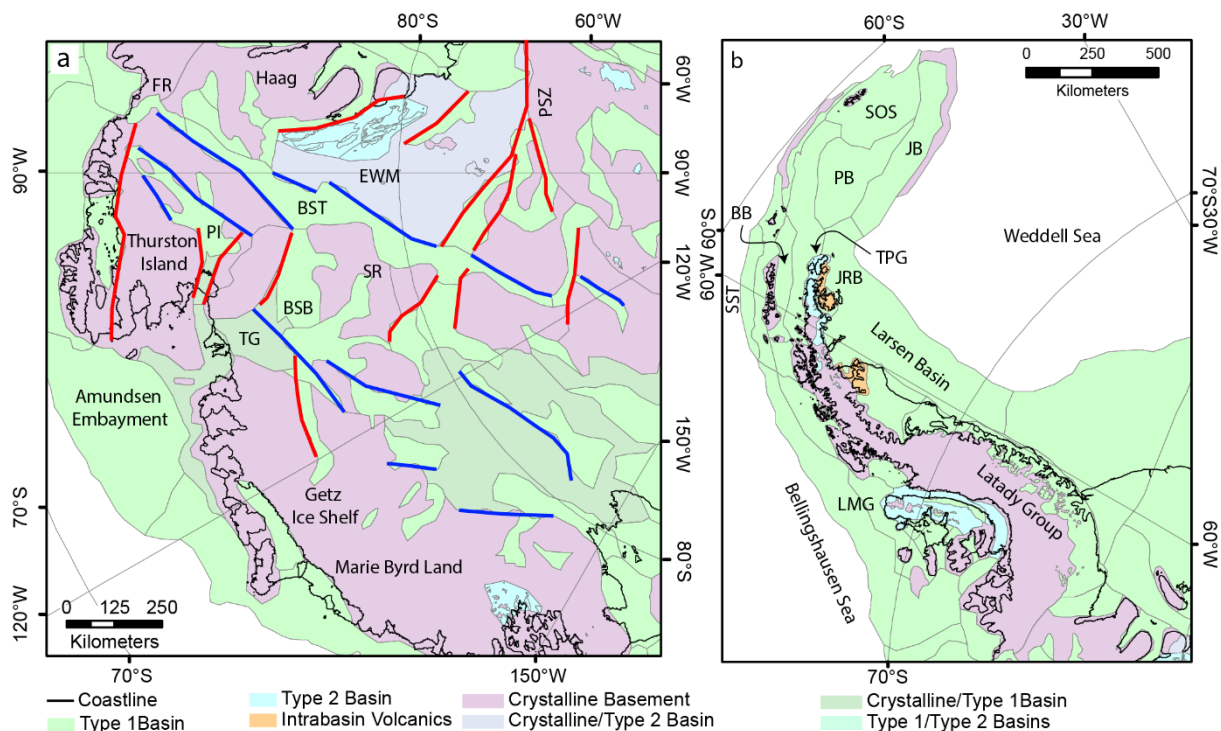
Figure 8: Sedimentary basins of the a) Central West Antarctica and b) Antarctic Peninsula Drake and eastern Weddell Sea regions. Structures in a) are reinterpreted from prior studies [Bell et al., 1998; Bingham et al., 2012; Haeger and Kaban, 2019; Jordan et al., 2010b; Jordan et al., 2013b; Jordan et al., 2020; Studinger et al., 2001] as associated with the WARS (blue) and WSRS (red). PI – Pine Island Rift Basin, FR – Ferrigno Rift, BSB – Byrd Subglacial Basin, BST – Bentley Subglacial Trough, EWM - Ellsworth Whitmore Mountains, SR – Sinuous Ridge, PSZ – Pagano Shear Zone, SST – South Shetland Trench, BB – Bransfield Basin, PB – Powell Basin, JB – Jane Basin, SOS – South Orkney Shelf, TPG – Trinity Peninsula Group, LMG – LeMay Group, JRB – James Ross Basin.

The nature of the bed in the glacial troughs connecting these inland basins to the coast is not clearly defined. Evidence from seismic and RES data suggests in each case a complex bed evolving with, in places thick and partially lithified sedimentary deposits, and in other places basement rocks or volcanoes [*Alley et al.*, 2021; *Bingham et al.*, 2012; *Brisbourne et al.*, 2017; *Muto et al.*, 2016; *Muto et al.*, 2019a; *Muto et al.*, 2019b; *Smith et al.*, 2013]. These are classed as mixed-crust, similar to the Siple Coast region, implying a bed condition that is not well resolved within the trough, and also is potentially quite time-variable but likely contains enough sedimentary material to support enhanced till production and hydrogeology [*Alley et al.*, 2021].

3.2.3 Pacific Margin

The Pacific margin of West Antarctica includes the basin regions of the Amundsen and Bellingshausen Seas, and the extension of this margin along the western Antarctic Peninsula (Fig 8). Each of these is characterized by a thick sequence of sedimentary rocks on the continental shelf, with up to 7 km in the Amundsen Sea and 5 km in the Bellingshausen Sea [*Hochmuth et al.*, 2020; *Lindeque et al.*, 2016b]. Based on a partial continuity

887   of Cenozoic seismic stratigraphy extending from the eastern Ross Sea, the Pacific margin preserves, from

888   west to east, a progressively younger base-of-basin, from 80-67 Ma in the Ross Sea to 36 Ma on the

889   Antarctic Peninsula margin, and correspondingly a younger onset of transitional glacial conditions, from 34-

890   30 Ma in the Ross Sea to 21 Ma in the eastern Amundsen Sea, and 25 Ma on the Antarctic Peninsula margin

891   [*Lindeque et al.*, 2016b]. In the transition to glacial Antarctica, and in subsequent glacial conditions these

892   basins record selective deposition focused especially in the Amundsen Sea Embayment and the eastern

893   Bellingshausen Sea [*Hochmuth et al.*, 2020; *Lindeque et al.*, 2016b]. This margin has substantial shelf-edge

894   progradation, since the middle to late Miocene in the Amundsen Sea and since the late Miocene/early

895   Pliocene for the Bellingshausen Sea, and the early Pliocene for the Antarctic Peninsula margin [*Hochmuth et*

896   *al.*, 2020].

897   The Amundsen Sea Embayment receives sediments from the Pine Island and Thwaites Glaciers and

898   possesses the thickest accumulation of sedimentary rocks on the Pacific margin. The inner shelf however is

899   dominated by exposed basement, extending 200 to 250 km from the coast [*Gohl et al.*, 2013a]. Within this

900   region some minor basin regions are interpreted where both the bed and the magnetic data are relatively

901   smooth. The middle and outer shelf are thickly sedimented, comprising basal strata from early Cretaceous

902   rifting, a thick passive-margin sequence of Late Cretaceous to Oligocene sediments, and Early/Middle

903   Miocene to Pleistocene characterized by episodic glacial advances and progradation of the shelf edge,

904   especially during the Pliocene [*Gohl et al.*, 2013a; *Gohl et al.*, 2013b; *Gohl et al.*, 2021].

905   ### 3.2.4   South Shetland and South Orkney Shelf

906   At the northern Antarctic Peninsula, the Pacific margin of Antarctica changes from a passive margin to a

907   convergent margin with the former Phoenix Plate (Antarctic Plate) descending under the South Shetland

908   Islands. The main features of this margin are the South Shetland trench and the active spreading centre in

909   Bransfield Strait behind, both associated with ongoing basin forming processes. At the South Shetland

910   Trench, the margin preserves a thick accretionary complex and fore-arc system imposed on the older

911   continental shelf [*Maldonado et al.*, 1994]. These sediments were predominantly accumulated during

912   subduction of the former Phoenix Plate, which ceased between 3.6-2.6 Ma, but also preserve evidence of

913   younger deformation suggesting ongoing thrust faulting [*Maldonado et al.*, 1994]. Since ~ 4 Ma, the

914   Bransfield Basin is actively subsiding through rifting with segmented depocenters up to 2 km thick, and with

915   active volcanism and seismicity [*Almendros et al.*, 2020].

916   On the opposite side of the Antarctic Peninsula shelf, the Powell Basin records rifting of the South Orkney

917   microcontinent from the Antarctic Peninsula, with rifting commencing in the late Eocene or early Oligocene,

918   progressing to seafloor spreading from ~30 to ~20 Ma [*Eagles and Livermore*, 2002]. The adjacent Jane Basin

919   opened in a back-arc setting from ~18 to ~14 Ma [*Bohoyo et al.*, 2002]. Across these basins, sediments are

920   deposited in several sequences including syn-to post rift packages initially in individual depocenters,

921 transitioning to a broader shared sequence since the mid-Miocene [*Lindeque et al.*, 2013; *Maldonado et al.*,
922 2006].

3.2.5   Antarctic Peninsula and Weddell Sea

924 The Antarctic Peninsula and the Weddell Sea record the evolution of the Weddell Sea Rift with a partly
925 shared basin evolution in the Mesozoic to Cenozoic. The oldest sedimentary rocks on the Antarctic Peninsula
926 are preserved in the Trinity Peninsula Group, outcropping on the northern Antarctic Peninsula. These rocks
927 comprise an upper Carboniferous to Triassic sequence that formed on the margin of Gondwana in
928 association with erosion of continental magmatic arc material [*Castillo et al.*, 2015]. The Triassic LeMay
929 Group outcropping on Alexander Island was deposited in a fore-arc accretionary complex coincident with
930 ongoing Triassic arc magmatism in southern Antarctic Peninsula [*Willan*, 2003]. The Late Jurassic to Early
931 Cretaceous Fossil Bluff Group represents a thick sequence of fore-arc deposits derived from adjacent
932 magmatic arc [*Riley et al.*, 2012]. Considering their current setting, all these basins are considered as type 2
933 basins in our classification.

934 The Jurassic-Cretaceous Latady Group outcrops on the south-eastern Antarctic Peninsula, representing the
935 formation of a progressively deepening basin from 185 to 140 Ma, with several kilometers of sediment
936 deposited [*Hunter and Cantrill*, 2006]. Early Jurassic to early-Middle Jurassic terrestrial to shallow marine
937 formations occupy smaller depocenters in grabens or half-grabens, with a transition to a deep marine
938 environment from the late-Middle Jurassic onwards associated with Weddell Sea rifting [*Hunter and Cantrill*,
939 2006]. More sparse outcrops of similarly aged rocks are found to the north in the Larsen basin. Although a
940 distinct depocenter, the Larsen Basin preserves a similar evolution from a terrestrial to shallow marine syn-
941 rift setting in the Early to Middle Jurassic, transitioning to a deep marine setting from the Late Jurassic
942 [*Hathway*, 2000]. The northern Antarctic Peninsula preserves key upper Mesozoic to lower Cenozoic
943 sequences exposed in the James Ross Basin. These sequences preserve a critical record of the high latitude
944 paleoenvironment at the Cretaceous-Tertiary boundary and also support a better knowledge of
945 paleogeography of Antarctica [*Bowman et al.*, 2016; *Francis et al.*, 2006].

946 The formation of the Weddell Sea Rift System is interpreted to commence in line with the above transition
947 from a magmatic-arc setting to back-arc extension at 180-177 Ma [*Riley et al.*, 2020] with the onset of
948 seafloor spreading by 147 Ma [*König and Jokat*, 2006]. The Weddell Sea contains the thickest known
949 sedimentary basin in Antarctica (Fig 6), with up to 15 km of sedimentary rocks [*Leitchenkov and Kudryavtzev*,
950 1997; *Straume et al.*, 2019]. *Jordan et al.* [2017a] define distinct northern and southern provinces from
951 magnetic fabrics, indicating two distinct phases of rifting: In the south, east-west extension is interpreted
952 due to the motion, and possibly rotation, of the Ellsworth-Whitmore and Haag blocks from a position
953 adjacent to the East Antarctic margin, north of the Pensacola Mountains. Movement of the Haag Ellsworth–
954 Whitmore microcontinent likely ceased by ~175 Ma, based on the ages of granites emplaced along the

marginal Pagano Shear Zone [*Jordan et al.*, 2013b]. Modelling of Bouguer gravity anomalies suggest highly thinned continental crust with a bowl-shaped basin geometry beneath the Ronne-Filchner Ice Shelf [*Jordan et al.*, 2017a; *Leitchenkov and Kudryavtzev*, 1997]. Distinct positive Bouguer gravity anomalies around the margins of the Ronne-Filchner ice shelf (Fig 2e), including the Weddell Rift Anomaly, Filchner Rift and Evans-Rutford Rift Basin represent areas with thinned crust and low topography, but less thick sedimentary fill than seen in the central basin.
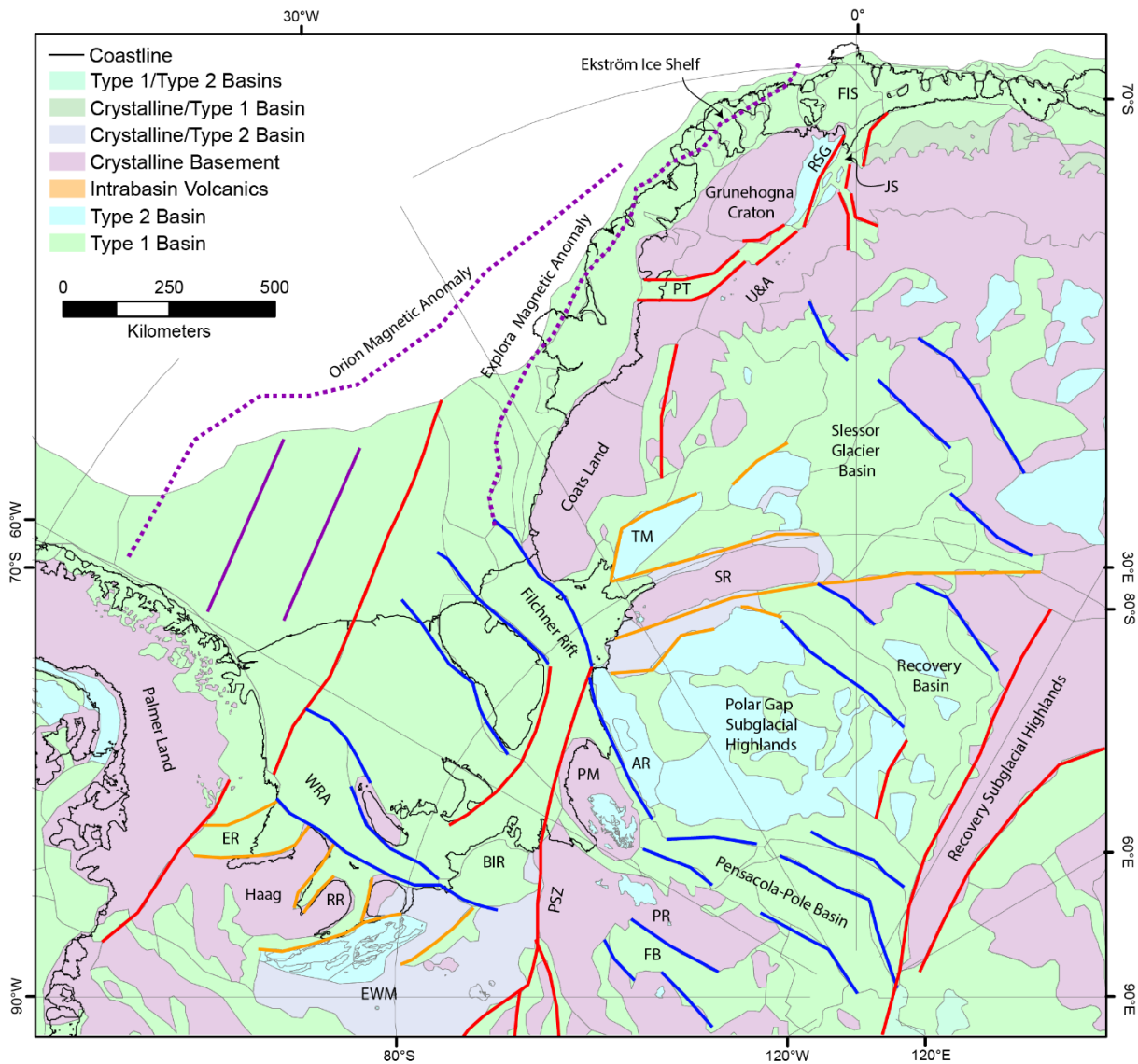
Figure 9: Sedimentary basins of the Weddell and Weddell Coast regions. Structures are reinterpreted from prior studies including [Bamber et al., 2006; Ferraccioli et al., 2005b; Jones et al., 2002; Jordan et al., 2013b; Jordan et al., 2017a; Paxman et al., 2017; Paxman et al., 2019a; Riedel et al., 2012]. Blue lines indicate structures parallel with the SWRS, Red lines structures aligned transverse to the SWRS, parallel to the Pagano Shear Zone. Orange lines indicate structures of other orientations. Purple lines indicate magnetic trends of the NWRS including the Orion and Explora Anomalies. ER - Evans Rift, RR - Rutford Rift, EWM – Ellsworth

968   *Whitmore Mountains, WRA – Weddell Rift Anomaly, BIR – Bungenstock Ice Rise, FB – Foundation Basin, PR*

969   *Patuxent Range, PM – Pensacola Mountains, AR – Argentina Range, SR -Shackleton Range, TM – Theron*

970   *Mountains, U&A – Urfjell and Amelang Groups, PT - Pencksokket Trough, RSG – Ritscherflya Supergroup, JS –*

971   *Jutulstraumen, FIS – Fimbul Ice Shelf*

972   After development of the Southern Weddell Sea Rift System, continental rifting between Southern Africa

973   and Antarctica became the dominant tectonic process [*König and Jokat*, 2006] forming the Northern

974   Weddell Sea Rift System. The northern province possesses a NE-SW magnetic fabric, and potentially oceanic

975   to transitional crust [*Jordan et al.*, 2020]. This phase of extension appears to crosscut the older back-arc

976   system [*Jordan et al.*, 2017a] and is associated with magmatism giving rise to the Orion and Explora magnetic

977   anomalies (Fig. 9). These magnetic anomalies approximately coincide with the continent-ocean transition,

978   and they may reflect seaward dipping reflector sequences [*Kristoffersen et al.*, 2014], potentially emplaced

979   ca 150-138 Ma [*König and Jokat*, 2006]. The onset-age of northern Weddell Sea rifting is not uniquely

980   defined: In one model, onset of extension is suggested by 167 Ma with ocean-crust forming by 147 Ma

981   [*König and Jokat*, 2006], however an alternative model suggests the Northern Weddell Sea Rift reflects

982   separation of a single Skytrain plate from Southern Africa and the Falkland Plateau between 180 and 156

983   Ma, followed by 90 degree rotation of the entire Skytrain plate into its current position by ~126 Ma [*Eagles*

984   *and Eisermann*, 2020].

985   Regardless of the tectonic model, interpreted sedimentary rock thicknesses and gravity anomalies are

986   continuous throughout the central part of the Weddell Embayment. This suggests that most of the

987   sedimentary fill has been deposited after tectonic motions ceased due to thermal subsidence associated

988   with ongoing slow spreading at the margin. The oldest sedimentary horizons were deposited over the

989   seaward dipping reflectors and the oceanic crust from ~160 to 145 Ma, with ongoing deposition continuing

990   until at least ~114 Ma in the southeastern Weddell Sea [*Rogenhagen et al.*, 2004], and progressively younger

991   toward the northwest, in line with the generation of oceanic crust and its subsidence [*Lindeque et al.*, 2013].

992   The youngest sediments of the pre-glacial regime may be as young as mid-Miocene, with deposition

993   controlled by the proto-Weddell gyre [*Lindeque et al.*, 2013].

994   Glacial influences on the northern Weddell Sea are substantial, with major sedimentary packages deposited

995   associated with the transition to glacial conditions, in the Oligocene (in the southeast) to early Miocene (in

996   the northwest), and to full glacial conditions in the mid-Miocene [*Lindeque et al.*, 2013], with substantial

997   shelf progradation since the late Miocene [*Hochmuth and Gohl*, 2019]. The youngest cover relates to

998   Quaternary sediments recovered in marine sediment cores which preserve normally consolidated, over-

999   compacted sediments and glacial till [*Hillenbrand et al.*, 2014] as well as glacio-marine landforms in seabed

1000 topography [*Arndt et al.*, 2017]. The distribution of these young units is not comprehensively mapped, and

1001 their thickness and age are likely to be highly variable. Nevertheless, we infer that the Weddell Sea has

1002 received sediment continuously since the Early Jurassic. To the south of the Weddell Ice Shelf, accumulations

1003 of water-saturated sediments are identified beneath the Bungenstock Ice Rise and extending into the

1004 Institute Ice Stream [*Siegert et al.*, 2016]. These sedimentary deposits overly a relatively shallow basement

1005 but are associated with elevated ice velocity suggesting control on ice sheet dynamics [*Siegert et al.*, 2016].

3.3 East Antarctic Basins

3.3.1 Weddell Coast

1008 The continental shelf in the eastern Weddell Sea preserves a sedimentary basin extending along the shelf

1009 from the Filchner Rift to the Fimbul Ice Shelf. The basin is associated with a volcanic rifted margin that

1010 initiated in the Jurassic [*Jokat and Herter*, 2016; *Kristoffersen et al.*, 2014], but also has upper Cenozoic to

1011 Quaternary sediment deposition [*Hillenbrand et al.*, 2014; *Huang and Jokat*, 2016; *Kristoffersen et al.*, 2014]

1012 recording repeated glacial advances. Magnetic data indicate the geology of the underlying basement with

1013 high frequency content indicating relatively thin basin cover throughout this basin. Magnetic data also image

1014 the Explora anomaly (Fig 9), associated with Jurassic magmatism [*Hunter et al.*, 1996] and a seaward-dipping

1015 reflector (SDR) sequence, the Explora Wedge [*Kristoffersen et al.*, 2014]. Seismic exploration on the Ekström

1016 Ice Shelf has demonstrated the Explora Wedge to extend beneath the ice shelf, with overlying sedimentary

1017 rocks of up to 1 km thickness [*Kristoffersen et al.*, 2014]. The boundary is marked by a prominent magnetic

1018 gradient that extends along the entire basin, which we infer to delineate the extent of the SDR sequence.

1019 Landward from this magnetic boundary, the basin is characterized by smooth topography with several ice

1020 rises interpreted as representing grounded ice on remnants of shelf sediments while adjacent troughs were

1021 eroded [*Kristoffersen et al.*, 2014].

1022 Inland, as well as extensive crystalline bed, several phases of basin formation are recorded. The oldest phase

1023 is preserved in outcrops on the Pensacola Mountains. The early Cambrian Hannah Ridge Formation was

1024 deposited after 563 Ma and prior to granite intrusion dated at 505 Ma [*Curtis et al.*, 2004]. The Hannah

1025 Ridge Formation is overlain by the Nelson Limestone and the Gambacorta Formation volcanics, dated at 501

1026 Ma. Overlying, the Late Cambrian Wiens Formation and Late Cambrian to Ordovician Neptune Group, were

1027 deposited during and after the Ross Orogeny [*Curtis et al.*, 2004]. Similar rocks may also be preserved in the

1028 Argentina and Shackleton Ranges [*Evans et al.*, 2018]. The second major phase comprises the Devonian to

1029 Permian Beacon Supergroup, including the Upper Devonian Dover Sandstone, the Carboniferous-Permian

1030 Gale Mudstone and the Permian Pecora Formation [*Curtis*, 2002]. As elsewhere, the Beacon Supergroup is

1031 preserved with characteristic mesa-like landforms in the Polar Gap Subglacial Highlands between Support

1032 Force and Recovery glaciers (Fig 9). Outliers of the Beacon Supergroup also occur on the Theron Mountains

1033 north of Slessor Glacier [*Cox et al.*, 2019]. There is no evidence for Beacon Supergroup to the north of the

1034 Theron Mountains, although the Paleozoic rocks of the Urfjell Group and Amelang Formation outcrop in

1035 western Dronning Maud Land [*Cox et al.*, 2019]

1036   Several type 1 basins are inferred, with a dominant westerly trend, and characterized by low topography,

1037   negative isostatic residual gravity and smooth beds. Major basins exist to the north and east and to the

1038   south of the Polar Gap Subglacial Highlands and are bounded to the east by the Recovery Subglacial

1039   Highlands (Fig 9). The southern basin, the Pensacola-Pole Basin, occupies an elongate trough 150-200 km

1040   wide. Sedimentary rocks in this basin thicken inland reaching a thickness of 3.6±1.1 km [*Paxman et al.*,

1041   2019a]. The basin fill is interpreted to be dominated by the Beacon Supergroup, indicated by the presence of

1042   magnetic features interpreted to represent Jurassic dolerites, but also there is interpreted younger cover of

1043   up to 1 km thickness [*Paxman et al.*, 2019a]. We define the Foundation Basin as a smaller aligned

1044   depocenter with similar characteristics. The northern Recovery Basin occurs inland from the Recovery

1045   Glacier. No thickness for this basin is defined, however, its geophysical character is similar to the Pensacola-

1046   Pole basin. We suggest that the Foundation, Pensacola-Pole and Recovery subglacial sedimentary basins

1047   formed during Jurassic-Cretaceous rifting. This event generated the distinctive topography that was later

1048   incised by glaciers, removing several kilometers of sediments from glacier troughs [*Paxman et al.*, 2017].

1049   These troughs today do not host major basin fill. another major basin is interpreted associated with the

1050   northern Slessor Glacier (Fig 9). This basin has a particularly smooth bed throughout [*Bamber et al.*, 2006;

1051   *Eisen et al.*, 2020] and models of magnetic data suggest 3 km of post-Jurassic fill [*Bamber et al.*, 2006].

1052   3.3.2   Dronning Maud Land and Enderby Land

1053   Dronning Maud Land preserves evidence for a series of basin forming events. The most prominent is the

1054   Jurassic rifting associated with the Jutul-Penck Graben system, associated with localized crustal thinning

1055   associated with the Jutulstraumen and Pencksokket troughs, with high isostatic residual gravity, and smooth

1056   magnetic field patterns [*Ferraccioli et al.*, 2005a; *Ferraccioli et al.*, 2005b; *Riedel et al.*, 2013]. Interpreted

1057   type 1 basins in interior Dronning Maud Land region are parallel and may also represent this event.

1058   Sedimentary rocks of the ca. 1.1 Ga Ritscherflya Supergroup are exposed adjacent to the Jutulstraumen,

1059   representing a ~2 km thick basin forming on the eastern edge of the Grunehogna Craton, in an interpreted

1060   arc-proximal setting [*Marschall et al.*, 2013]. A series of north-south oriented ancient basins is interpreted in

1061   Interior Dronning Maud Land based on negative isostatic residual gravity and reduced subglacial roughness

1062   relative to their surroundings (Fig 3). One of these was modelled in the work of *Eagles et al.* [2018] who

1063   identified a sedimentary bed incised by a preserved fluvial landscape. The age of these basins is highly

1064   uncertain, however they overlie magnetic trends of the Tonian Ocean Arc Super Terrane [*Ruppel et al.*,

1065   2018], and are aligned with interpreted late Pan-African structures in the Sør Rondane region [*Mieth and*

1066   *Jokat*, 2014].

1067   The Dronning Maud Land escarpment separates the type 2 basins of the interior from interpreted type 1

1068   basins along the front of the escarpment, on the coastal plain and continental shelf. These basins are

1069   characterized by low, flat and smooth bed topography, sloping gently southward overall [*Eisen et al.*, 2020]

1070 and, onshore, negative isostatic residual gravity. Numerous ice-rises are present associated with

1071 sedimentary banks, interpreted as remnant shelf sediments following erosion of adjacent troughs. These

1072 basins are interpreted to reflect depocenters formed initially during the late Jurassic to Cretaceous

1073 denudation of the Great Escarpment, and received sediment as part of the sedimentary pathway to the

1074 major depocenters of the Riiser-Larsen Sea [*Eagles et al.*, 2018]. Further regions along the front of the

1075 escarpment, and in localized topographic lows, also have relatively high basin likelihood [*Li et al.*, 2022], and

1076 may represent piedmont deposits.
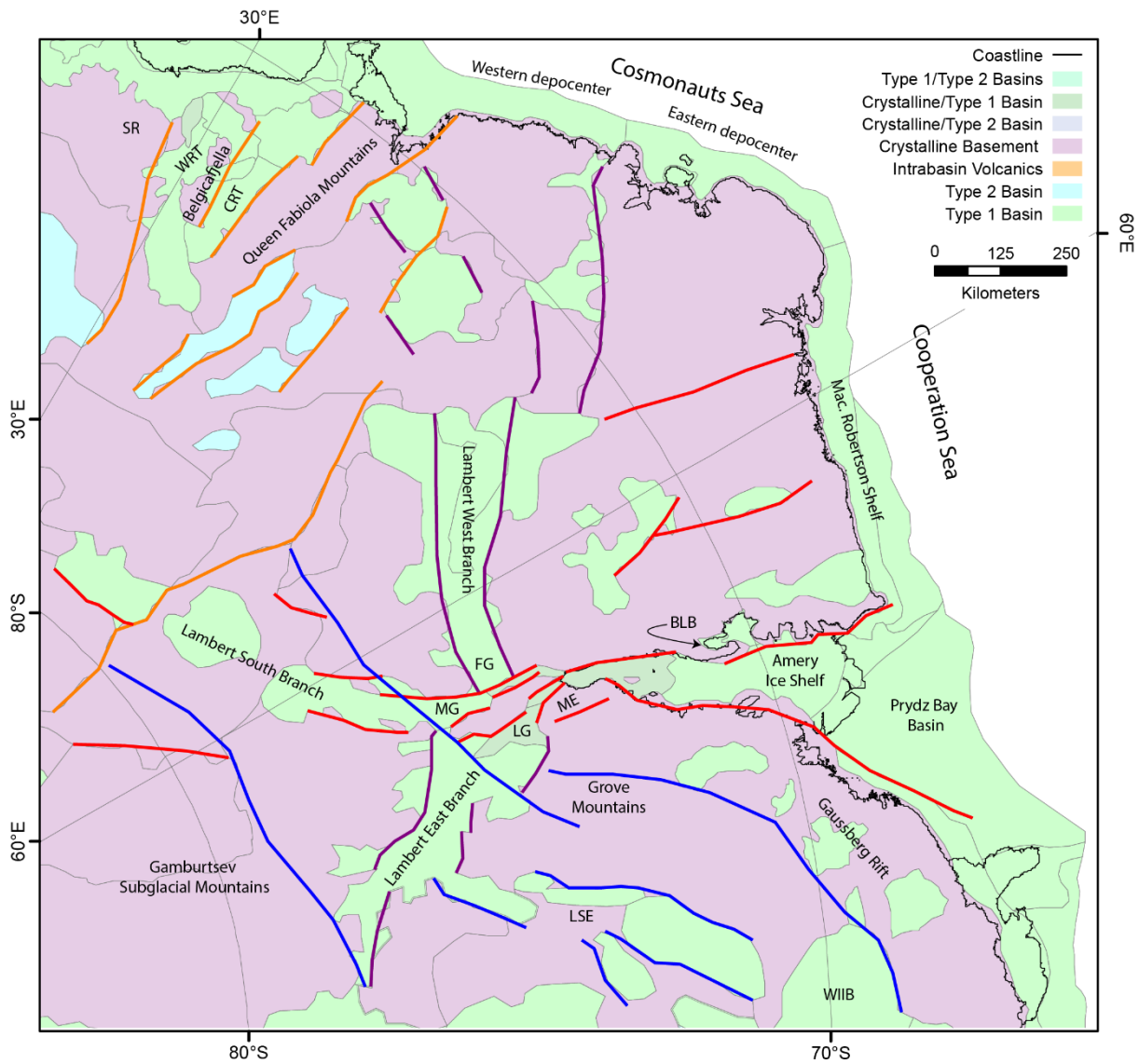
1077

1078 *Figure 10: Sedimentary basins of the Enderby-Mac. Robertson and Lambert regions. Red structures indicate*

1079 *structures aligned with the main north-south Lambert Rift trend while purple structures are aligned with the*

1080 *east-west trend. Blue structures are aligned with Precambrian structures including the Gamburtsev Suture*

1081 *[Ferraccioli et al., 2011], the Ruker anomaly and Proterozoic basins in the southern Prince Charles Mountains*

1082 *[McLean et al., 2008]. Orange lines indicate structures associated with the Fuji Subglacial Highlands block. SR*

1083 *– Sør Rondane, WRT – West Ragnhild Trough, CRT – Central Ragnhild Trough BLB – Beaver Lake Basin, FG –*

Fisher Glacier, MG – Mellor Glacier, LG – Lambert Glacier, ME – Mawson Escarpment, LSE – Lake Snow Eagle,

WIIB – Wilhelm II Basin.

1086 The Ragnhild Trough (Fig 10) is a major topographic feature cutting through the escarpment and in its

1087 coastal portion is interpreted to possess a fill of low-density sedimentary material [*Eagles et al.*, 2018], which

1088 is also topographically smooth [*Eisen et al.*, 2020], included here in the escarpment basin. The trough forms

1089 two ~100 km wide sub-troughs either side of Belgica Highlands (Belgicafjella), called West and Central

1090 Ragnhild Troughs, with low gravity, low to moderate topographic roughness and low magnetic roughness. To

1091 the east is the crystalline bed of the Queen Fabiola Mountains block. These linear troughs are interpreted as

1092 rifts forming during Paleozoic to Mesozoic rifting. Similar troughs are interpreted in Enderby Land,

1093 connecting to the west branch of the Lambert Rift System (Fig 10).

1094 The continental shelf fringing the Cosmonauts Sea is narrow, at ca 70 km width [*Davis et al.*, 2018]. Two

1095 separate depocenters are defined with the western depocenter having less rugged topography and lesser

1096 offshore sediment volume relative to the eastern depocenter [*Davis et al.*, 2018]. Seismic data over the shelf

1097 edge image a relatively thin package (0.5 to 2 km) of pre-to syn-rift sediments, with a more voluminous post-

1098 rift sequence [*Stagg et al.*, 2004]. While sedimentation on the shelf may be relatively limited, a substantial

1099 sediment volume was transported to the continental rise since the late Miocene [*Hochmuth et al.*, 2020].

3.3.3   Lambert Graben and Prydz Bay

1101 Mac. Robertson Land is dominated by crystalline basement, with basins associated with the Lambert Rift

1102 System. The Lambert Rift System has a cruciform geometry, with the north-south aligned main branch

1103 extending inland for over 1500 km, complemented by eastern and western branches (Fig 10). Subsidence is

1104 greatest in the northern portion of the main branch, with more limited subsidence to the south, suggesting

1105 that the East and West branches may have accommodated differential strain. Smaller aligned basins are

1106 found on Mac. Robertson land, including the exposed Beaver Lake Basin. The Beaver Lake Basin preserves

1107 the mid-Permian to upper-Triassic Amery Group, comprising clastic sedimentary rocks, with coals in the

1108 lower sequence [*McLoughlin and Drinnan*, 1997]. These rocks represent a terrestrial depositional setting

1109 with overall north-directed sediment transport. Seismic studies on the Amery Ice Shelf resolve multiple

1110 layers of sedimentary rocks, with a thin layer of young sediments overlying an older package of interpreted

1111 glaciomarine origin [*McMahon and Lackie*, 2006]. In turn this overlies a > 5 km thick sequence of rift-related

1112 sedimentary rocks [*Mishra et al.*, 1999]. Cenozoic glaciomarine fjordal sedimentary rocks are mapped from

1113 within the Lambert Graben, indicating a series of glacial retreat events since the Oligocene or younger, and

1114 also significant Cenozoic uplift, with exposures preserved at up to 1500 m elevation [*Hambrey and McKelvey*,

1115 2000].

1116   Inland, the southern branch of the Lambert Rift System occupies the trough to the Mellor Glacier, while the

1117   eastern branch occupies the trough to the Lambert Glacier, and the western branch occupies the catchment

1118   of the Fisher Glacier [*Ferraccioli et al.*, 2011]. Each has characteristics of low isostatic residual gravity

1119   anomalies and smooth topography. The southern branch has several further depocenters indicated

1120   upstream (Fig 10).

1121   Offshore, the Prydz Bay Basin is well-surveyed with relatively dense seismic coverage and multiple drill cores

1122   (Fig 1). The inner shelf is dominated by thick accumulations of Permian to Early Cretaceous sediments, with a

1123   thin veneer of Cenozoic cover [*Stagg et al.*, 2004]. On the outer shelf a sequence is recorded prograding

1124   toward the northeast through the Cenozoic, marked by a number of erosion surfaces and marine deposition

1125   events [*Whitehead et al.*, 2006]. Quaternary deposition is inferred to be present throughout the region

1126   [*Whitehead et al.*, 2006]. The Mac. Robertson Shelf preserves a relatively thin cover of syn- to post-rift

1127   sedimentary rocks [*Stagg et al.*, 2004], with a comparable Cenozoic sequence to the Prydz Bay Basin

1128   [*Whitehead et al.*, 2006].

3.3.4   Princess Elizabeth Land and Queen Mary Land

1130   The Princess Elizabeth Land shelf preserves a thin cover of upper Paleozoic to Cenozoic sedimentary rocks

1131   [*Davis et al.*, 2018], with interpreted Precambrian basement at Drygalski Island, and, at Gaussberg, a volcano

1132   dated at 56±5ka [*Smellie and Collerson*, 2021]. Inland, the Princess Elizabeth Land region is dominated by

1133   crystalline basement, however, several regions are identified with subdued magnetic responses and

1134   relatively smooth topography that may represent remnant sedimentary basins. These are arrayed along the

1135   tectonic structure of the Gaussberg Rift, which may share an evolution with the Lambert Rift system

1136   [*Golynsky and Golynsky*, 2007]. A large basin (the Wilhelm II Basin) is identified with similar characteristics to

1137   the better-known Knox Basin further east (Fig 11). The interior of Princess Elizabeth Land until recently had

1138   one of the largest data gaps in Antarctica [*Cui et al.*, 2020]. Early work identified a significant lake (Lake Snow

1139   Eagle) and associated canyon system [*Jamieson et al.*, 2016] likely aligned with tectonic structures (Fig 10).

1140   More recent subglacial topography [*Cui et al.*, 2020] identified a topographic depression that is aligned en-

1141   echelon with the Wilhelm II Basin and Lake Snow Eagle (Fig 10). We infer a sedimentary basin in this

1142   depression although other geophysical results are not yet available for corroboration.

1143   Queen Mary Land has the well-resolved and substantial Knox Rift system including several sedimentary

1144   depocenters aligned perpendicular to the coast [*Maritati et al.*, 2016]. The basin system may extend over

1145   1000 km inland (Fig 11). This basin possesses up to 3 km of sedimentary rock fill that is interpreted to date

1146   primarily to the Permian-Triassic [*Maritati et al.*, 2016; *Maritati et al.*, 2020]. The region also preserves the

1147   Neoproterozoic to Ediacaran Sandow Group, exposed at the fringes of the Knox Basin [*Mikhalsky et al.*,

1148   2020]. The coastal region is dominated by Precambrian crystalline basement, including beneath the

1149   Shackleton Ice Shelf, with moderate to thin sedimentary cover interpreted for the Bruce Rise and the Knox

1150 Coast shelf. The Knox coastal plain preserves a low-relief surface [*Eisen et al.*, 2020] potentially indicative of

1151 a thin and relatively young sedimentary cover.

3.3.5   Vostok and Gamburtsev Highlands

1153 The East Antarctic interior is defined by the subglacial highlands of the Vostok and Gamburstev regions (Fig

1154 11). Subglacial Lake Vostok has been investigated with seismic techniques that return equivocal results

1155 [*Siegert et al.*, 2011]. Receiver function studies record a low-velocity zone beneath the lake bed, interpreted

1156 to represent a 4-5 km thickness of sedimentary rocks above a crystalline bed [*Isanina et al.*, 2009]. However,

1157 later seismic refraction experiments suggest instead that the lake bed is characterized by a relatively thin

1158 cover of sediments over an acoustically fast basement, likely to be crystalline basement [*Leitchenkov et al.*,

1159 2016]. The same study resolved a lower velocity bedrock for the highlands to the west of Lake Vostok. The

1160 western shore of Lake Vostok, and the lake itself possesses areas with predicted moderate to high

1161 sedimentary basin likelihood [*Li et al.*, 2022], indicated by low isostatic residual gravity anomalies and

1162 smooth magnetic field anomalies [*Studinger et al.*, 2003]. These characteristics notably do not extend to the

1163 eastern shore. While a thick type 1 sedimentary basin in Lake Vostok may not be supported, a type 2 basin is

1164 interpreted extending along the Vostok Subglacial Highland to the west of and beneath Lake Vostok (Fig 11).

1165 This may represent a flexural basin formed in response to collisional processes in the Neoproterozoic

1166 [*Studinger et al.*, 2003].

1167 The Vostok Highlands are separated from the Gamburtsev Subglacial Mountains by a prominent a low-lying

1168 region with relatively smooth bed, also including Lake Sovetskaya and Lake 90°E (Fig 11), forming the eastern

1169 branch of the EARS [*Ferraccioli et al.*, 2011]. This region is interpreted as a type 1 sedimentary basin

1170 although it is not associated with a gravity low, suggesting sedimentary fill is limited in thickness. The main

1171 range of the Gamburtsev Subglacial Mountains (GSM) is dominated by high elevation topography, high

1172 along-track roughness, and high spatial variability in elevation and magnetic data (Fig 2), all indicative of

1173 crystalline basement. To the west, a broad area with low and smooth topography, and low gravity separates

1174 the GSM from the Recovery Subglacial Highlands, suggesting a basin with substantial sedimentary fill,

1175 forming the western branch of the EARS [*Ferraccioli et al.*, 2011]. The southern flank of the GSM is also

1176 marked by a substantial gravity low, and relatively low roughness, indicating a possible sedimentary basin

1177 (Fig 3). The origin of this basin is not known, but it is aligned parallel to the South Pole Basin, and it may be

1178 an uplifted remnant that basin or part of an older basin system [cf *McLean et al.*, 2008].

3.3.6   Wilkes Land and Terre Adelie

1180 Wilkes Land preserves an extensive sedimentary basin system including several major depocenters including

1181 the Aurora, Vincennes and Sabrina basins [*Aitken et al.*, 2014]. These basins are characterized by thick

1182 accumulations of sedimentary rocks, with as much as 10 km of fill possible in the Aurora Basin, but more

typically ~5 km in Aurora, ~4 km in Vincennes and ~2 km in Sabrina Basin [*Aitken et al.*, 2014; *Aitken et al.*,
2016b]. The Aurora and Vincennes basins are characterized most fundamentally by low gravity, a very
smooth surface, and subdued magnetic signals - this same characteristic defining southward extension of the
Aurora basin (Fig 11). The Sabrina basin has less smooth topography and magnetic data, nevertheless,
geophysical models suggest a preserved sedimentary basin of up to 3 km thickness that has been variably
eroded by ice sheet activity, exposing basement in places [*Aitken et al.*, 2016b]. These inland basins are
separated from the Sabrina Coast by a basement ridge, likely also a feature of glacial erosion.
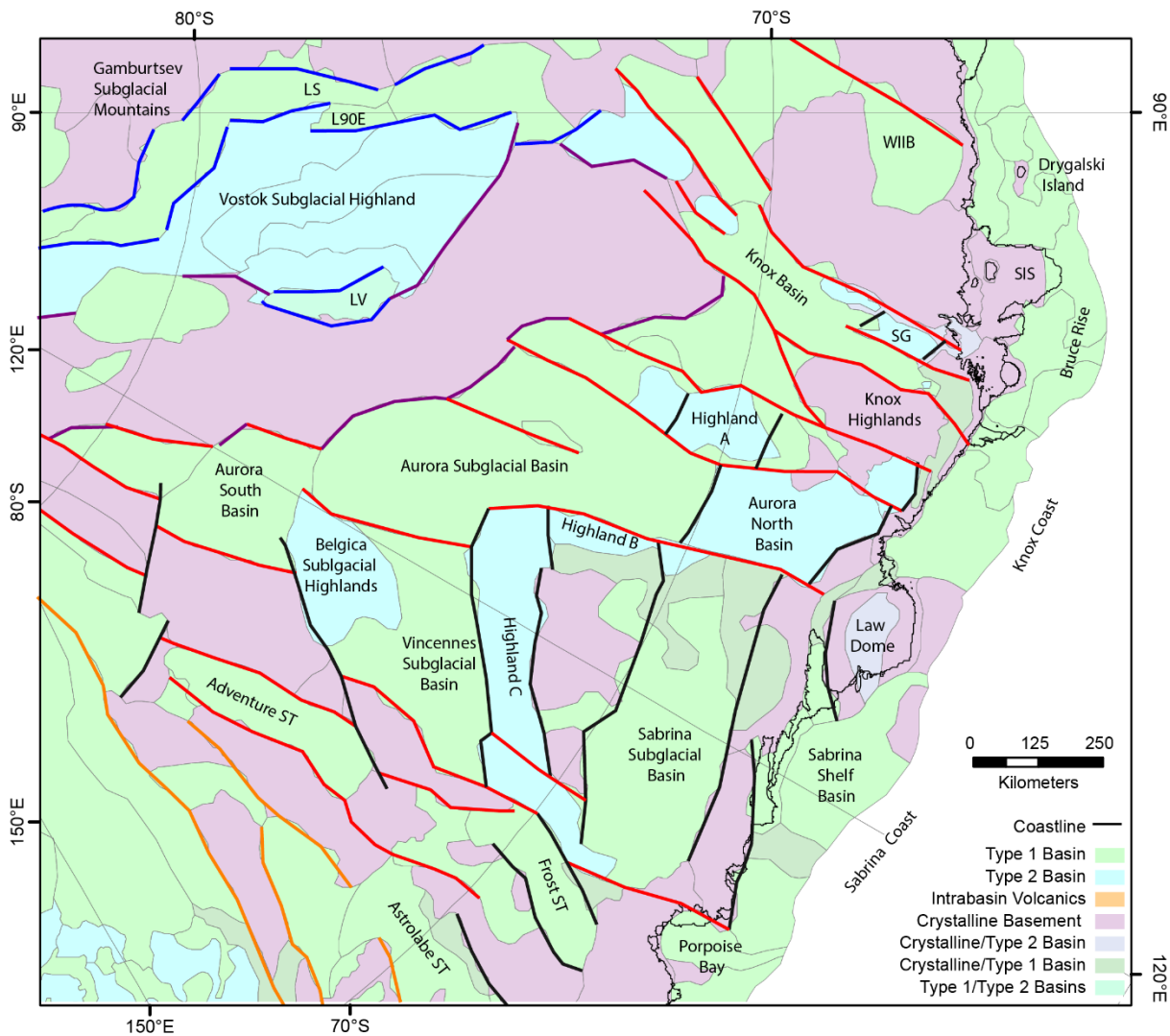
Figure 11: Sedimentary basins of the Vostok, Queen Mary Land, Aurora, and Terre Adelie regions. Purple lines
indicate older structures associated with collisional events [Studinger et al., 2003] while the blue lines
indicate interpreted EARS structures [Ferraccioli et al., 2011]. Black and Red structures indicate Paleozoic-
Mesozoic structures linked to the Knox, Aurora, Vincennes and Sabrina subglacial basins. Orange structures
indicate structures associated with the Wilkes Subglacial Basin, with slightly different trend. Structures
reinterpreted from prior studies [Aitken et al., 2014; Aitken et al., 2016a; Cianfarra and Salvini, 2016; Maggi

1199 Tonian to Ediacaran sedimentary rocks have been found in glacial erratics, indicating an early basin forming

1200 phase with potential links to the Centralian Superbasin of Australia [*Maritati et al.*, 2019]. The region

1201 preserves several subglacial highlands that are interpreted in gravity models to be sedimentary in nature,

1202 including Highlands A, B and C, the region north of the Aurora Basin, and the Belgica Subglacial Highlands

1203 [*Aitken et al.*, 2016b]. Thermochronology suggests that the highlands were uplifted and peneplained in the

1204 Permian-Triassic [*Maritati et al.*, 2020], with the main phase of rifting at this time. Although the region was

1205 potentially reactivated during Jurassic-Cretaceous rifting events, to date, no evidence of this exists locally.

1206 Offshore sedimentary sequences along the Australian-Antarctic margin define four major sequences

1207 separated by unconformities of age 95-80 Ma, 65-58 Ma, 50-45 Ma and 34 Ma [*Sauermilch et al.*, 2019]. The

1208 first sequence represents the rift-derived basin; the sequence is characterized by deltaic sediment

1209 deposition derived from continental river systems, while the third may derive from clockwise-circulating

1210 bottom currents developing in the Paleocene – Eocene with a decrease in sediment input [*Sauermilch et al.*,

1211 2019]. The Sabrina Shelf sedimentary basin may have begun forming at this time, with a distinctive

1212 terrestrial palynoflora interpreted to date to the latest Paleocene to earliest Eocene [*Smith et al.*, 2019a].

1213 The Sabrina Shelf is covered by post-Cretaceous sedimentary cover with variable thickness up to 1.3 km

1214 seismically imaged [*Gulick et al.*, 2017; *Montelli et al.*, 2019]. Paleocene to late-Miocene strata record a

1215 history of Cenozoic ice sheet evolution including the identification of marine-terminating glaciers in the early

1216 to middle Eocene, a series of retreat and advance events in the Oligocene and Miocene, and an expanded

1217 EAIS since the late Miocene [*Gulick et al.*, 2017]. The fourth offshore sequence represents the glacial

1218 development of the margin with in particular the deposition of a high-volume of sediments since the

1219 Oligocene, including apparently variable supply from glacial outlets through time [*Hochmuth et al.*, 2020;

1220 *Hochmuth et al.*, 2022].

1221 The Terre Adelie Craton provides the eastern boundary to this basin region, with a basement-dominated

1222 ridge extending 1800 km inland from Porpoise Bay. Several smaller basins are identified within this ridge

1223 including the Frost Subglacial Basin, and the Astrolabe and Adventure Subglacial troughs. Smooth beds [*Eisen*

1224 *et al.*, 2020] and low gravity suggest these depressions host sedimentary basins, although their age is not

1225 known [*Aitken et al.*, 2014; *Frederick et al.*, 2016]. Offshore Terre Adelie, seismic data record the transition

1226 from a deformed Cretaceous rift on the innermost shelf, through a Paleocene to Eocene transpressional

1227 phase, younging to Plio-Pleistocene strata at the shelf edge [*De Santis et al.*, 2003], representing

1228 progradation of the shelf through since the Eocene [*Hochmuth and Gohl*, 2019]. Maximum observed

1229 sedimentary thickness is 1.6 km [*De Santis et al.*, 2003]. The Mertz and Adelie banks are prominent

1230 bathymetric features representing remnant shelf-sediments, with adjacent basins incised by past glacial
1231 action [*Beaman et al.*, 2011].

3.3.7 Wilkes Subglacial Basin, South Pole Basin and Transantarctic Mountains

1233 The Beacon Supergroup are prominent along the Transantarctic Mountains (TAM) extending from northern
1234 Victoria Land, where outcrop is relatively sparse, to prominent and near continuous exposures extending
1235 from David Glacier to the Ohio Range [*Elliot et al.*, 2017]. The Beacon Supergroup comprises the basal Taylor
1236 Group and the overlying Victoria Group. The Taylor Group consists of Devonian clastic sedimentary rocks,
1237 predominated by shallow marine sediments grading to fluvial sediments [*Bradshaw*, 2013]. The
1238 unconformably overlying Victoria Group and regional equivalents consists of Permian-Triassic siliciclastic and
1239 volcaniclastic rocks also including glacial deposits and coal beds [*Elliot et al.*, 2017]. Ongoing sedimentation
1240 into the Jurassic is identified from younger rocks exposed along the Transantarctic Mountains including the
1241 Jurassic Section Peak Formation of northern Victoria land, the Mawson Formation of southern Victoria Land
1242 and the Hanson Formation in the central TAM [*Elliot et al.*, 2017]. The sequence is overlain and intruded by
1243 mafic magmatic rocks of the Ferrar Group, often forming the caps to mesa-like exposures. In the context of
1244 their exposed extent the Beacon Supergroup are classed as type 2 basins.

1245 Likely Beacon Supergroup correlatives are exposed at Horn Bluff, on the Wilkes Land coast and also,
1246 magnetic features consistent with Ferrar Group dolerite intrusions are found throughout the northern
1247 Wilkes Subglacial Basin [*Ferraccioli et al.*, 2009a]. From these observations we may infer the Beacon
1248 Supergroup as the dominant sedimentary fill in the Wilkes Subglacial Basin. The Wilkes Subglacial Basin
1249 extends for 1600 km along the edge of the Terre Adelie Craton. The basin may be divided into a southern
1250 sub basin, which consists of a single broad depocenter, with a substantial thickness of sedimentary rocks (~ 5
1251 km) extending to 81°S, in line with the Byrd Glacier [*Frederick et al.*, 2016]. Thinner cover extends
1252 southwards to roughly 84°S, in line with the southern end of the Miller Range. The northern sub-basin
1253 consists of three smaller depocenters and more variable sedimentary cover [*Frederick et al.*, 2016]. Magnetic
1254 analysis suggests possible rifting post-dating the intrusion of the Ferrar Group, and interpreted to be
1255 Cretaceous in age, possibly with Cenozoic reactivation [*Ferraccioli et al.*, 2009a; *Jordan et al.*, 2013a]. The
1256 discontinuity between these basin regimes (Fig 12) connects to the David Glacier and is aligned with several
1257 right-lateral transcurrent faults in northern Victoria Land [*Ferraccioli et al.*, 2009a], that also influenced the
1258 Cenozoic evolution of the Ross Sea [*Salvini et al.*, 1997]. The Wilkes Subglacial Basin is continuous with a
1259 further subglacial sedimentary basin located near the South Pole [*Wannamaker et al.*, 2004]. The furthest
1260 extent of the South Pole Basin is aligned with a structural lineament extending from the South Pole through
1261 the TAM near the Reedy Glacier (Fig 12).
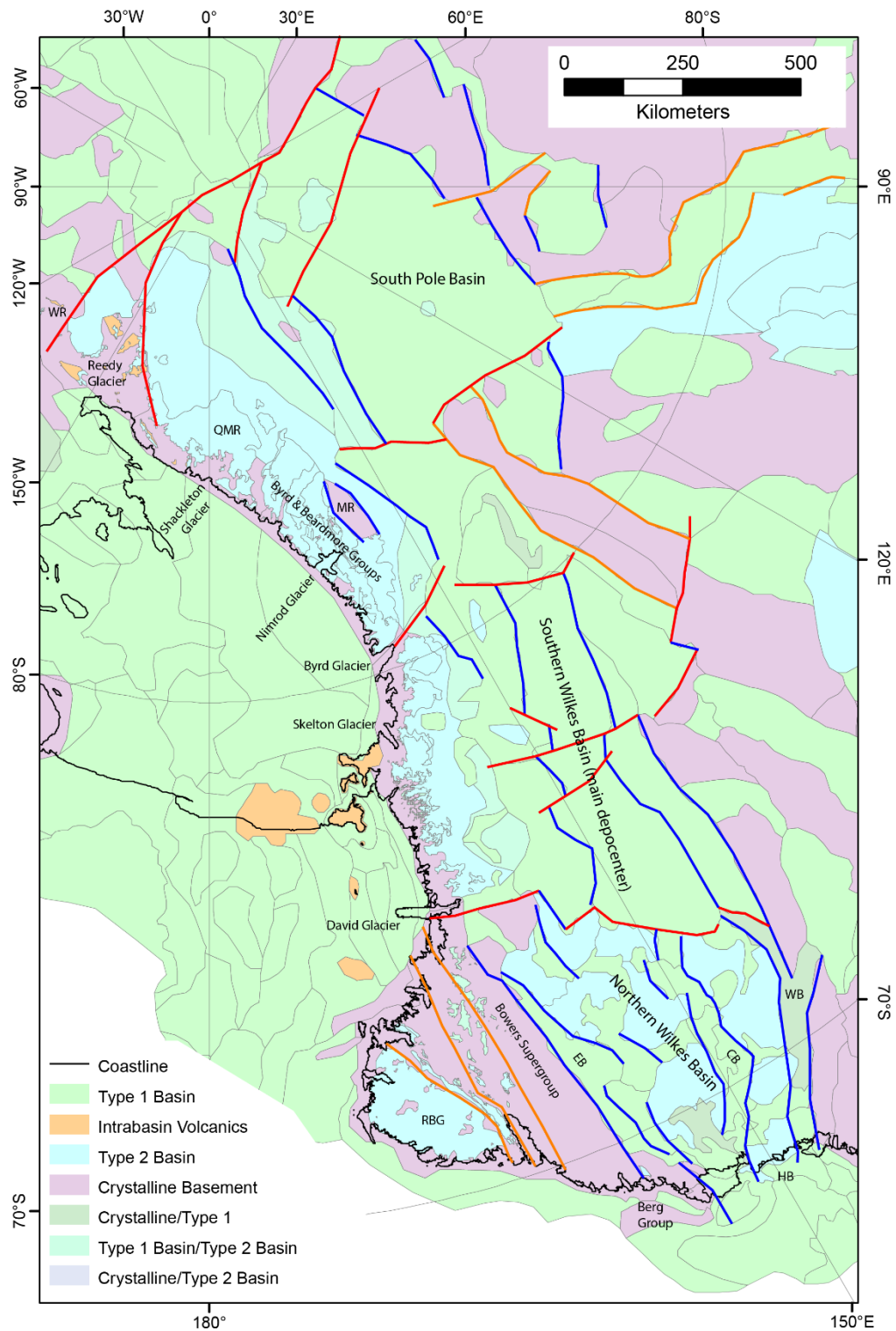
1262

Figure 12: The Transantarctic Mountains and the Wilkes and South Pole subglacial sedimentary basins. Blue lines indicate major rift structures of the Wilkes and South Pole subglacial basins and red lines major cross-basin discontinuities. Orange lines indicate structures from other events. Structures reinterpreted from [Ferraccioli and Bozzo, 2003; Ferraccioli et al., 2009a; Frederick et al., 2016; Jordan et al., 2013a; Wilson, 1999]. WR – Wisconsin Range, QMR – Queen Maud Range, MR – Miller Range

Several Neoproterozoic to early Paleozoic sedimentary packages occur along the TAM. Ediacaran sedimentary rocks are preserved including the Berg Group (northern Victoria Land) and the Beardmore Group (central and southern TAM), with also metasedimentary units including the Rennick Schist and Priestley Formation (northern Victoria Land) and Skelton Group (southern Victoria Land) [*Goodge*, 2020]. Detrital zircon populations indicate these units were deposited after ca 1000 Ma, while Ross Orogeny metamorphism and granite intrusions provide a lower bound of 600 – 550 Ma; volcanic horizons in the Skelton Glacier area and Beardmore Group return compatible ages of 670-650 Ma [*Goodge*, 2020]. The TAM also preserves extensive lower Paleozoic successions. These include in northern Victoria Land the Bowers Supergroup, comprising the Sledgers, Mariners and Leap Year Groups, exposed in the Bowers Terrane and the Robertson Bay Group exposed in the Robertson Bay Terrane. The Bowers Supergroup was deposited in a marine to terrestrial setting in the Cambrian, deposition beginning prior to 520 Ma and ceasing after 480 Ma [*Goodge*, 2020]. The Robertson Bay Group was deposited in a deep marine setting in the early Ordovician, after 490-465 Ma. The TAM between David Glacier and Byrd Glacier does not preserve a comparable lower Paleozoic sequence but south of Byrd Glacier the Cambrian-Ordovician Byrd Group is interpreted to extend to the Shackleton Glacier [*Goodge*, 2020]. The Byrd Group contains a lower sequence of carbonate rocks (Shackleton Limestone, 525-515 Ma) transitioning upwards to carbonate-clastics (Holyoake Formation) and then siliciclastic sedimentary rocks (Starshot Formation and Douglas Conglomerate, 515 – 480 Ma). These are interpreted to represent the transition from a pre-Ross Orogeny carbonate platform to syn-orogenic molasse deposit [*Goodge*, 2020]. The southern TAM, extending from the Queen Maud Range to the Wisconsin Range preserves the lower Paleozoic siliciclastic LaGorce Formation and Duncan Formation. These formations contain detrital zircons dated at ~ 560-550 Ma suggesting they were deposited in the early Cambrian and are intruded by hypabyssal volcanic rocks of the Liv Group dated at 526 Ma. The Liv Group preserves an early Cambrian lower sequence of silicic volcanics and a middle to late Cambrian upper sequence of bimodal volcanics.

4   Tectonic architecture, basin formation and the paleolandscape of Antarctica

Antarctica's sedimentary basins have developed in several key phases in accordance with the evolving plate-tectonic system. Early phases associated with Pre-Ediacaran tectonic events are well defined at regional scale, however, their plate tectonic setting remains in many cases cryptic with respect to the global plate system. The type 1 basins recognized in this study have predominantly developed since the Ediacaran and we focus on these.

4.1 Tectonic structure of Antarctica's lithosphere

The development of sedimentary basins occurs in parallel with the development of the crust and the lithospheric mantle beneath. The structure of the crust and mantle have been investigated in a number of recent studies that reveal key features of relevance to understanding the basin distribution [*An et al.*, 2015; *Pappa et al.*, 2019a; *Shen et al.*, 2017; *Shen et al.*, 2018] [*Chaput et al.*, 2014; *Hazzard et al.*, 2022; *Lloyd et al.*, 2015; *Lloyd et al.*, 2020]. Most critical to basin forming is the development of accommodation space due to tectonic subsidence. Most commonly, the thinning of the lithosphere under extension is the main driver of subsidence.

Antarctica's crustal thickness (Fig 13a) reflects to a large degree the history of extension events that have occurred since Pangea times, and thinner crust is highly correlated with the presence of major basins, whereas basement dominated regions tend to have substantially thicker crust. This is most notable in the Ross and Weddell regions where very thin crust (h < 15 km) is linked to the major basin systems in these regions. This relationship is not universal, and the southern Wilkes Basin and the Aurora Basin are underlain by thicker crust (h > 30 km), suggesting that basin subsidence here was not driven by crustal thinning. Type 2 basins including those in the Vostok Highlands, TAM and Dronning Maud Land regions often overlie thick crust.

In addition to crustal thickness lithospheric thinning may lead to the upwelling of asthenospheric mantle. Initially surface uplift is typical due to mantle heating, and then a prolonged post-rift thermal subsidence phase as the mantle cools over hundreds of millions of years. Lithospheric thickness (Fig 13b) is closely associated with the thermal state of the mantle, and areas of thin lithosphere are associated with recent to ongoing tectonic events. Thin lithosphere in West Antarctica is associated with the WARS, and recent higher-resolution models [*Hazzard et al.*, 2022] suggest it may be less than 30 km thick in regions with recent volcanism including the Terror Rift, Marie Byrd Land, the Siple Coast and the Antarctic Peninsula. Thicker lithosphere is found through the Eastern Basin of the Ross Sea, central West Antarctica and Ellsworth-Whitmore and Haag regions. The Jurassic Weddell Sea Rift System has a lithosphere thickness of ~ 100 km.

In central East Antarctica the thickest lithosphere exceeding 200 km thickness, is centered on the Recovery Subglacial Highlands, the Gamburtsev Mountains and the Vostok Highlands. The effect of the EARS on the lithosphere is not clearly delineated, although narrow rifts of ca 100 km width may be below the resolution of the seismic models for East Antarctica. The major basins of East Antarctica are not all clearly associated with thinned lithosphere and notably Aurora, Vincennes, South Pole and Southern Wilkes basins all overly lithosphere exceeding 150 km thickness. The lack of a basin-aligned thermal anomalies suggests that these basins are probably associated with rifting occurring prior to the Jurassic. The Pensacola-Pole, Recovery and Sabrina basins rest on more moderate lithosphere thickness, potentially representing partial reactivation,

1332 although other influences on the lithosphere thickness are complicating factors. The Lambert, Slessor Glacier

1333 and northern Wilkes basins are associated with thinner lithosphere, supporting a more recent (post-Triassic)

1334 rifting and thermal reactivation in those basins. Thinned lithosphere is observed around the East Antarctic

1335 margin including lithospheric embayments beneath northern Victoria Land, the southern TAM, Dronning

1336 Maud Land, Enderby Land, the Sabrina Coast and Terre Adelie.

1337
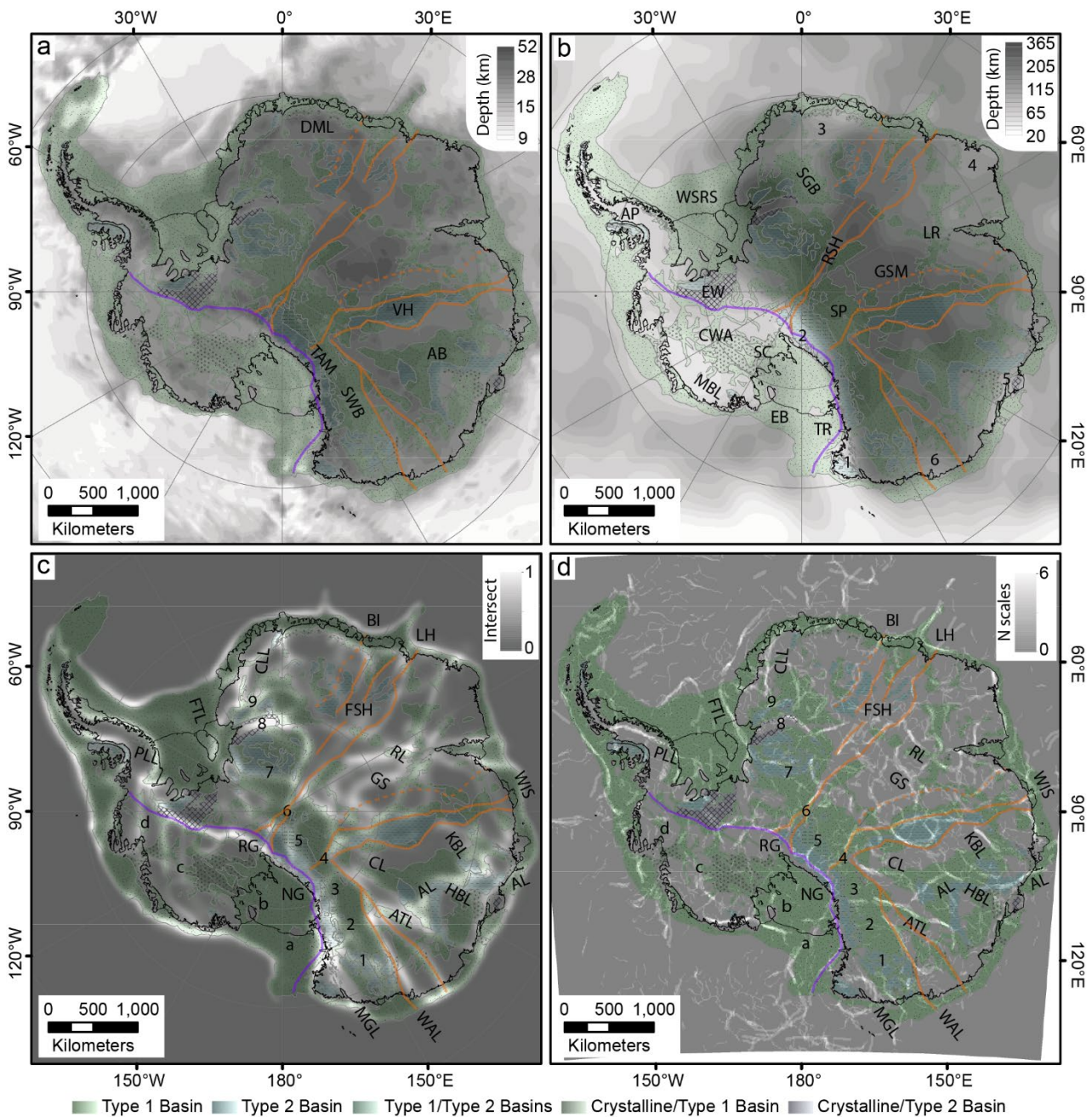
1338 *Figure 13: Structure of the Antarctic lithosphere showing basins over a) Moho depth [Pappa et al., 2019a], b)*

1339 *lithosphere-asthenosphere boundary depth [Hazzard et al., 2022], 1 to 6 indicate lithospheric embayments*

1340 *around the East Antarctic margin c) multidata lineament analysis [Stål et al., 2019] and d) multiscale gravity*

1341 *edge analysis. Labelling: a to d cross-rift structures in the WARS, 1 to 9 cross-basin structures in the Beacon*

1342 *Basin, PLL – Palmer Land Lineament, FTL – Filchner Trough Lineament, CLL – Coats Land Lineament, RL –*

1343 *Ruker Lineament, GS – Gamburtsev Suture, KBL Knox Basin Lineament, AL -Aurora lineament, HBL – Highland*

1352   In rifting, crust and lithospheric scale structures control the locus of deformation, and strongly influence the

1353   shape and internal structure of basins. Integrated lithospheric scale structures were investigated by [*Stål et*

1354   *al.*, 2019], who analyzed bed topography, gravity, and seismic tomography models to delineate indicate the

1355   major boundaries of the lithosphere (Fig 13c). We apply a multiscale gravity edge detection approach to the

1356   Bouguer anomaly (Fig 13d). Phase-congruent multiscale edges [*Kovesi*, 1999] were delineated for 6 scales

1357   with upward continued datasets at 20, 30, 40, 50, 60 and 80 km height; for each of these three sub-scales

1358   were analyzed for phase congruency using windows of 3, 6 and 12 times the height. Ultimately, the analysis

1359   resolves phase-congruent structures between 60 km and 960 km width. Overall, the gravity analysis provides

1360   finer-scaled structures than the integrated lithospheric analysis.

1361   Both analyses indicate major basin-bounding structures of the lithosphere including the WARS-bounding

1362   structures of the TAM front and Bentley Subglacial Trough but also several more subtle basin-aligned

1363   features including in the Ross Sea, and along the Siple Coast, the Pine Island Rift and the Byrd Subglacial

1364   Basin (Fig 10c). The boundaries of the Weddell Sea Rift system are clearly defined including the boundary

1365   with Palmer Land (the Palmer Land Lineament) and the Filchner Trough (the Filchner Trough Lineament),

1366   with again several smaller structures associated with the internal structure of the basin. The gravity analysis

1367   defines additional lineaments associated with the Orion and Explora magnetic anomalies (Fig 13d)

1368   In East Antarctica, key basin-bounding features defined include both the eastern and western edges of the

1369   northern Wilkes Subglacial Basin, with the western boundary (the Wilkes Adelie Lineament) extending inland

1370   for at least 1200 km, while the eastern boundary (the Matusevich Glacier Lineament) is truncated against

1371   the TAM front near David Glacier. Numerous cross-basin structures are seen including the division of

1372   northern and southern WSB, near David Glacier, the boundary with the South Pole Basin near Nimrod

1373   Glacier, and the truncation of the South Pole Basin near Reedy Glacier (Fig 13). Beyond, the Polar Gap

1374   Subglacial Highland is bounded by lineaments associated with Support Force and Recovery Glaciers, and the

1375   final boundary of the Beacon Supergroup basin is seen aligned with Bailey Glacier. Beyond Bailey Glacier the

1376   north-south oriented Coats Land lineament relates to basement structures, likely of Precambrian age, with a

1377   minor basin formed to its west.

1378   The Adventure Subglacial Trench is bounded to the west by a prominent north-south oriented lineament

1379   (the Adventure Trough Lineament) while a parallel structure to the west bounds the Belgica Subglacial

1380   Highlands from the Aurora Subglacial Basin (the Concordia Lineament). The southern boundary of the ASB

1381   possesses a substantial gravity boundary, linked to topographic boundary and truncation of magnetic trends

1382   [*Aitken et al.*, 2014], however it is not associated with a lineament in either analysis. This indicates a diffuse

1383   gradient that is not phase-congruent and may indicate a shallow-dipping structure. The northern edge of the

1384   ASB is associated with a lineament (the Aurora Lineament) trending northwest-southeast towards the Knox

1385   Coast. The northwest-southeast lineament is disrupted by the north-south trending Highland B lineament

1386   and a similar structure to the west defines the eastern boundary of the Knox Subglacial Basin (the Knox Basin

1387   Lineament). Lambert also has a complex structure including the analysis of [*Stål et al.*, 2019] the main north-

1388   south graben, although this is less obvious in the gravity analysis and in both east-west to northwest-

1389   southeast boundaries aligned with basins. In the gravity data analysis, additional northeast-southwest

1390   lineaments are identified aligned with the magnetic Ruker magnetic anomaly (the Ruker Lineament) and the

1391   Gamburtsev suture representing structures in the Precambrian basement [*Ferraccioli et al.*, 2011; *McLean et*

1392   *al.*, 2009].

1393   At the largest scale, we can see in these analyses and models the division of East Antarctica into several

1394   major domains by prominent sets of lineaments along structural culminations. The first lineament set is

1395   observed extending along the Terre Adelie Highlands, bounding the Wilkes Subglacial Basin from the Aurora

1396   region. This trend reflects fundamental boundaries in the geometry of the Mawson continent and its

1397   Neoproterozoic margin [*Aitken et al.*, 2016a; *Studinger et al.*, 2004].

1398   The second set extends from near Nimrod Glacier, along the Vostok Subglacial highlands, where they bound

1399   the Vostok Highlands Basin and lake Vostok Basin, and reaching the coast near the West Ice Shelf. A

1400   potential sub-set to the west extends along a similar trend transecting the Gamburtsev Subglacial

1401   Mountains, Princess Elizabeth Land and emerging into Prydz Bay. In part this trend may represents the EARS

1402   [*Ferraccioli et al.*, 2011], which dominates the domain to the west but likely also is aligned with a more

1403   fundamental lithospheric boundary associated with Neoproterozoic collision [*Mulder et al.*, 2019; *Studinger*

1404   *et al.*, 2003].

1405   A third set of lineaments extends from Reedy Glacier, through South Pole, extending along the Recovery

1406   Subglacial Highland, and then either side of the Fuji Subglacial Highlands, with branches emerging into

1407   Lutzow-Holm bay, the West Ragnhild Trough and possibly also Borchgrevinkisen. In its southern portion, this

1408   structure separates the South Pole Basin from the Pensacola Pole Basin and is linked to the formation of the

1409   Pensacola Embayment, interpreted in the late Neoproterozoic [*Jordan et al.*, 2022]. To the north, the Fuji

1410   Subglacial Highlands culmination separates the basin-dominated regions to the west (Recovery, Slessor and

1411   Interior DML), and east (Lambert).

1412   These lineament sets represent fundamental structures of the Antarctic lithosphere dating to at least the

1413   Neoproterozoic, but their impact on later tectonics and basins is profound. In a Gondwana reconstruction,

1414   the Fuji Subglacial Highlands lineament trend is aligned with the eventual Africa-Madagascar-Sri Lanka triple

1415   junction, the Vostok Highlands lineament trend is aligned with the Kerguelen Plateau, and the Terre Adelie

1416   Highlands trend is linked to the George V fracture zone of Australian-Antarctic basin (Fig 14). The four

1417   domains of East Antarctica have clearly different basin systems with distinct geometries and structural

1418   trends, with broadly the Pensacola-Recovery-Slessor rift system [*Paxman et al.*, 2017; *Paxman et al.*, 2019a],

1419   the EARS [*Ferraccioli et al.*, 2011], the Aurora-Vincennes-Sabrina system [*Aitken et al.*, 2014], and the Wilkes

1420   Subglacial Basin system [*Ferraccioli et al.*, 2009a; *Jordan et al.*, 2013a; *Jordan et al.*, 2022].

4.2 Phase 1 - Ediacaran to Carboniferous

1421

1422   During the Ediacaran to early Cambrian, a continuous East Antarctica was formed as part of Gondwana,

1423   assembled through the East-African (~650 to ~550 Ma) and Kuunga (~550 to ~490 Ma) orogens. The exact

1424   locations of the associated lithospheric boundaries beneath the ice sheet are not known well, however, it is

1425   likely that type 2 basins in the continental interior potentially formed during these events, including in

1426   Dronning Maud Land, the Vostok Highlands, the Aurora/Sabrina region and the Knox region. In the same

1427   timeframe, the edge of East Antarctica was evolving as a passive margin [*Jordan et al.*, 2022] with associated

1428   basin forming events [*Goodge*, 2020]. Ediacaran subduction was initiated along the paleo-Pacific margin of

1429   Gondwana. The onset of the Ross Orogeny, marked by metamorphism from 615 Ma and magmatism from

1430   590- 565 Ma [*Goodge*, 2020] and associated deformation events, saw a change in the locus and nature of

1431   basin formation towards the edge of the craton, with the orogeny ending ~470 Ma when the margin

1432   retreated [*Goodge*, 2020].

1433   Cambrian to Ordovician sedimentary basins deposited along this margin are interpreted to have formed in

1434   association with arc-related magmatism of the Ross Orogeny, continuing into the post-tectonic phase. Basins

1435   typically include an Early to Middle Cambrian sequence of pre- to syn-orogenic units (e.g. Bowers

1436   Supergroup, Byrd Group, Hannah Ridge Formation, Heritage Group) and a Late Cambrian to Ordovician syn-

1437   to post-orogenic sequence (e.g. the Robertson Bay Group, the Swanson Formation, Neptune Group,

1438   Crashsite Group). Both the Ellsworth-Whitmore and western Marie Byrd blocks were probably adjacent to

1439   East Antarctica at this time [*Jordan et al.*, 2020]. Global tectonic reconstructions of this time period lack

1440   detail relative to those from the Devonian onwards and for regional tectonic reconstructions of this time

1441   period the reader is referred to several regional syntheses [*Boger*, 2011; *Goodge*, 2020]. Cambro-Ordovician

1442   basement exhumation occurred inland from the central TAM region as recorded in low temperature

1443   thermochronology [*Fitzgerald and Goodge*, 2022].
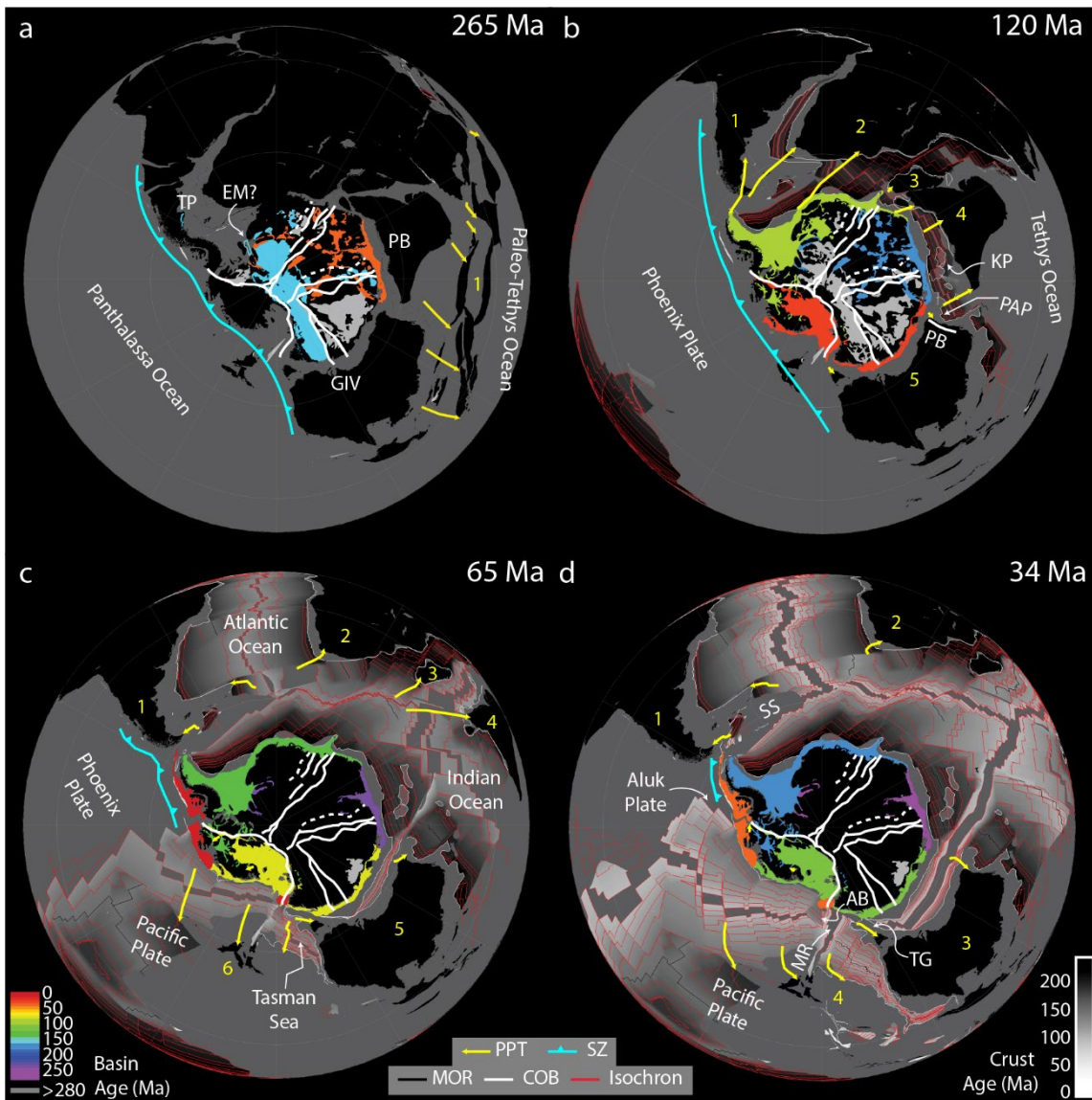
Figure 14: Tectonic reconstruction snapshots a) 265 Ma, b) 120 Ma, c) 65 Ma and d) 34 Ma showing the context of basin formation since Pangea [Müller et al., 2019; Young et al., 2019]. East Antarctica is held fixed in this reconstruction which also does not include rift block motions not involving ocean spreading. Basins are shown from their base-of-basin age to their top-of-basin age, with basin age indicating the time elapsed since the former. Each image also shows the major lithospheric boundaries (see Fig 13). Past plate trajectories (PPTs) are shown for departing plates for the following time periods a) 280 to 265 Ma 1 - Cimmeria, b) 180 to 120 Ma 1 – South America, 2 – Africa, 3 – Madagascar, 4 -Greater India, 5 - Australia c) 90 to 65 Ma 1 – South America, 2 – Africa, 3 – Madagascar, 4 -Greater India, 5 – Australia, 6 – Zealandia, and d) 64 to 34 Ma, 1 – South America, 2 – Africa, 3 –Indo-Australia 4 – Zealandia/Pacific. TP – Trinity Peninsula, EM – Ellsworth Mountains (inferred location) PrB – Prydz Bay, GIV George IV land, KP – Kergualen Plateasu PAP - Perth Abyssal Plain. PeB – Perth Basin, DP – Drake Passage, SS – Scotia Sea, AB – Adare Basin TG – Tasman Gateway.

1457 The Devonian is marked by the deposition of the lower Beacon Supergroup in an interpreted continental
1458 retro-arc setting within Gondwana [*Bradshaw*, 2013]. This basin is exposed as type 2 in the mountains from
1459 Northern Victoria Land to the Theron Mountains and is also preserved as type 1 in the hinterland. The
1460 distinction of type 1 and type 2 in this case is primarily a consequence of later uplift of the TAM and
1461 potentially also downfaulting of the hinterland [*Ferraccioli et al.*, 2009a], and we infer for the Devonian a
1462 single sedimentary basin system (the Beacon Basin) with low-elevation throughout. The system was divided
1463 along-strike into distinct depocenters with up to 9 major divisions along its length (Fig 13). The internal
1464 divisions are marked by changing thickness and morphology of the type 1 basins, while for type 2 basin in
1465 the TAM the variable extent of Beacon Supergroup exposures along strike may represent thickness
1466 variations coupled with differential uplift in later events [*Brenn et al.*, 2017; *Shen et al.*, 2017; *Wannamaker*
1467 *et al.*, 2017] . Offsets to the basin margins and the uplifted parts are also seen (Fig 12). The end of this
1468 subsidence episode is not well constrained but must predate lower-Permian glaciogenic deposits that mark
1469 the onset of the second phase [*Elliot et al.*, 2017].

4.3 Phase 2 - Permian to Triassic

1470

1471 Following the amalgamation of Pangea at ~320 Ma, the Permian marked a distinct change in the tectonic
1472 setting of Antarctica. Permian-Triassic Antarctica saw ongoing subduction at the West Antarctic-
1473 Panthalassan margin, while the Tethyan margin was subjected to rifting from ca 300 Ma to ca 200 Ma
1474 [*Müller et al.*, 2019; *Young et al.*, 2019]. During this period several microcontinents rifted at different times,
1475 but the main Cimmerian terranes separated from Pangea from 280 to 270 Ma (Fig 14a). The Antarctic
1476 Peninsula preserves arc-proximal sedimentary rocks from this period [*Castillo et al.*, 2015], however the
1477 most extensive known sedimentary deposits are found along the Transantarctic Mountains, including
1478 exposures from Northern Victoria Land to the Shackleton Range [*Elliot et al.*, 2017] all considered
1479 equivalents of the Victoria Group of the Beacon Supergroup. Similar rocks in the Ellsworth mountains may
1480 also be stratigraphic correlatives, since relocated due to motion of the Ellsworth-Whitmore block [*Jordan et*
1481 *al.*, 2017a] (Fig 14a). A continuation of Victoria Group equivalent sequences into the Wilkes Subglacial basin,
1482 South Pole Basin and Pensacola-Pole Basin is likely [*Ferraccioli et al.*, 2009a; *Paxman et al.*, 2019a;
1483 *Wannamaker et al.*, 2004].

1484 Exhumation of the East Antarctic coast at least from Prydz Bay to George IV Land occurred between ~350
1485 and ~200 Ma, likely in response to Tethyan rifting [*Lisker et al.*, 2007; *Maritati et al.*, 2020; *Tochilin et al.*,
1486 2012] although influenced by glacial erosion [*Rolland et al.*, 2019]. This was accompanied by formation of
1487 several major basins including Lambert, Knox and Aurora basins [*Maritati et al.*, 2020] and likely an extensive
1488 network of smaller basins within East Antarctica (Fig 14a). The Pangean landscape and basins persisted until
1489 the Early Jurassic Karoo-Ferrar LIP (183 Ma) when Gondwana breakup commenced.

4.4   Phase 3 - Jurassic to Eocene

The Jurassic to Eocene tectonic setting of Antarctica was dominated by the protracted and progressive fragmentation of Gondwana (Fig 14), which led to the formation of marginal basins and ultimately led to an isolated Antarctic continent. Rifting progressed in a 'clockwise' direction with first South America and Africa (from 177 Ma), India and Madagascar (from 135 Ma), Australia (from 100 Ma), and Zealandia (from 82 Ma). This process is relatively well recorded in the sedimentary basins of the Antarctic margin.

Subsidence linked to Gondwana dispersal began in the Weddell Sea region ~180-177 Ma [*Riley et al.*, 2020]. The pre-cursor to continental breakup is thought to have been extensive magmatism and emplacement of the Karoo-Ferrar Large Igneous Province at ~183 Ma [*Burgess et al.*, 2015]. For the main Weddell Sea basins, one suite of models suggest a two-stage development with Early Jurassic motion of the Haag Ellsworth– Whitmore microcontinent that led to the development of the Southern Weddell Sea Rift System [*Jordan et al.*, 2017a], including rifting at the margins of the Weddell Sea (Evans-Rutford Basin and Filchner Trough). Subsequently, rifting occurred in the Northern Weddell Sea Rift Basin and the Riiser-Larsen Sea, beginning associated with breakup between Southern Africa and Antarctica before ~167 Ma [*König and Jokat*, 2006]. The Weddell and Riiser-Larsen seas continued to open together, with associated basin formation offshore, until 126 Ma after which time Atlantic Ocean (Fig 14b) opening led to separate kinematics for these regions [*König and Jokat*, 2006]. In East Antarctica, the Jutul-Pencke-Graben system [*Ferraccioli et al.*, 2005b; *Riedel et al.*, 2012] and the Slessor Glacier Basin have experienced Jurassic to early Cretaceous extension in line with the departure of Africa and South America (Fig 14b). The thermal history of the Shackleton Range suggests a heating episode between 180 – 135 Ma indicating possible sedimentary burial during this time, before rapid cooling at ca 130 Ma [*Krohne et al.*, 2016].

An alternative tectonic model for the Weddell Sea region suggests that the entire Weddell Sea Rift System is part of a single larger Skytrain tectonic plate, including much of the central and southern Antarctic Peninsula [*Eagles and Eisermann*, 2020]. In this model the Northern Weddell Sea Rift reflects separation of the Skytrain plate from Southern Africa and the Falkland Plateau between 180 and 156 Ma, followed by 90° counterclockwise rotation of the entire Skytrain plate into its current position by ~126 Ma [*Eagles and Eisermann*, 2020]. In contrast with the previous model this model does not include Jurassic opening of the southern Weddell Sea, and the plate-motion implies 200-400 km of shortening between the Skytrain plate and East Antarctica during the Cretaceous.

Rifting of Madagascar and greater India from Antarctica had commenced by the early Cretaceous with oceanic crust forming in the Enderby Basin from 133 Ma [*Jokat et al.*, 2021]. This process may have involved an initial separation between East Antarctica and the Elan Bank and Southern Kerguelen Plateau, with by ~ 115 Ma a ridge-jump to north of the Elan Bank associated with the Kerguelen plume [*Gaina et al.*, 2007;

1523 *Gibbons et al.*, 2013], although an entirely pre-Kerguelen evolution is possible [*Jokat et al.*, 2021]. From 120

1524 Ma, igneous rocks from the Kerguelen plume formed much of the Southern Kerguelen Plateau and also are

1525 prominent in the basins of Enderby and Davis Seas [*Davis et al.*, 2018]. The potential effects of the rifting of

1526 greater India on East Antarctica's landscape and onshore basins remains ill-defined. Limited

1527 thermochronology detects early Cretaceous cooling in the Lambert region [*Lisker et al.*, 2007], linked to

1528 brittle deformation structures [*Phillips and Läufer*, 2009], although later studies propose an igneous origin

1529 for thermal resetting [*Tochilin et al.*, 2012], while the Shackleton range experienced rapid cooling at ca 130

1530 Ma [*Krohne et al.*, 2016].

1531 The geometry of the Lambert Rift is characteristic of two distinct structural orientations that dominate this

1532 sector of East Antarctica: one is aligned parallel to early spreading in the Cosmonauts Sea margin, and the

1533 other to early spreading direction of the Enderby Basin (Fig 14b). These structural orientations may be

1534 associated with much older events, and reactivation may have occurred in response to events associated

1535 with the opening of the Enderby Basin (130 – 115 Ma [*Gibbons et al.*, 2013]) and the Cosmonauts Sea (<120

1536 Ma [*Jokat et al.*, 2010]), either separately, or due to strain-partitioning associated with contemporaneous

1537 rifting.

1538 The impact of greater India rifting on the margin of Western Australia, at the time contiguous, is more well

1539 defined, and may form a key template to understand East Antarctica. After the end of Permian-Triassic

1540 rifting, renewed subsidence of the Perth and Mentelle basins occurred from the mid-Jurassic to early

1541 Cretaceous, with the breakup phase associated with oblique northwest-southeast extension aligned with

1542 spreading in the Perth Abyssal Plain [*Williams et al.*, 2013]. Onshore structures for this period include dextral

1543 strike-slip on north-south oriented structures, en-echelon folding and sinistral motion on northwest-

1544 southeast transfer faults [*Song and Cawood*, 2000]. The late Jurassic sedimentary fill of the Mentelle Basin

1545 suggests dominant detrital sources located in East Antarctica during this time, indicating active erosion of

1546 inland regions [*Maritati et al.*, 2021]. Following these a widespread Valanginian unconformity and eruption

1547 of the Bunbury Basalt at 137 - 130 Ma [*Olierook et al.*, 2016] mark breakup and widespread uplift. The Perth

1548 Basin is continuous with the Knox and Aurora Subglacial basins, which are structurally similar (Fig 14b).

1549 In the mid-Cretaceous the oblique motion of Australia from Antarctica (Fig 14c) commenced at ca. 100 Ma,

1550 however, did not proceed to separation until 83 Ma [*Williams et al.*, 2019]. In contrast to Africa and India,

1551 Australia did not rapidly move away, with slow spreading until ~45 Ma [*Williams et al.*, 2019], and the

1552 Tasman Gateway was not opened until 33 Ma [*Scher et al.*, 2015]. Spreading on this margin west of the

1553 George V fracture zone between 57-50 Ma may have been accommodated by sinistral transtension in East

1554 Antarctica and tectonic deepening of the Adventure and Astrolabe Subglacial Troughs [*Eagles*, 2019]. The

1555 adjacent margins preserve the evolution of this post-rift system including, since the early Paleogene, a major

1556 influence from evolving glacial and oceanographic systems [*De Santis et al.*, 2003; *Escutia et al.*, 2005;

1557 *Hochmuth et al.*, 2020; *Sauermilch et al.*, 2019].

1558 Initial east-west extension in the Ross Sea is interpreted with a broad basin evolving between 105 to 83 Ma

1559 [*Jordan et al.*, 2020]. This phase of rifting in the Ross Sea is characterized by lower-crustal exhumation along

1560 low-angle detachment faults [*Siddoway et al.*, 2004]. Up to 100 km of diffuse extension may be

1561 accommodated on these shear zones [*Siddoway*, 2008], and this phase of extension is associated with

1562 crustal thinning and magmatism but not the development of major accommodation space [*Lindeque et al.*,

1563 2016a]. The predominance of crustal thinning over basin development may a consequence of weak lower

1564 crust [*Karner et al.*, 2005]. This wide rift event has also been associated with a potential plateau collapse

1565 [*Bialas et al.*, 2007]. With separation of Zealandia at 83 Ma the translation of Marie-Byrd Land trends

1566 towards the northwest and the rift system is interpreted to extend southward into the Siple Coast and

1567 Amundsen regions [*Jordan et al.*, 2020], also evolving from a more diffuse wide-rift to a more focused

1568 narrow-rift mode, likely due to increasing rheological strength [*Harry et al.*, 2018; *Huerta and Harry*, 2007].

1569 The opening of the Tasman Sea and Pacific-Antarctic Ridge from 83 Ma to 52 Ma accommodated the

1570 majority of the relative motion of Zealandia and the Pacific plate relative to Antarctica [*Gibbons et al.*, 2013].

1571 In the northern Ross Sea, opening of the Central Basin is interpreted between 61- 53 Ma [*Davey et al.*, 2021].

1572 From 52 Ma, the opening of the Macquarie Ridge and Adare basin is associated with translation and rotation

1573 of Marie-Byrd Land and the Eastern Basin, initially to the northeast, and then to the east (Fig 14).

1574 ## 4.5   Phase 4 – Eocene to Present

1575 Post mid-Eocene, plate tectonic motions in Antarctica were restricted to a few key areas. The western Ross

1576 Sea was in extension with corresponding seafloor spreading in the Adare Basin from 43 to 26 Ma, and also

1577 extension in the Terror Rift [*Davey et al.*, 2016; *Granot and Dyment*, 2018]. Although the amount of

1578 extension was limited, the effects on the bathymetry of the continental shelf, and the association with

1579 volcanism were important local drivers of basin evolution. Neogene rifting is interpreted to extend into the

1580 interior West Antarctica including the Bentley Subglacial Trough [*Lloyd et al.*, 2015], Pine Island Rift [*Jordan*

1581 *et al.*, 2010b], Byrd Subglacial Basin [*Shen et al.*, 2018] and the Ferrigno Rift [*Bingham et al.*, 2012]. Tectonic

1582 subsidence through this period has occurred in the Ross, Siple Coast and Central West Antarctica regions (Fig

1583 12) [*Paxman et al.*, 2019b].

1584 Subduction of the Aluk plate (part of the Phoenix plate) progressively ceased from south to north over time,

1585 as the West Antarctic-Aluk ridge moved north and ultimately ceased subduction in the Neogene [*Burton-*

1586 *Johnson and Riley*, 2015]. The evolution of a more complex margin to the north occurred in line with

1587 complex tectonics of the Scotia Sea [*van de Lagemaat et al.*, 2021]. This included the opening of the Powell

1588 (30-20 Ma) and Jane (18-14 Ma) basins in a back-arc setting, and the convergent South Shetland margin,

1589   comprising a fore-arc basin and accretionary prism [*Maldonado et al.*, 1994], and, since 4 Ma rifting in the

1590   Bransfield Basin [*Almendros et al.*, 2020]. In the Eocene tectonic processes occurring to the north of

1591   Antarctica remained important as the Drake Passage allowed throughflow by 42 Ma [*Scher and Martin*,

1592   2006] and the Tasman gateway by 33 Ma [*Scher et al.*, 2015]. Through the Oligocene these gateways

1593   developed more fully [*van de Lagemaat et al.*, 2021], allowing by the Miocene a fully developed Antarctic

1594   Circumpolar Current.
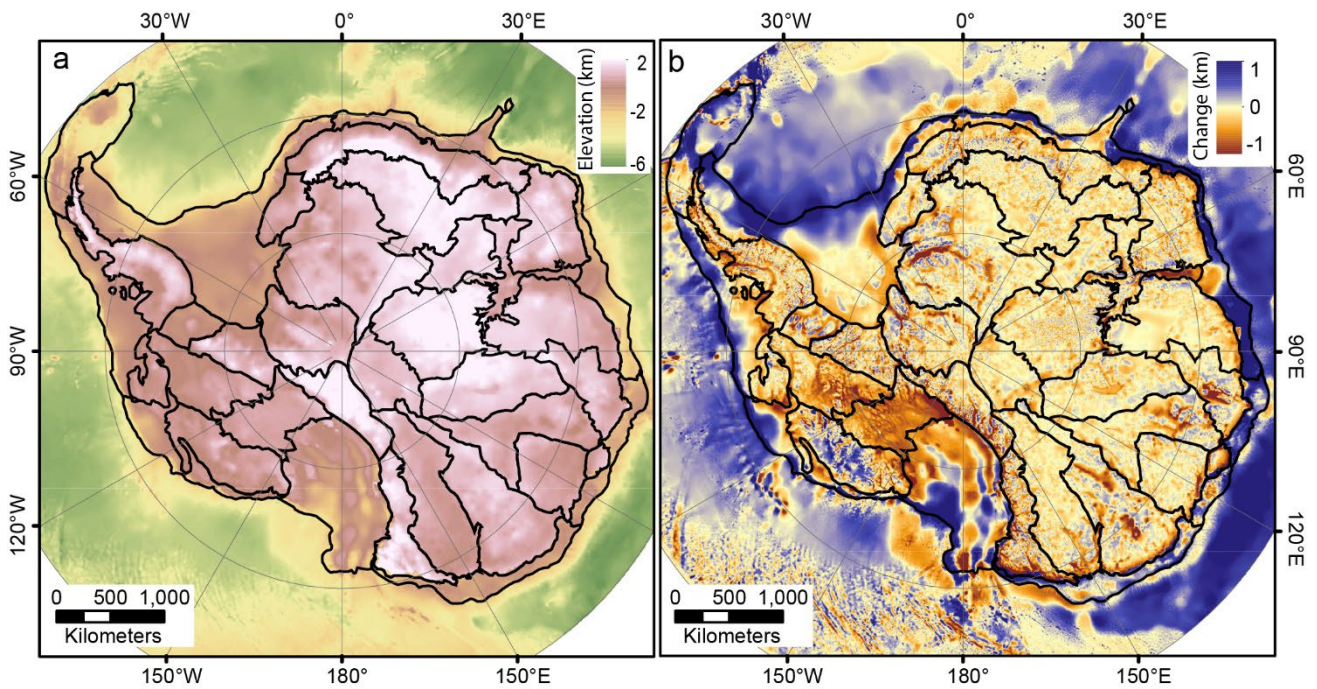
1595

1596   *Figure 15: a) paleotopography at the Eocene Oligocene boundary [Paxman et al., 2019b] and b) the*

1597   *difference with the present day. Negative values indicate surface lowering due to tectonic subsidence and or*

1598   *glacial erosion.*

1599   Despite these regional tectonic events, by far the major influence on Antarctica's basin forming processes in

1600   this period was the glacial influence as the ice sheet developed, with many cycles of advance and retreat

1601   causing major unconformities, substantial onshore erosion [*Paxman et al.*, 2019b] and fluctuating sediment

1602   volumes deposited around the margins [*Hochmuth and Gohl*, 2019; *Pérez et al.*, 2021]. The resulting

1603   landscape of eroded basement regions, post-glacial sedimentary basins and the geomorphological features

1604   from both tectonic and glacial processes are essential for understanding the past present and future

1605   behavior of the Antarctic Ice Sheet.

1606   # 5   Implications for Antarctic Ice Sheet dynamics

1607   ## 5.1   Basin-associated processes and their potential impact on the cryosphere

1608   Ice sheets and glaciers flow by three main mechanisms: internal ice deformation, basal sliding and

1609   deformation of basal material. The first of these is ubiquitous among ice masses, but the second and third

1610 are conditional on the presence of basal water. Furthermore, the third is dependent on the availability of

1611 deformable sediments at the bed. For water to exist beneath an ice sheet basal heat is needed: This can

1612 come from geothermal sources and, especially if ice flow is rapid, from basal motion and internal ice-

1613 deformation. Thus, the dynamics of fast flowing ice is dominated by basal flow processes that allow speeds

1614 more than 50 m yr^{-1}, and often several 100 m yr^{-1}.

1615 The availability of subglacial water is essential to both basal sliding and sediment deformation. In addition to

1616 ice sheet melting, for a permeable bed, we must consider the potential for water to be exchanged between

1617 the ice sheet bed interface, the active deforming till layer, and the strata beneath which may tap deep

1618 groundwater reserves [*Gustafson et al.*, 2022]. The role of groundwater in subglacial hydrological systems is

1619 important to ice flow for two main reasons. The first reason is a source of water in addition to that melted

1620 from ice. For example, *Christoffersen et al.* [2014] suggest groundwater may contribute up to half of the

1621 water available beneath ice streams in the Siple Coast and *Li et al.* [2022] model groundwater discharge of

1622 similar scale to melt-derived water. The second reason is that groundwater flow allows heat to be

1623 transported vertically and laterally through the subglacial system [*Gooch et al.*, 2016; *Kulessa et al.*, 2019]

1624 thus representing a governing mechanism of advective heat transport to the ice sheet base.

1625 Hydraulic gradients in subglacial sedimentary basins vary over glacial cycles during the growth and decay of

1626 the ice sheet. This process has a positive feedback with ice sheet retreat and advance, as retreating ice

1627 sheets thin, unloading the basin causes groundwater to be discharged into the subglacial system [*Gooch et*

1628 *al.*, 2016; *Li et al.*, 2022; *Person et al.*, 2012,]. The opposite may occur when the ice sheet thickens, directing

1629 water away from the ice sheet base and storing it in subglacial sedimentary basins [*Gooch et al.*, 2016]. In

1630 this manner, the groundwater system modulates interactions between basal water systems and the

1631 underlying sedimentary basins to exert control on the lubrication of the ice sheet base and thus impact ice

1632 flow. Numerical modelling indicates that, even in situations of fast retreat, the groundwater discharge-rate

1633 can be of comparable magnitude to the expected basal melt rate, and this feedback is likely to contribute

1634 substantially to ice sheet dynamics [*Li et al.*, 2022]. Furthermore, past retreat and advance events can store

1635 'fossil' hydraulic head in aquifers for later release [*Gooch et al.*, 2016; *Person et al.*, 2012].

1636 From what we understand from formerly glaciated regions [*Evans et al.*, 2006] and from geophysical

1637 observations of subglacial Antarctica [*Alley et al.*, 2021; *Anandakrishnan et al.*, 1998; *Christianson et al.*,

1638 2016; *Muto et al.*, 2019a; *Siegert et al.*, 2016], the deformation of basal material is a dominant process

1639 within major ice streams and, consequently, exerts control on ice sheet flow. InSAR depiction of surface ice

1640 flow velocities [*Mouginot et al.*, 2019] and geophysical measurements of the subglacial system

1641 [*Anandakrishnan et al.*, 1998; *Christianson et al.*, 2016; *Muto et al.*, 2016; *Muto et al.*, 2019a; *Peters et al.*,

1642 2006] allow us to pinpoint the onset of enhanced ice flow and the basal boundary conditions that permit it:

1643 For example, the onset of Whillans Ice Stream coincides with the availability of sedimentary material

1644 identified through aerogeophysical [*Bell et al.*, 1998] and seismic [*Anandakrishnan et al.*, 1998] data. The

1645 mechanics of subglacial sediment is complex and time variable, with in general hydration and fluid

1646 overpressure leading to weaker rheology while compaction and de-watering lead to stiffer rheology. This

1647 sensitivity to water supply can lead to relatively abrupt changes in flow [*Catania et al.*, 2012; *Christoffersen*

1648 *et al.*, 2014; *Smith et al.*, 2013]. Meanwhile, sediment deposition in a grounding zone wedge and subsequent

1649 compaction associated with tidal loading may stabilize the grounding zone [*Christianson et al.*, 2016]. The

1650 deformation of the sediment commonly involves two layers: a relatively thin upper active zone, at most a

1651 few meters thick dilated by high-pressure water within pores that acts to reduce its material strength; and a

1652 thicker over-compacted basal unit that is stiffer and contributes little to flow [*Evans et al.*, 2006].

1653 Basal sediments originate from two main sources: accumulations of marine sediments during previous times

1654 of deglaciation, and from the erosion of bedrock either locally or upstream. Recent marine deposits are likely

1655 to be present at lower-elevations and will often be widespread, prompting zones of more continuous bed

1656 deformation [*Evans et al.*, 2006]. Without recent marine sediments, sediment supply must be sustained

1657 through glacial erosion, and this may be a limiting factor on till continuity. Glacial erosion is accomplished

1658 through a variety of processes, and these are fundamentally reliant on heterogeneities in the bedrock,

1659 including joints, especially their spacing and orientation [*Hooyer et al.*, 2012], and lithological variations

1660 including competency contrasts, layer thicknesses, and structural orientation relative to flow [*Krabbendam*

1661 *and Glasser*, 2011; *Lane et al.*, 2015]. In comparison to the competent and massive structure more typical of

1662 igneous and metamorphic basement, sedimentary rocks provide more opportunities for quarrying to occur,

1663 and also a higher likelihood of abrasion, where the rocks are less competent [*Krabbendam and Glasser*,

1664 2011]. Finally, to sustain a continuous till layer, sediments eroded upstream must be transported, which is

1665 predominantly achieved via the subglacial hydrology system, which depending on erosion rate and water

1666 flux may be supply-limited or transport capacity limited [*Delaney et al.*, 2019].

1667 Both subglacial water and thin horizons of weak basal sediments may be present in areas of crystalline

1668 basement as well as in sedimentary basin regions. Before considering basin settings, it is instructive to

1669 consider an ice stream catchment with a structurally massive and impermeable bed throughout, such as a

1670 granite or gneiss bedrock. For such a bed we may consider as a first priority the supply of basal water, which

1671 must be derived from basal melting and/or surface melting transported to the bed via fractures and moulins

1672 [*Schoof*, 2010]. The latter, while certainly an important processes, depends on surface melting conditions

1673 that in Antarctica are, for now, limited to certain coastal regions, although they may be more important in

1674 the future [*Tuckett et al.*, 2019]. For the former, a sustained high flow-speed and/or geothermal heat flux is

1675 needed. With an impermeable bed, geothermal heat flux for a given location will be near constant, and so

1676 temporal variations in basal melt rate will depend solely on ice-stream flow processes. In addition to water,

1677 sediment must be supplied through erosion of the crystalline basement, which is likely to be highly resistant

1678   to erosion [*Krabbendam and Glasser*, 2011] potentially restricting supply. We may now consider how the

1679   presence of a sedimentary bed influences ice sheet dynamics.

1680   Several factors associated with sedimentary basin formation increase the likelihood that regions containing

1681   sedimentary basins will possess enhanced ice flow. These are 1) a favorable source for sustained supply of

1682   sediment from more erodible bedrock and/or recent marine sediments [*Bell et al.*, 1998]; 2) the supply of

1683   subglacial water through groundwater discharge, tied to glacial unloading [*Christoffersen et al.*, 2014; *Siegert*

1684   *et al.*, 2018]; 3) different organization of subglacial water systems including transitions between distributed

1685   and channelized flow, and routing between catchments [*Christoffersen et al.*, 2014; *Schroeder et al.*, 2013];

1686   4) the opportunity through groundwater circulation to advect heat from depth to the ice sheet bed [*Gooch*

1687   *et al.*, 2016]. In addition, the tendency for basin-dominated regions to possess relatively smooth topography

1688   at all scales promotes ice-stream boundaries defined by ice sheet dynamics, including basal processes

1689   [*Catania et al.*, 2012]. Finally, we may consider the effects of ongoing basin-forming processes on the

1690   morphology of ice shelf cavities that are critical for ice sheet stability [*Smith et al.*, 2019b].

5.2   Antarctic sedimentary basins and ice sheet dynamics

1691

1692   Although the specifics of when, where and how sedimentary basins have influenced ice sheet dynamics in

1693   Antarctica remain to be defined, the mechanisms listed above are more able to occur in catchments

1694   containing sedimentary basins. Consequently, we may consider if the presence of subglacial sedimentary

1695   basins within a glacial catchment is associated with more dynamic behaviour, and if this impact on ice sheet

1696   dynamics may be expressed for the modern-day ice sheet.
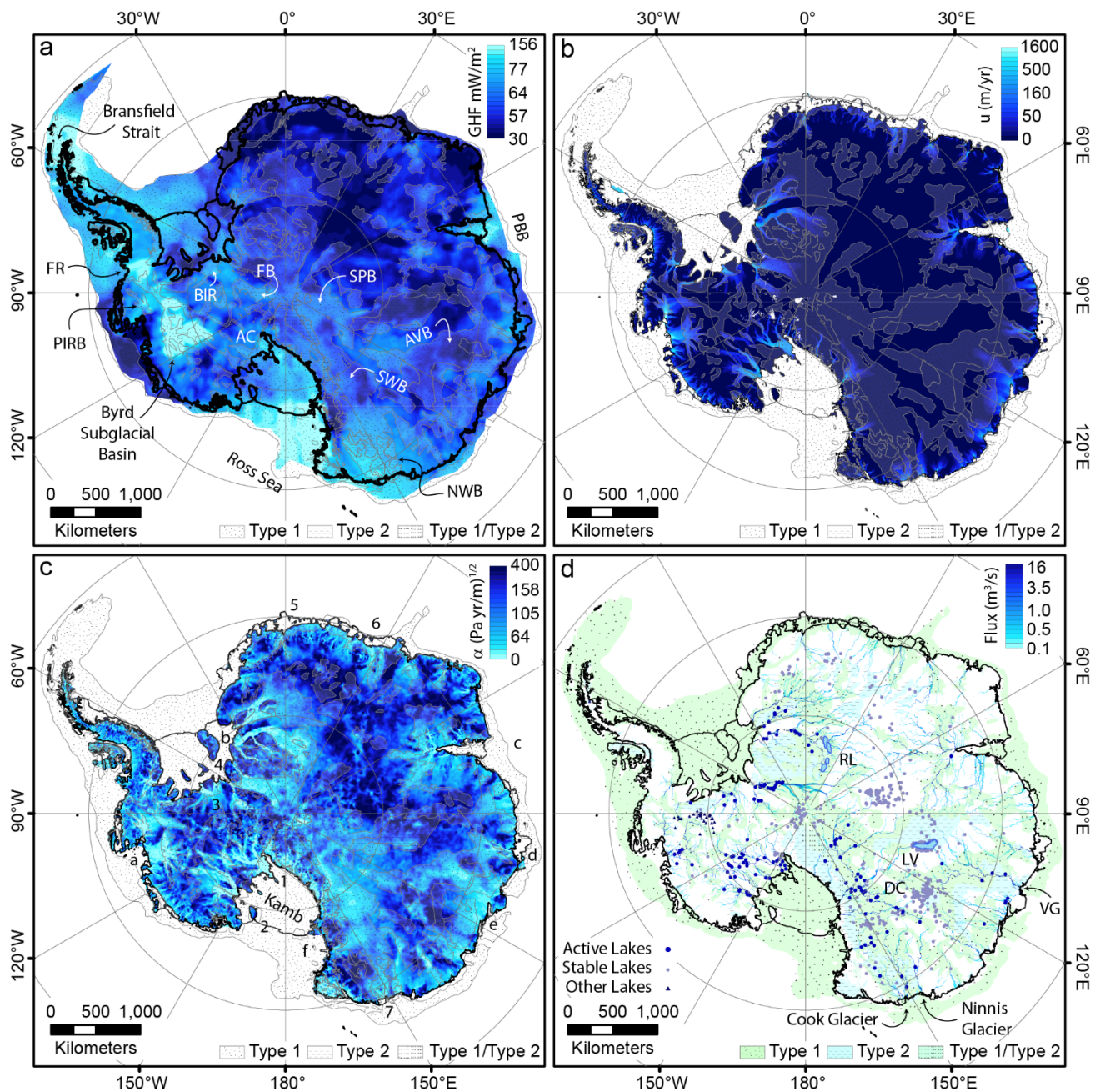
1697

Figure 16: a) deep-seated geothermal heat flux [Lösing and Ebbing, 2021] b) surface ice sheet velocity from InSAR phase mapping [Mouginot et al., 2019] c) inferred basal friction coefficient derived by inverting for basal conditions using the Ice sheet and Sea level System Model [Dawson et al., 2022]. Numbers indicate ice stream systems with sedimentary basins beneath fast flowing ice including 1 – Mercer and Whillans, 2 – Bindschadler and MacAyeal 3 – Insitute , 4 - Academy and Support Force 5 – Jutulstraumen 6 – West and Central Ragnhild, 7 – Cook. Letters indicate ice stream systems with basins upstream including a – Thwaites and Pine Island, b – Recovery and Slessor d – Lambert, Mellor and Fisher, d – Denman and Scott e – Totten f – David, Skelton and Byrd d) subglacial hydrology, including subglacial lakes [Livingstone et al., 2022], and a modern-day drainage network [Le Brocq et al., 2013]. FR – Ferrigno Rift, PIRB – Pine Island Rift Basin, BIR – Bungenstock Ice Rise, AC – Amundsen Coast Basin, FB – Foundation Basin, SPB – South Pole Basin, AVB –

1710 Basins are important modulating influence on geothermal heat flux (GHF) and can act either to inhibit or

1711 enhance surface GHF. In Antarctica, the overall statistical relationship with heat flux from deep-seated

1712 sources [*Lösing and Ebbing*, 2021] is almost null for type 1 basins relative to crystalline basement, although

1713 type 2 basins are systematically associated with lower GHF (small effect size). In West Antarctica where heat

1714 flux is generally high, higher heat flux is found within basin regions (Fig 15a). These regions include the Siple

1715 Coast with especially high heat flux in the Amundsen Coast Basin, but less to the north. From the Byrd

1716 Subglacial Basin to the Ferrigno Rift is an elevated high heat flux region, with concentrations beneath basins

1717 including the Byrd Subglacial basin and the Pine Island Rift Basin. The western Ross Sea, including the active

1718 Terror Rift and the similarly active Bransfield Strait region has high heat flux. Tectonically older regions such

1719 as the Weddell Sea possess more moderate heat flux, but higher towards the west and the south near

1720 Bungenstock Ice Rise (Fig 15a). Variations in heat flux in East Antarctica are not so clearly associated with

1721 basins except for the tendency for very low values to be restricted to areas without type 1 basins. Selected

1722 areas, including the Foundation Basin South Pole Basin, the Northern Wilkes Basin, and the Prydz Bay Basin

1723 show elevated heat flux relative to their surrounding area while the Aurora-Vincennes and southern Wilkes

1724 subglacial basins show reduced heat flux. With respect to ice sheet dynamics, the large-scale heat flux

1725 shown here represents the crustal structure beneath the basin, and excepting volcanism, is a stable

1726 boundary condition. The time-variable influence of basins on heat flux at the bed is likely to be substantial

1727 where fluid circulation is coupled with a high thermal gradient, with fluid conduits such as deformation

1728 zones also important [*Tankersley et al.*, 2022].

1729 Fast flowing ice, as defined by surface ice velocity [*Mouginot et al.*, 2019] has overall only a weak spatial

1730 association with the presence of basins (Fig 15b). Type 1 basins do have a higher average velocity (24 m yr^{-1})

1731 than either crystalline bed (19 m yr^{-1}) or type 2 basins (11 m yr^{-1}), but with very small effect size given the

1732 large spatial variability ($\sigma \approx 70$ m yr^{-1}). However, although many of Antarctica's fastest flowing glaciers flow

1733 over crystalline bedrock or a mixed bed, many of these possess sedimentary basins preserved in the upper

1734 catchment (Fig 15b).

1735 The slipperiness at the ice-bed interface is expressed by the basal friction coefficient, which relates basal

1736 sliding velocity to basal shear stress. It is a direct measure of the subglacial environment and encapsulates

1737 the effect of both subglacial water and deformable sediment. Model inferred basal friction coefficient is

1738 generally lower where there is fast flowing ice and higher near topographic divides, but also may associate

1739 with the presence of basins (Fig 15c). In comparison with velocity, model-inferred basal friction coefficient is

1740 closely correlated with the basin distribution, with a mean for type 1 basins of 93 (Pa yr/m)$^{1/2}$ contrasting

1741   with a mean of 127 and 134 $(Pa\ yr/m)^{1/2}$ in crystalline basement and type 2 basins respectively. Overall, this

1742   relationship has a medium effect size given regional variability ($\sigma \approx 70$ $(Pa\ yr/m)^{1/2}$).

1743   Basal friction coefficient is related to basin coverage in several ways. In several ice stream systems, basin

1744   coverage occurs in the fast-flowing lower catchment and low basal friction coefficient is seen. Examples

1745   include Mercer and Whillans; MacAyeal and Bindschadler; and Institute ice streams draining the West

1746   Antarctic Ice sheet and Academy and Support Force; Jutulstraumen; West and Central Ragnhild; and Cook ice

1747   streams draining the East Antarctic Ice Sheet. Often however for major catchments the fast-flowing lower

1748   catchments flows over a crystalline or mixed bed, with the basin confined to the upper catchment, the

1749   downstream part having been eroded [*Aitken et al.*, 2016b; *Paxman et al.*, 2017]. Examples include Thwaites

1750   and Pine Island; Recovery and Slessor; Lambert, Mellor and Fisher; Denman and Scott; Totten and the ice

1751   streams draining from the southern Wilkes Subglacial Basin through the TAM including Byrd, Skelton and

1752   David glaciers. For these ice streams low basal friction coefficient extends far into the sedimentary basin

1753   region despite the surface velocity being relatively slow, suggesting that basal sliding can propagate into the

1754   upstream basin. A final relationship is that for slow-moving ice such as at Kamb Ice Stream, and at drainage

1755   divides (e.g. for South Pole) where we see basin regions associated with moderate to high basal friction

1756   coefficient, indicating that basal sliding is limited in these areas.

1757   We may also review the association of basins with the subglacial hydrology system (Fig 13d). Subglacial

1758   lakes are found throughout Antarctica [*Livingstone et al.*, 2022] and occur across all bed classes. Of 675

1759   lakes, 260 (39%) occur over crystalline bedrock, while 239 (35%) occur over type 1 basins, and 114 (17%)

1760   over type 2 basins. In comparison, the areas taken up by these bed classes is 40%, 47% and 8% respectively.

1761   Furthermore, of 140 hydraulically active lakes we find 96 (69%) occur over type 1 basins, while of 502 stable

1762   lakes only 137 occur over this class (27%.). This represents a tendency for stable lakes to occur close to ice

1763   divides, while active lakes occur more frequently towards the ice sheet margins [*Livingstone et al.*, 2022].

1764   Besides subglacial lakes, basal fluid flux is driven by hydraulic potential gradients from the high-potential

1765   divides towards the ice sheet margins. These networks do not necessarily follow the same flow-routing as

1766   the ice and can cross boundaries to ice flow (Fig 15d). Unless the ice sheet surface slope is steep and

1767   oriented transverse to the bed slope, the subglacial water flux will be preferentially concentrated into

1768   topographic basins and form highly dynamic flow networks [*Dow et al.*, 2022; *Le Brocq et al.*, 2013], and so

1769   there is a natural association of high-volume subglacial water flux and sedimentary basins (Fig 13d). Several

1770   notable examples include the Recovery Lakes that overly the Recovery Basin with flow directed towards

1771   Recovery glaciers, the Pensacola-Pole Basin with flow directed to Academy and Support Force glaciers, the

1772   Byrd Subglacial Basin with flow directed towards Thwaites Glacier. Lake Vostok draining into the Wilkes

1773   Subglacial Basin, and from there flow directed towards Cook Glacier, and also through the TAM, and Finally

1774   Dome C with flow directed into the Aurora Subglacial Basin and towards Vanderford Glacier.

1775 At Thwaites, the transition from distributed to channelized flow may be correlated to the change from
1776 sedimentary basin to crystalline bed [*Schroeder et al.*, 2013] and bed-type transitions in other catchments
1777 (Fig 15d) may also be critical thresholds for the hydrology system. The interaction of high-flux hydrology
1778 networks including active lakes with higher-permeability sedimentary beds is fundamental to the subglacial
1779 hydrology of Antarctica and may exert a critical influence on ice sheet dynamics. An important consideration
1780 is where subglacial hydrology follows different routing to the ice flow: Ice retreat and unloading in one
1781 catchment, along with increased basal melting, may enhance water flux that is potentially routed into
1782 another catchment, and so may help propagate dynamic behavior from one catchment to another [*Wright*
1783 *et al.*, 2008].

1784 The preceding indicates associations between the presence of sedimentary basins and enhanced ice sheet
1785 flow. In a sedimentary basin setting, this sliding may occur in deformable till layers facilitated by more
1786 extensive basal till and from hydrogeological processes that may provide substantial amounts of subglacial
1787 water. Enhanced groundwater discharge to the bed is associated with additional feedbacks, including heat
1788 advection within the basin and temporally variable water discharge and recharge coupled with ice unloading
1789 and loading histories. The expected groundwater response includes an ongoing long-term response from
1790 deep aquifers activated by unloading since Last Glacial Maximum, and shorter-term responses from
1791 shallower aquifers activated by more recent mass loss [*Christoffersen et al.*, 2014; *Gustafson et al.*, 2022; *Li*
1792 *et al.*, 2022]. In some regions, high sensitivity to variable subglacial hydrology network structure may lead to
1793 cross-catchment vulnerabilities and the propagation of dynamic behavior between ice streams [*Alley et al.*,
1794 1994; *Vaughan et al.*, 2008; *Wright et al.*, 2008].

1795 A substantial role for subglacial sedimentary basins in governing the basal conditions of the ice sheet is well
1796 supported by both models and data, but a well-defined relationship between subglacial sedimentary basins
1797 and ice sheet flow remains elusive, with many cross-associations with other boundary conditions and
1798 complex time and space variable interactions. In particular, the potential effects of these basin processes on
1799 large scale glacial flow are yet to be systematically assessed.

6 Future directions in Antarctic Subglacial Sedimentary Basins research

1801 Knowledge of sedimentary basins beneath the Antarctic ice sheet has expanded greatly in recent decades,
1802 and key concepts relating to their influence on ice sheet dynamics are identified. Despite this, for a full
1803 realization of their value for understanding global tectonics, paleolandscape evolution and the dynamic
1804 behavior of ice sheets with changing climate, there is a pressing need to continue to progress several key
1805 themes.

6.1   Sedimentary basin definition and characterization

Despite substantial recent advances, mapping the presence of sedimentary rocks beneath thick ice remains a significant challenge. The more widely available datasets from airborne geophysics can provide a strong indication of the presence of a sedimentary basin, subject to certain ambiguities.

Small-scale variations in the solid earth, for example heat flux [*McCormack et al.*, 2022] and topography [*MacKie et al.*, 2020] may have large impacts on ice sheet dynamics. For consistent mapping at a continent scale, improved coverage is needed both to fill remaining data gaps, and in areas with typically older, low resolution, less accurate or poorly geolocated data. The newest compilation Bedmap3 [*Frémand et al.*, 2022b] is based on a 500m along-line resolution. Taking this as a benchmark, we summarize the requirements for airborne data to reach this resolution: To maximize non-aliased signal, magnetic intensity data should be collected with a line-separation comparable to the source-sensor separation [*Reid*, 1980]. Gravity data may be more widely separated without loss of non-aliased signal. In much of Antarctica, due to thick ice, the source-sensor separation is several kilometers, and there is little gain from closely spaced magnetic and gravity surveys. Regions with thinner ice however may benefit in principle but are limited by several additional factors. Airborne gravity systems require along-line data filtering that, for fixed-wing platforms, limit viable resolution to 5 -10 kilometers wavelength.

Radar has no similar physical limitation on resolution and the bed can be sampled at fine scales along lines. The fine scale along line sampling allows for sub-survey resolution data products to be generated in 2D using physical and/or statistical techniques [*Frémand et al.*, 2022b; *MacKie et al.*, 2020; *Morlighem et al.*, 2020]. The need for closely spaced data, depends on the characteristics of the ice sheet bed and the ice sheet flow, and a variable radar line-spacing of 500 to 2.5 km across the continent is likely to improve the fidelity of bed topography data products across all scales. To enable finer resolution it is necessary to reduce aircraft velocity, and helicopter surveys are one practical solution [*Wei et al.*, 2020], or alternatively, slow-flying UAVs may be an emerging technology for practical deployment in the future [*Teisberg et al.*, 2022]. Ship-based operation may also allow to reach key coastal data gaps.

Ground-based geophysical data collection, including by active and passive seismic and magnetotelluric methods, remains limited in Antarctica and it is a significant challenge to achieve a systematic continent-wide coverage. Large-scale passive seismic deployments, with stations spaced tens of kilometers apart or more, have been used with success to image the nature of the crust and the mantle including basins [*Shen et al.*, 2018; *Zhou et al.*, 2022]. The current network of passive seismic stations (n ~ 1600), mostly in West Antarctica could feasibly be expanded to a continent-scale network with accompanying magnetotelluric data within a manageable logistical footprint. Smaller-scale deployments with station spacings of kilometers are capable of imaging the geology conditions at the bed of individual ice streams and are fundamental to

understanding the impact of sedimentary basins on ice sheet dynamics [*Anandakrishnan and Winberry*, 2004; *Gustafson et al.*, 2022; *Peters et al.*, 2006]. Active seismic experiments remain resource-intensive and logistically challenging although the implementation of vibrator sources and snow-streamer technologies is a substantial step forward to increase the efficiency, resolution and accuracy of data collection [*Eisen et al.*, 2015]. These more intensive approaches initially may be targeted towards key catchments, however expanded deployment of these technologies would be of immense benefit to understanding geologic bed conditions for ice dynamics.

Finally, it is necessary to enhance capability for field-verification of bed characteristics to inform and constrain geophysical observations. Several initiatives are under way to develop further drilling technologies to access the subglacial geology, including systems designed with differing logistical footprints and with different capacity to reach the bed through thick ice [*Gong et al.*, 2019; *Goodge et al.*, 2021; *Hodgson et al.*, 2016; *Kuhl et al.*, 2021; *Talalay et al.*, 2021]. Maintaining strong engagement with ice-coring and hot-water drilling communities is desirable to synergize efforts where feasible. For the context of basins research, and the study of their interactions with glacial systems, a critical problem remains that representative samples are likely to be found under thick and especially wet-based ice, for which drilling technologies are not yet optimized. The capacity to recover long stratigraphic cores is of particular value to basins research.

As well as the detection of basins, we may seek to better define the geometry of basins, including their thickness and overall morphology but also their internal structure. Defining the thickness of Antarctica's sedimentary basins is a clear next step that demands a new approach able to combine multiple diverse datasets so that all are accommodated in the problem formulation, and the solution. Also important are faults and stratigraphy, which provide critical controls on fluid flow within the basins. Consequently, these dictate the hydrogeological response to changing glacial load and so advective heat transport to the ice sheet bed [*Tankersley et al.*, 2022]. The sensitivity of gravity and magnetic data to internal basin structure may be limited by density and magnetization contrasts between sedimentary rocks which are relatively low in comparison to the contrast with the basement and other features such as intrusions and volcanic rocks. While passive seismic and magnetotelluric data provide some additional constraints, active seismic data are most effective for developing a good appreciation of intra-basin structure.

Finally, while the physical properties of the basins, including density, seismic velocity and its anisotropy, electrical conductivity and other characteristics may be defined from geophysical data, to define their relationship with ice sheet dynamics it is necessary to translate these into mechanical and hydrogeological properties. A particular challenge are 'topological' properties defined largely by orientations and connections (e.g. permeability, stratigraphic layering and its orientation, fracture density and orientation) that have most bearing on both the hydrogeological system [*Person et al.*, 2012] and also the erodibility of sedimentary bedrock [*Krabbendam and Glasser*, 2011; *Lane et al.*, 2015].

6.2 Sedimentary basins as a record of glacial change

A profound quality of sedimentary basins is their capacity to record sensitively the conditions of their formation, which amongst other things provides knowledge of tectonic and surface processes, and past ice, ocean, and climate conditions. Sampling of sedimentary records from basins provides key benchmarks and constraints on the behavior of the ice sheet in the past, which supports the capacity to define ice sheet processes in models of potential future ice sheet change. While many studies have investigated the Antarctic margin, these studies remain limited in extent and are clustered in a few areas (Fig 1). With dynamic instabilities dominating catchment scale ice stream behavior, more comprehensive coverage is required to understand the dynamic response of the Antarctic ice sheet to changing climate. Innovative approaches to marine drilling [e.g. *Gohl et al.*, 2017] may allow more agile, safer and less logistically demanding investigations.

In addition to obtaining records of changing conditions from drill cores, spatial patterns of erosion and sedimentation are closely linked to past glacial cycles [*Anderson et al.*, 2019; *Hochmuth et al.*, 2020; *Pérez et al.*, 2021] and can be used to understand systematic instabilities within catchments [*Aitken et al.*, 2016b]. The structure of sedimentary basins can be used for the reconstruction of paleo-landscapes, offshore and onshore, which is important for understanding the long-term stability of the ice sheet structure [*Hochmuth et al.*, 2020; *Jamieson et al.*, 2010; *Paxman et al.*, 2019b]. Paleotopographic reconstruction is also critical in the effort to model past ice sheet behavior with realistic topographic and basal boundary conditions, rather than relying on modern-day formulations [*Hochmuth and Gohl*, 2019; *Paxman et al.*, 2020]. An important factor here is not just the reconstruction of topographic elevation, but also the changing nature of the ice sheet bed through time.

6.3 Understanding cryosphere interactions

While the fundamental principles of the interactions between sedimentary basins, sediments and water at the ice sheet bed and ice sheet flow have been known for some time [*Alley et al.*, 1987; *Bell et al.*, 1998; *Blankenship et al.*, 1986; *Christoffersen et al.*, 2014] their overall role in controlling Antarctic ice sheet dynamics is ill-defined. Knowledge of these interactions in Antarctica is growing, but it is evident that much further work needs be done to provide a systematic understanding of how these complex boundary conditions interact with the ice sheet to focus, enhance, constrain or otherwise influence glacial change processes associated with a warming climate [*Kennicutt et al.*, 2019].

Hydrogeologic interactions of sedimentary basins with subglacial hydrology and cryosphere are understood largely through model studies [*Christoffersen et al.*, 2014; *Gooch et al.*, 2016; *Li et al.*, 2022] and through studies of the former northern hemisphere ice sheets [*Person et al.*, 2007]. It is not clear yet how these model concepts may affect Antarctic conditions, and a robust and Antarctic-specific understanding of their

role in the dynamics of the Antarctic ice sheet is a core challenge requiring both targeted model studies and expanded observations of the bed. Critical concepts to be defined further include the role of sedimentary basins for sustaining subglacial water supply, and the interactions of aquifer systems with subglacial lakes and hydrological flow organization on different timescales. Understanding how Antarctica's aquifers respond to a changing ice sheet may be an essential factor in understanding their vulnerability in retreat, as the release of water during glacial unloading, if substantial, could be a critical positive feedback promoting accelerated ice sheet flow [*Schoof*, 2010] and also ice-shelf destabilization [*Le Brocq et al.*, 2013].

Sedimentary basins are an important factor in controlling heat flux, firstly through the tendency to insulate the crust beneath, leading to warmer conditions beneath and secondly, the capacity for fluid circulation within the basin to efficiently transport heat from depth to the surface, also potentially accessing saline waters [*Gustafson et al.*, 2022]. Heat advection is especially important as a positive feedback associated with ice sheet unloading [*Gooch et al.*, 2016]. Essential concepts to be defined further include mapping temperature gradients, water contents and salinity within basins, as well as the association of these with high ambient temperatures associated with rifting, magmatism, or high crustal heat production. Perhaps the most limiting factor is the identification of the internal basin structure, and so the necessary conduits for fluid circulation, their orientation and connectivity.

A sustained supply of flow-capable sediment is an important factor enabling sustained fast ice sheet flow. This requires either a base of marine sediments, deposited during a past retreat, or a reliably erodible bedrock. In the latter case, while the presence of the sedimentary bed is known to be an important condition, studies of formerly glaciated regions show there is a high degree of sensitivity to the nature of the sedimentary rocks, including the dip and strike of the strata, bedding-layer thicknesses, the competency of the different lithologies, and the intensity and spacing of joints and other fractures [*Hooyer et al.*, 2012; *Krabbendam and Glasser*, 2011; *Lane et al.*, 2015]. Characterization of these fine-scale details in a subglacial setting is problematic in the absence of high-resolution seismic reflection data, however, an understanding of the depositional setting, large-scale structure and broad lithology variations within basins may allow these factors to be assessed in a probabilistic sense bearing in mind analogues from formerly glaciated regions.

6.4   Coupling mapping with ice sheet models for predictive capacity

A major frontier for basins research in Antarctica is the coupling of the knowledge of subglacial geology with ice sheet models to understand the influence of the main processes and to enable better predictions of sea level change and other impacts on ocean and climate. The first challenge in doing so is the identification of the basin characteristics and processes that are most relevant to dynamic ice sheet behavior, in particular we may wish to understand more precisely the influence of basin location within the catchment relative to the grounding zone, the effects of variable basin thickness, and variations at different scales of properties

such as porosity, lithology, permeability, structural orientation and mechanical erodibility. The incorporation of these in ice sheet models may in the future be enabled through inclusion of adaptive sliding laws and better coupled hydrology and hydrogeology modelling.

Other challenges include the successful representation in ice sheet models of evolving sedimentary systems under ice, including spatially variable and anisotropic bedrock erosion, the re-distribution of subglacial sediments through subglacial sediment transport and time-variable subglacial hydrology on ice sheet flow, water outflux and sediment deposition on ice shelves and their cavities. Many ice sheet models are now able to accommodate at least some of these processes in parameterized forms, allowing their influence to be assessed alongside other processes [e.g. *Delaney et al.*, 2019; *Lowry et al.*, 2020; *Pollard and DeConto*, 2020].

7 Conclusion

The presence of sedimentary basins in Antarctica, their potential impact on ice sheet dynamics, and their ability to record change has long been known. Except in some regions with access to outcrops and/or ship-based science, a comprehensive understanding has been lacking due to ice cover and remoteness restricting access. The geophysical community has in recent years developed improved approaches to characterize subglacial geology, through improved equipment and data collection, and advances in data processing and analysis targeted to the unique environment of Antarctica. The community also has collected large amounts of data, and crucially these are available to the community in compilations at continent-scale. Numerical data analysis techniques including machine learning are providing advanced capability to map the distribution of sedimentary basins.

Key outcomes from the growing understanding of Antarctica's basins are the definition of feedbacks with ice sheet processes that have the capacity to influence the future Antarctic Ice Sheet, in particular through the potential supply of increased water and heat to the ice sheet bed as a consequence of retreat. Around the continent, a system-level understanding is emerging that ties subglacial processes at the ice sheet bed and marine depositional systems [Hochmuth et al., 2020; Paxman et al., 2019b; Pollard and DeConto, 2020]. A persistent finding beneath the ice sheet, on the continental shelf and beyond is that glacial processes are the dominant factor in the development of Antarctica's basins since at least the Eocene, signifying the dynamic nature of the Antarctic Ice Sheet [Noble et al., 2020].

Despite the progress made it is notable that the records we have are, relative to many other parts of the world, very limited in their distribution, resolution and scope. Across all data, critical gaps remain in our coverage of Antarctica's basins, and, due to high logistical thresholds, data redundancy and repeatability is often low. There is a critical need to define in expanded form the importance of subglacial sedimentary basins for controlling dynamic ice sheet flow, especially to characterize the feedbacks and instabilities that may dictate the response of Antarctica's ice sheet to changing climate. Finally, it is essential that these

1972 findings are incorporated in future numerical ice sheet models to underpin a better predictive capacity for
1973 future ice sheet change.

8 Acknowledgements

9 Open Research

1986 The map of Antarctica's sedimentary basins presented here is available from the Pangaea repository (Details
1987 TBC) via [DOI, persistent identifier link] with [license, access conditions]. A version for ongoing development
1988 is available form GitHub []. Data used in mapping are available from sources as cited in text.

10 References

1990 Aitken, A. R. A., et al. (2014), The subglacial geology of Wilkes Land, East Antarctica, *Geophysical Research*
1991 *Letters*, *41*(7), 2390-2400.

1992 Aitken, A. R. A., et al. (2016a), The Australo-Antarctic Columbia to Gondwana transition, *Gondwana*
1993 *Research*, *29*(0), 136-152.

1994 Aitken, A. R. A., et al. (2016b), Repeated large-scale retreat and advance of Totten Glacier indicated by inland
1995 bed erosion., *Nature*, *533*, 385-389.

1996 Aitken, A. R. A., et al. (2018), A role for data richness mapping in exploration decision making, *Ore Geology*
1997 *Reviews*, *99*, 398-410.

1998 Aitken, A. R. A., et al. (2020), A Magnetic Data Correction Workflow for Sparse, Four-Dimensional Data,
1999 *Journal of Geophysical Research: Solid Earth*, *125*(10).

2000 Allen, P. A., et al. (2015), Chapter 2 Classification of basins, with special reference to Proterozoic examples,
2001 *Geological Society, London, Memoirs*, *43*(1), 5-28.

2002 Alley, R. B., et al. (1987), Till beneath ice stream B: 3. Till deformation: Evidence and implications, *Journal of*
2003 *Geophysical Research: Solid Earth*, *92*(B9), 8921-8929.

2004 Alley, R. B., et al. (1994), A water-piracy hypothesis for the stagnation of Ice Stream C, Antarctica, *Annals of*
2005 *Glaciology*, *20*, 187-194.

2006 Alley, R. B., et al. (2021), Bedforms of Thwaites Glacier, West Antarctica: Character and Origin, *Journal of*
2007 *Geophysical Research: Earth Surface*, *126*(12).

2008 Almendros, J., et al. (2020), BRAVOSEIS: Geophysical investigation of rifting and volcanism in the Bransfield
2009 Strait, Antarctica, *Journal of South American Earth Sciences*, *104*, 102834.

2010 Ammon, C. J. (1991), The isolation of receiver effects from teleseismic P waveforms, *Bulletin - Seismological*
2011 *Society of America*, *81*(6), 2504-2510.

2012 An, M., et al. (2015), S-velocity model and inferred Moho topography beneath the Antarctic Plate from
2013 Rayleigh waves, *Journal of Geophysical Research: Solid Earth*, *120*(1), 2014JB011332.

2014 Anandakrishnan, S., et al. (1998), Influence of subglacial geology on the position of a West Antarctic ice
2015 stream from seismic observations, *Nature*, *394*(6688), 62-65.

2016 Anandakrishnan, S., et al. (2000), Deployment of a broadband seismic network in West Antarctica,
2017 *Geophysical Research Letters*, *27*(14), 2053-2056.

2018 Anandakrishnan, S., and J. P. Winberry (2004), Antarctic subglacial sedimentary layer thickness from receiver
2019 function analysis, *Global and Planetary Change*, *42*(1-4), 167-176.

2020 Anderson, J. B., et al. (2019), Seismic and geomorphic records of Antarctic Ice Sheet evolution in the Ross Sea
2021 and controlling factors in its behaviour, *Geological Society, London, Special Publications*, *475*(1), 223-240.

2022 Anderson, J. J. (1965), Bedrock Geology of Antarctica: A Summary of Exploration, 1831–1962, in *Geology and*
2023 *Paleontology of the Antarctic*, edited by J. B. Hadley, pp. 1-70, AGU, Washington, DC, USA.

2024 Arndt, J. E., et al. (2017), Evidence for a dynamic grounding line in outer Filchner Trough, Antarctica, until the
2025 early Holocene, *Geology*, *45*(11), 1035-1038.

2026 Arnold, E., et al. (2020), CReSIS airborne radars and platforms for ice and snow sounding, *Annals of*
2027 *Glaciology*, *61*(81), 58-67.

2028 Bailey, J. T., et al. (1964), Radio echo sounding of polar ice sheets, *Nature*, *204*(4957), 420-421.

2029 Bamber, J. L., et al. (2006), East Antarctic ice stream tributary underlain by major sedimentary basin, *Geology*,
2030 *34*(1), 33-36.

2031 Baranov, A., et al. (2021), ANTASed – An Updated Sediment Model for Antarctica, *Frontiers in Earth Science*,
2032 *9*.

2033 Bart, P. J., et al. (2000), Seismic data from the Northern basin, Ross Sea, record extreme expansions of the
2034 East Antarctic Ice Sheet during the late Neogene, *Marine Geology*, *166*(1-4), 31-50.

2035 Bart, P. J. (2003), Were West Antarctic ice sheet grounding events in the Ross Sea a consequence of East
2036 Antarctic ice sheet expansion during the middle Miocene?, *Earth and Planetary Science Letters*, *216*(1-2), 93-
2037 107.

2038 Batchelor, C. L., et al. (2020), New insights into the formation of submarine glacial landforms from high-
2039 resolution Autonomous Underwater Vehicle data, *Geomorphology*, *370*.

2040 Beaman, R. J., et al. (2011), A new high-resolution bathymetry model for the Terre Adélie and George V
2041 continental margin, East Antarctica, *Antarctic Science*, *23*(1), 95-103.

2042 Behrendt, J. C., et al. (1966), Airborne geophysical study in the Pensacola Mountains of Antarctica, *Science*,
2043 *153*(3742), 1373-1376.

2044 Bell, R., et al. (1999a), Development of a new generation gravity map of Antarctica: ADGRAV Antarctic Digital
2045 Gravity Synthesis, *Annali di Geofisica*, *42*.

2046 Bell, R. E., et al. (1998), Influence of subglacial geology on the onset of a West antarctic ice stream from
2047 aerogeophysical observations, *Nature*, *394*(6688), 58-62.

2048   Bell, R. E., et al. (1999b), Airborne gravity and precise positioning for geologic applications, *Journal of*
2049   *Geophysical Research: Solid Earth*, *104*(B7), 15281-15292.

2050   Bentley, C. R., et al. (1960), Structure of West Antarctica, *Science*, *131*(3394), 131-136.

2051   Bialas, R., et al. (2007), Plateau collapse model for the Transantarctic Mountains--West Antarctic Rift System:
2052   Insights from numerical experiments, *Geology*, *35*, 687-690.

2053   Bienert, N. L., et al. (2022), Post-Processing Synchronized Bistatic Radar for Long Offset Glacier Sounding,
2054   *IEEE Transactions on Geoscience and Remote Sensing*, 1-1.

2055   Bingham, R. G., and M. J. Siegert (2007a), Radio-echo sounding over polar ice masses, *Journal of*
2056   *Environmental and Engineering Geophysics*, *12*(1), 47-62.

2057   Bingham, R. G., and M. J. Siegert (2007b), Radar-derived bed roughness characterization of Institute and
2058   Möller ice streams, West Antarctica, and comparison with Siple Coast ice streams, *Geophysical Research*
2059   *Letters*, *34*(21).

2060   Bingham, R. G., and M. J. Siegert (2009), Quantifying subglacial bed roughness in Antarctica: implications for
2061   ice-sheet dynamics and history, *Quaternary Science Reviews*, *28*(3), 223-236.

2062   Bingham, R. G., et al. (2012), Inland thinning of West Antarctic Ice Sheet steered along subglacial rifts,
2063   *Nature*, *487*(7408), 468-471.

2064   Blankenship, D. D., et al. (1986), Seismic measurements reveal a saturated porous layer beneath an active
2065   Antarctic ice stream, *Nature*, *322*(6074), 54-57.

2066   Boger, S. D. (2011), Antarctica — Before and after Gondwana, *Gondwana Research*, *19*(2), 335-371.

2067   Bohoyo, F., et al. (2002), Basin development subsequent to ridge-trench collision: The Jane Basin, Antarctica,
2068   *Marine Geophysical Research*, *23*(5-6), 413-421.

2069   Bowman, V., et al. (2016), The Paleocene of Antarctica: Dinoflagellate cyst biostratigraphy,
2070   chronostratigraphy and implications for the palaeo-Pacific margin of Gondwana, *Gondwana Research*, *38*,
2071   132-148.

2072   Bradshaw, M. A. (2013), The Taylor Group (Beacon Supergroup): the Devonian sediments of Antarctica,
2073   *Geological Society, London, Special Publications*, *381*(1), 67-97.

2074   Brenn, G. R., et al. (2017), Variable thermal loading and flexural uplift along the Transantarctic Mountains,
2075   Antarctica, *Geology*, *45*(5), 463-466.

2076   Brisbourne, A. M., et al. (2017), Bed conditions of Pine Island Glacier, West Antarctica, *Journal of Geophysical*
2077   *Research: Earth Surface*, *122*(1), 419-433.

2078   Broome, A. L., and D. M. Schroeder (2022), A Radiometrically Precise Multi-Frequency Ice-Penetrating Radar
2079   Architecture, *IEEE Transactions on Geoscience and Remote Sensing*, *60*, 1-15.

2080   Burgess, S. D., et al. (2015), High-precision geochronology links the Ferrar large igneous province with early-
2081   Jurassic ocean anoxia and biotic crisis, *Earth and Planetary Science Letters*, *415*, 90-99.

2082   Burton-Johnson, A., and T. R. Riley (2015), Autochthonous v. accreted terrane development of continental
2083   margins: a revised in situ tectonic history of the Antarctic Peninsula, *Journal of the Geological Society*, *172*(6),
2084   822-835.

2085   Cande, S. C., and J. M. Stock (2004), Cenozoic reconstructions of the australia-new zealand-south pacific
2086   sector of antarctica, in *Geophysical Monograph Series*, edited, pp. 5-17.

2087   Capponi, M., et al. (2022), Antarctica 3-D crustal structure investigation by means of the Bayesian gravity
2088   inversion: the Wilkes Land case study, *Geophysical Journal International*, *229*(3), 2147-2161.

2089   Castillo, P., et al. (2015), Petrography and geochemistry of the Carboniferous-Triassic Trinity Peninsula
2090   Group, West Antarctica: Implications for provenance and tectonic setting, *Geological Magazine*, *152*(4), 575-
2091   588.

2092   Castillo, P., et al. (2017), Provenance and age constraints of Paleozoic siliciclastic rocks from the Ellsworth
2093   Mountains in West Antarctica, as determined by detrital zircon geochronology, *GSA Bulletin*, *129*(11-12),
2094   1568-1584.

2095   Catania, G., et al. (2012), Variability in the mass flux of the Ross ice streams, West Antarctica, over the last
2096   millennium, *Journal of Glaciology*, *58*(210), 741-752.

2097   Chaput, J., et al. (2014), The crustal thickness of West Antarctica, *Journal of Geophysical Research: Solid
2098   Earth*, *119*(1), 378-395.

2099   Christianson, K., et al. (2016), Basal conditions at the grounding zone of Whillans Ice Stream, West
2100   Antarctica, from ice-penetrating radar, *Journal of Geophysical Research: Earth Surface*, *121*(11), 1954-1983.

2101   Christoffersen, P., et al. (2014), Significant groundwater contribution to Antarctic ice streams hydrologic
2102   budget, *Geophysical Research Letters*, *41*(6), 2003-2010.

2103   Chu, W., et al. (2018), Complex Basal Thermal Transition Near the Onset of Petermann Glacier, Greenland,
2104   *Journal of Geophysical Research: Earth Surface*, *123*(5), 985-995.

2105   Cianfarra, P., and F. Salvini (2016), Origin of the Adventure Subglacial Trench linked to Cenozoic extension in
2106   the East Antarctic Craton, *Tectonophysics*, *670*, 30-37.

2107   Cooper, M. A., et al. (2019), Subglacial roughness of the Greenland Ice Sheet: relationship with
2108   contemporary ice velocity and geology, *The Cryosphere*, *13*(11), 3093-3115.

2109   Corr, H., et al. (2007), Airborne radio-echo sounding of the Wilkes Subglacial Basin, the Transantarctic
2110   Mountains, and the Dome C region, 55-63.

2111   Cox, S. C., et al. (2019), ATA SCAR GeoMAP geology, edited by G. Science'.

2112   Craddock, J. P., et al. (2017), Detrital zircon provenance of upper Cambrian-Permian strata and tectonic
2113   evolution of the Ellsworth Mountains, West Antarctica, *Gondwana Research*, *45*, 191-207.

2114   Cui, X., et al. (2020), Bed topography of Princess Elizabeth Land in East Antarctica, *Earth Syst. Sci. Data*, *12*(4),
2115   2765-2774.

2116   Curtis, M. L., and S. A. Lomas (1999), Late Cambrian stratigraphy of the Heritage Range, Ellsworth Mountains:
2117   Implications for basin evolution, *Antarctic Science*, *11*(1), 63-77.

2118   Curtis, M. L. (2002), Palaeozoic to Mesozoic polyphase deformation of the Patuxent Range, Pensacola
2119   Mountains, Antarctica, *Antarctic Science*, *14*(2), 175-183.

2120   Curtis, M. L., et al. (2004), Structural and geochronological constraints of early Ross orogenic deformation in
2121   the Pensacola Mountains, Antarctica, *Bulletin of the Geological Society of America*, *116*(5-6), 619-636.

2122   Dall, J., et al. (2010), ESA'S POLarimetric Airborne Radar Ice Sounder (POLARIS): design and first
2123   results, *IET Radar, Sonar & Navigation, 4*(3), 488-496.

2124   Damaske, D., et al. (2003), Aeromagnetic anomaly investigations along the antarctic coast between Yule Bay
2125   and Mertz Glacier, *Terra Antartica*, *10*, 85-96.

2126   Davey, F. J., and G. Brancolini (1995), The Late Mesozoic and Cenozoic structural setting of the Ross Sea
2127   region, *Geology and Seismic Stratigraphy of the Antarctic Margin*, *68*, 167-182.

2128   Davey, F. J., et al. (2000), A revised correlation of the seismic stratigraphy at the Cape Roberts drill sites with
2129   the seismic stratigraphy of the Victoria Land Basin, Antarctica, *Terra Antartica*, *7*(3), 215-220.

2130   Davey, F. J., et al. (2016), Synchronous oceanic spreading and continental rifting in West Antarctica,
2131   *Geophysical Research Letters*, *43*(12), 6162-6169.

Davey, F. J., et al. (2021), Cenozoic continental rifting in the north-western Ross Sea, *New Zealand Journal of Geology and Geophysics*, 1-8.

Davies, D., et al. (2017), High-resolution sub-ice-shelf seafloor records of twentieth century ungrounding and retreat of Pine Island Glacier, West Antarctica, *Journal of Geophysical Research: Earth Surface*, *122*(9), 1698-1714.

Davis, J. K., et al. (2018), The crustal structure of the Enderby Basin, East Antarctica, *Marine Geophysical Research*, *40*, 1-16.

Dawson, E. J., et al. (2022), Ice mass loss sensitivity to the Antarctic ice sheet basal thermal state, *Nature Communications*, *13*(1), 4957.

De Santis, L., et al. (1999), The Eastern Ross Sea continental shelf during the Cenozoic: Implications for the West Antarctic ice sheet development, *Global and Planetary Change*, *23*(1-4), 173-196.

De Santis, L., et al. (2003), Seismo-stratigraphic analysis of the Wilkes Land continental margin (East Antarctica): Influence of glacially driven processes on the Cenozoic deposition, *Deep-Sea Research Part II: Topical Studies in Oceanography*, *50*(8-9), 1563-1594.

Delaney, I., et al. (2019), A Numerical Model for Fluvial Transport of Subglacial Sediment, *Journal of Geophysical Research: Earth Surface*, *124*(8), 2197-2223.

Dow, C. F., et al. (2022), Antarctic basal environment shaped by high-pressure flow through a subglacial river system, *Nature Geoscience*, *15*(11), 892-898.

Dowdeswell, J. A., et al. (2008), Autonomous underwater vehicles (AUVs) and investigations of the ice-ocean interface in Antarctic and Arctic waters, *Journal of Glaciology*, *54*(187), 661-672.

Dunham, C. K., et al. (2020), A joint inversion of receiver function and Rayleigh wave phase velocity dispersion data to estimate crustal structure in West Antarctica, *Geophysical Journal International*, *223*(3), 1644-1657.

Eagles, G., and R. A. Livermore (2002), Opening history of Powell Basin, Antarctic Peninsula, *Marine Geology*, *185*(3-4), 195-205.

Eagles, G., et al. (2018), Erosion at extended continental margins: Insights from new aerogeophysical data in eastern Dronning Maud Land, *Gondwana Research*, *63*, 105-116.

Eagles, G. (2019), A little spin in the Indian Ocean plate circuit, *Tectonophysics*, *754*, 80-100.

Eagles, G., and H. Eisermann (2020), The Skytrain plate and tectonic evolution of southwest Gondwana since Jurassic times, *Scientific Reports*, *10*(1), 19994.

Ebbing, J., et al. (2018), Earth tectonics as seen by GOCE - Enhanced satellite gravity gradient imaging, *Scientific Reports*, *8*(1).

Ebbing, J., et al. (2021), East Antarctica magnetically linked to its ancient neighbours in Gondwana, *Scientific Reports*, *11*(1).

Eisen, O., et al. (2015), On-ice vibroseis and snowstreamer systems for geoscientific research, *Polar Science*, *9*(1), 51-65.

Eisen, O., et al. (2020), Basal roughness of the East Antarctic Ice Sheet in relation to flow speed and basal thermal state, *Annals of Glaciology*, *61*(81), 162-175.

Eisermann, H., et al. (2020), Bathymetry Beneath Ice Shelves of Western Dronning Maud Land, East Antarctica, and Implications on Ice Shelf Stability, *Geophysical Research Letters*, *47*(12), e2019GL086724.

Elliot, D. H., et al. (2017), The Permo-Triassic Gondwana sequence, central Transantarctic Mountains, Antarctica: Zircon geochronology, provenance, and basin evolution, *Geosphere*, *13*(1), 155-178.

Enkin, R. J., et al. (2020), The Henkel Petrophysical Plot: Mineralogy and Lithology From Physical Properties, *Geochemistry, Geophysics, Geosystems*, *21*(1), e2019GC008818.

Escutia, C., et al. (2005), Cenozoic ice sheet history from East Antarctic Wilkes Land continental margin sediments, *Global and Planetary Change*, *45*(1), 51-81.

Evans, D. J. A., et al. (2006), Subglacial till: Formation, sedimentary characteristics and classification, *Earth-Science Reviews*, *78*(1), 115-176.

Evans, K. R., et al. (2018), Geology of the Nelson Limestone, Postel Nunatak, Patuxent Range, Antarctica, *Antarctic Science*, *30*(1), 29-43.

Evans, S., and G. D. Q. Robin (1966), Glacier depth-sounding from the air, *Nature*, *210*(5039), 883-885.

Evenick, J. C. (2021), Glimpses into Earth's history using a revised global sedimentary basin map, *Earth-Science Reviews*, *215*.

Ferraccioli, F., and E. Bozzo (2003), Cenozoic strike-slip faulting from the eastern margin of the Wilkes Subglacial Basin to the western margin of the Ross Sea Rift: an aeromagnetic connection, *Geological Society, London, Special Publications*, *210*(1), 109-133.

Ferraccioli, F., et al. (2005a), Subglacial imprints of early Gondwana break-up as identified from high resolution aerogeophysical data over western Dronning Maud Land, East Antarctica, *Terra Nova*, *17*(6), 573-579.

Ferraccioli, F., et al. (2005b), Tectonic and magmatic patterns in the Jutulstraumen rift (?) region, East Antarctica, as imaged by high-resolution aeromagnetic data, *Earth, Planets and Space*, *57*(8), 767-780.

Ferraccioli, F., et al. (2009a), Aeromagnetic exploration over the East Antarctic Ice Sheet: A new view of the Wilkes Subglacial Basin, *Tectonophysics*, *478*(1), 62-77.

Ferraccioli, F., et al. (2009b), Magmatic and tectonic patterns over the Northern Victoria Land sector of the Transantarctic Mountains from new aeromagnetic imaging, *Tectonophysics*, *478*(1-2), 43-61.

Ferraccioli, F., et al. (2011), East Antarctic rifting triggers uplift of the Gamburtsev Mountains, *Nature*, *479*(7373), 388-392.

Ferraccioli, F., et al. (2020), Processed line aeromagnetic data over the Recovery Lakes region and interior Dronning Maud Land, East Antarctica (2013) [Data set]. UK Polar Data Centre, Natural Environment Research Council, UK Research & Innovation. , edited.

Ferrar, H. (1907), Report on the field-geology of the region explored during the "Discovery" Antarctic Expedition, 1901-1904, Natl. Antarctic Expedition 1901-1904, Nat. Hist.,Geol.

Fielding, C. R., et al. (2008), Seismic facies and stratigraphy of the Cenozoic succession in McMurdo Sound, Antarctica: Implications for tectonic, climatic and glacial history, *Palaeogeography, Palaeoclimatology, Palaeoecology*, *260*(1-2), 8-29.

Fitzgerald, P. G., and J. W. Goodge (2022), Exhumation and tectonic history of inaccessible subglacial interior East Antarctica from thermochronology on glacial erratics, *Nature Communications*, *13*(1), 6217.

Foley, N., et al. (2015), Helicopter-borne transient electromagnetics in high-latitude environments: An application in the McMurdo Dry Valleys, Antarctica, *GEOPHYSICS*, *81*, WA87-WA99.

Forsberg, R., et al. (2018), Exploring the Recovery Lakes region and interior Dronning Maud Land, East Antarctica, with airborne gravity, magnetic and radar measurements, *Geological Society, London, Special Publications*, *461*(1), 23-34.

Francis, J. E., et al. (2006), *Cretaceous–Tertiary High-Latitude Palaeoenvironments: James Ross Basin, Antarctica*, Geological Society of London.

Frederick, B. C., et al. (2016), Distribution of subglacial sediments across the Wilkes Subglacial Basin, East Antarctica, *Journal of Geophysical Research F: Earth Surface*, *121*(4), 790-813.

Frémand, A. C., et al. (2022a), British Antarctic Survey's aerogeophysical data: releasing 25 years of airborne gravity, magnetic, and radar datasets over Antarctica, *Earth Syst. Sci. Data*, *14*(7), 3379-3410.

Frémand, A. C., et al. (2022b), Antarctic Bedmap data: FAIR sharing of 60 years of ice bed, surface and thickness data, *Earth Syst. Sci. Data Discuss.*, *2022*, 1-25.

Fretwell, P., et al. (2013), Bedmap2: Improved ice bed, surface and thickness datasets for Antarctica, *Cryosphere*, *7*(1), 375-393.

Gaina, C., et al. (2007), Breakup and early seafloor spreading between India and Antarctica, *Geophysical Journal International*, *170*(1), 151-169.

Gibbons, A. D., et al. (2013), The breakup of East Gondwana: Assimilating constraints from Cretaceous ocean basins around India into a best-fit tectonic model, *Journal of Geophysical Research: Solid Earth*, *118*(3), 808-822.

Gibson, C., et al. (2020), RAM-2 Drill system development: an upgrade of the Rapid Air Movement Drill, *Annals of Glaciology*, *62*, 1-10.

Glover, P. (2016), Archie's law – a reappraisal, *Solid Earth*, *7*, 1157-1169.

Gogineni, S., et al. (1998), An improved coherent radar depth sounder, *Journal of Glaciology*, *44*(148), 659-669.

Gohl, K., et al. (2013a), Deciphering tectonic phases of the Amundsen Sea Embayment shelf, West Antarctica, From a magnetic anomaly grid, *Tectonophysics*, *585*, 113-123.

Gohl, K., et al. (2013b), Seismic stratigraphic record of the Amundsen Sea Embayment shelf from pre-glacial to recent times: Evidence for a dynamic West Antarctic ice sheet, *Marine Geology*, *344*, 115-131.

Gohl, K., et al. (2017), MeBo70 Seabed Drilling on a Polar Continental Shelf: Operational Report and Lessons From Drilling in the Amundsen Sea Embayment of West Antarctica, *Geochemistry, Geophysics, Geosystems*, *18*(11), 4235-4250.

Gohl, K., et al. (2021), Evidence for a Highly Dynamic West Antarctic Ice Sheet During the Pliocene, *Geophysical Research Letters*, *48*(14), e2021GL093103.

Golynsky, A., et al. (2001), ADMAP – Magnetic anomaly map of the Antarctic, 1: 10 000 000 scale map, British Antarctic Survey, Cambridge, UK.

Golynsky, A., et al. (2006), ADMAP — A Digital Magnetic Anomaly Map of the Antarctic, in *Antarctica: Contributions to Global Earth Sciences*, edited by D. K. Fütterer, et al., pp. 109-116, Springer Berlin Heidelberg, Berlin, Heidelberg.

Golynsky, A. V., et al. (2018), New Magnetic Anomaly Map of the Antarctic, *Geophysical Research Letters*, *45*(13), 6437-6449.

Golynsky, D. A., and A. V. Golynsky (2007), Gaussberg rift - illusion or reality?, in *Antarctica: A Keystone in a Changing World--Online Proceedings of the 10th ISAES*, edited by A. K. Cooper and C. R. Raymond, USGS Open-File Report 2007-1047, Extended Abstract 168, 5 p.

Gong, D., et al. (2019), Coring of antarctic subglacial sediments, *Journal of Marine Science and Engineering*, *7*(6).

Gooch, B. T., et al. (2016), Potential groundwater and heterogeneous heat source contributions to ice sheet dynamics in critical submarine basins of East Antarctica, *Geochemistry, Geophysics, Geosystems*, *17*(2), 395-409.

Goodge, J. W. (2020), Geological and tectonic evolution of the Transantarctic Mountains, from ancient craton to recent enigma, *Gondwana Research*, *80*, 50-122.

Goodge, J. W., et al. (2021), Deep ice drilling, bedrock coring and dust logging with the Rapid Access Ice Drill (RAID) at Minna Bluff, Antarctica, *Annals of Glaciology*.

Granot, R., and J. Dyment (2018), Late Cenozoic unification of East and West Antarctica, *Nature Communications*, *9*(1), 3189.

Grikurov, G., et al. (2003), Antarctic tectonic and minerogenic provinces, *Arctic and Antarctic, Russian Academy of Sciences*, *2*, 26-47.

Grima, C., et al. (2019), Surface and basal boundary conditions at the Southern McMurdo and Ross Ice Shelves, Antarctica, *Journal of Glaciology*, *65*(252), 675-688.

Gulick, S. P. S., et al. (2017), Initiation and long-term instability of the East Antarctic Ice Sheet, *Nature*, *552*(7684), 225-229.

Gustafson, C. D., et al. (2022), A dynamic saline groundwater system mapped beneath an Antarctic ice stream, *Science*, *376*(6593), 640-644.

Haeger, C., and M. K. Kaban (2019), Decompensative Gravity Anomalies Reveal the Structure of the Upper Crust of Antarctica, *Pure and Applied Geophysics*, *176*(10), 4401-4414.

Halberstadt, A. R. W., et al. (2018), Characteristics of the deforming bed: Till properties on the deglaciated Antarctic continental shelf, *Journal of Glaciology*, *64*(248), 1014-1027.

Hale, R., et al. (2016), Multi-channel ultra-wideband radar sounder and imager, paper presented at 2016 IEEE International Geoscience and Remote Sensing Symposium (IGARSS), 10-15 July 2016.

Hambrey, M. J., and B. McKelvey (2000), Major Neogene fluctuations of the East Antarctic ice sheet: Stratigraphic evidence from the Lambert Glacier region, *Geology*, *28*(10), 887-890.

Harry, D. L., et al. (2018), Geodynamic models of the West Antarctic Rift System: Implications for the mantle thermal state, *Geosphere*, *14*(6), 2407-2429.

Hathway, B. (2000), Continental rift to back-arc basin: Jurassic-Cretaceous stratigraphical and structural evolution of the Larsen Basin, Antarctic Peninsula, *Journal of the Geological Society*, *157*(2), 417-432.

Haynes, M. S., et al. (2018), Geometric Power Fall-Off in Radar Sounding, *IEEE Transactions on Geoscience and Remote Sensing*, *56*(11), 6571-6585.

Hazzard, J., et al. (2022), Probabilistic Assessment of Antarctic Thermomechanical Structure: Impacts on Ice Sheet Stability, *EarthArXiv*.

Heliere, F., et al. (2007), Radio Echo Sounding of Pine Island Glacier, West Antarctica: Aperture Synthesis Processing and Analysis of Feasibility From Space, *IEEE Transactions on Geoscience and Remote Sensing*, *45*(8), 2573-2582.

Hill, G. J. (2020), On the Use of Electromagnetics for Earth Imaging of the Polar Regions, *Surveys in Geophysics*, *41*(1), 5-45.

Hillenbrand, C. D., et al. (2014), Reconstruction of changes in the Weddell Sea sector of the Antarctic Ice Sheet since the Last Glacial Maximum, *Quaternary Science Reviews*, *100*, 111-136.

Hirt, C., et al. (2016), A new degree-2190 (10 km resolution) gravity field model for Antarctica developed from GRACE, GOCE and Bedmap2 data, *Journal of Geodesy*, *90*(2), 105-127.

Hochmuth, K., and K. Gohl (2019), Seaward growth of Antarctic continental shelves since establishment of a continent-wide ice sheet: Patterns and mechanisms, *Palaeogeography, Palaeoclimatology, Palaeoecology*, *520*, 44-54.

2300 Hochmuth, K., et al. (2020), The Evolving Paleobathymetry of the Circum-Antarctic Southern Ocean Since 34
2301 Ma: A Key to Understanding Past Cryosphere-Ocean Developments, *Geochemistry, Geophysics, Geosystems*,
2302 *21*(8), e2020GC009122.

2303 Hochmuth, K., et al. (2022), Southern Ocean biogenic blooms freezing-in Oligocene colder climates, *Nature*
2304 *Communications*, *13*(1), 6785.

2305 Hodgson, D. A., et al. (2016), Technologies for retrieving sediment cores in Antarctic subglacial settings,
2306 *Philosophical Transactions of the Royal Society A: Mathematical, Physical and Engineering Sciences*,
2307 *374*(2059).

2308 Holschuh, N., et al. (2020), Linking postglacial landscapes to glacier dynamics using swath radar at Thwaites
2309 Glacier, Antarctica, *Geology*, *48*(3), 268-272.

2310 Hooyer, T. S., et al. (2012), Control of glacial quarrying by bedrock joints, *Geomorphology*, *153-154*, 91-101.

2311 Horgan, H., et al. (2005), Seismic stratigraphy of the Plio-Pleistocene Ross Island flexural moat-fill: A
2312 prognosis for ANDRILL Program drilling beneath McMurdo-Ross Ice Shelf, *Global and Planetary Change*,
2313 *45*(1-3 SPEC. ISS.), 83-97.

2314 Horgan, H. J., et al. (2021), Grounding zone subglacial properties from calibrated active-source seismic
2315 methods, *Cryosphere*, *15*(4), 1863-1880.

2316 Huang, X., and W. Jokat (2016), Sedimentation and potential venting on the rifted continental margin of
2317 Dronning Maud Land, *Marine Geophysical Research*, *37*.

2318 Huerta, A. D., and D. L. Harry (2007), The transition from diffuse to focused extension: Modeled evolution of
2319 the West Antarctic Rift system, *Earth and Planetary Science Letters*, *255*(1), 133-147.

2320 Hunter, M. A., and D. J. Cantrill (2006), A new stratigraphy for the Latady Basin, Antarctic Peninsula: Part 2,
2321 Latady Group and basin evolution, *Geological Magazine*, *143*(6), 797-819.

2322 Hunter, R. J., et al. (1996), Aeromagnetic data from the southern Weddell Sea embayment and adjacent
2323 areas: Synthesis and interpretation, in *Geological Society Special Publication*, edited, pp. 143-154.

2324 Isanina, E., et al. (2009), Deep structure of the Vostok Basin, East Antarctica as deduced from seismological
2325 observations, *Geotectonics*, *43*, 221-225.

2326 Isbell, J. L., et al. (2008), Permian glacigenic deposits in the Transantarctic Mountains, Antarctica, in *Special*
2327 *Paper of the Geological Society of America*, edited, pp. 59-70.

2328 Jamieson, S. S., et al. (2010), The evolution of the subglacial landscape of Antarctica, *Earth and Planetary*
2329 *Science Letters*, *293*(1-2), 1-27.

2330 Jamieson, S. S. R., et al. (2014), The glacial geomorphology of the Antarctic ice sheet bed, *Antarctic Science*,
2331 *26*(6), 724-741.

2332 Jamieson, S. S. R., et al. (2016), An extensive subglacial lake and canyon system in Princess Elizabeth Land,
2333 East Antarctica, *Geology*, *44*(2), 87-90.

2334 Jensen, T. E., and R. Forsberg (2018), Helicopter Test of a Strapdown Airborne Gravimetry System, *Sensors*
2335 *(Basel, Switzerland)*, *18*(9), 3121.

2336 Johnston, L., et al. (2008), Cenozoic basin evolution beneath the southern McMurdo Ice Shelf, Antarctica,
2337 *Global and Planetary Change*, *62*, 61-76.

2338 Jokat, W., et al. (2010), New aeromagnetic data from the western Enderby Basin and consequences for
2339 Antarctic-India break-up, *Geophysical Research Letters*, *37*(21).

2340 Jokat, W., and U. Herter (2016), Jurassic failed rift system below the Filchner-Ronne-Shelf, Antarctica: New
2341 evidence from geophysical data, *Tectonophysics*, *688*, 65-83.

2342 Jokat, W., et al. (2021), The early drift of the Indian plate, *Sci Rep*, *11*(1), 10796.

Jones, P., et al. (2002), Detecting rift basins in the Evans Ice Stream region of West Antarctica using airborne gravity data, *Tectonophysics*, *347*, 25-41.

Jordan, T. A., et al. (2010a), Hypothesis for mega-outburst flooding from a palaeo-subglacial lake beneath the East Antarctic Ice Sheet, *Terra Nova*, *22*(4), 283-289.

Jordan, T. A., et al. (2010b), Aerogravity evidence for major crustal thinning under the Pine Island Glacier region (West Antarctica), *Bulletin of the Geological Society of America*, *122*(5-6), 714-726.

Jordan, T. A., et al. (2013a), Crustal architecture of the Wilkes Subglacial Basin in East Antarctica, as revealed from airborne gravity data, *Tectonophysics*, *585*, 196-206.

Jordan, T. A., et al. (2013b), Inland extent of the Weddell Sea Rift imaged by new aerogeophysical data, *Tectonophysics*, *585*, 137-160.

Jordan, T. A., et al. (2017a), New geophysical compilations link crustal block motion to Jurassic extension and strike-slip faulting in the Weddell Sea Rift System of West Antarctica, *Gondwana Research*, *42*, 29-48.

Jordan, T. A., and D. Becker (2018), Investigating the distribution of magmatism at the onset of Gondwana breakup with novel strapdown gravity and aeromagnetic data, *Physics of the Earth and Planetary Interiors*, *282*, 77-88.

Jordan, T. A., et al. (2020), The geological history and evolution of West Antarctica, *Nature Reviews Earth & Environment*, *1*(2), 117-133.

Jordan, T. A., et al. (2022), An embayment in the East Antarctic basement constrains the shape of the Rodinian continental margin, *Communications Earth & Environment*, *3*(1), 52.

Jordan, T. M., et al. (2017b), Self-affine subglacial roughness: consequences for radar scattering and basal water discrimination in northern Greenland, *The Cryosphere*, *11*(3), 1247-1264.

Karner, G. D., et al. (2005), Gravity anomalies of sedimentary basins and their mechanical implications: Application to the Ross Sea basins, West Antarctica, *Earth and Planetary Science Letters*, *235*(3-4), 577-596.

Kennicutt, M. C., et al. (2019), Sustained Antarctic Research: A 21st Century Imperative, *One Earth*, *1*(1), 95-113.

Key, K., and M. R. Siegfried (2017), The feasibility of imaging subglacial hydrology beneath ice streams with ground-based electromagnetics, *Journal of Glaciology*, *63*(241), 755-771.

Kim, S., et al. (2018), Seismic stratigraphy of the Central Basin in northwestern Ross Sea slope and rise, Antarctica: Clues to the late Cenozoic ice-sheet dynamics and bottom-current activity, *Marine Geology*, *395*, 363-379.

Kjær, K. H., et al. (2018), A large impact crater beneath Hiawatha Glacier in northwest Greenland, *Sci Adv*, *4*(11), eaar8173.

König, M., and W. Jokat (2006), The Mesozoic breakup of the Weddell Sea, *Journal of Geophysical Research: Solid Earth*, *111*(12).

Kovesi, P. (1999), Image Features from Phase Congruency, *VIDERE*, *1*(3), 2-26.

Krabbendam, M., and N. F. Glasser (2011), Glacial erosion and bedrock properties in NW Scotland: Abrasion and plucking, hardness and joint spacing, *Geomorphology*, *130*(3), 374-383.

Kristoffersen, Y., et al. (2014), Reassembling Gondwana: A new high quality constraint from vibroseis exploration of the sub-ice shelf geology of the East Antarctic continental margin, *Journal of Geophysical Research: Solid Earth*, *119*(12), 9171-9182.

Krohne, N., et al. (2016), The Shackleton Range (East Antarctica): an alien block at the rim of Gondwana?, *Geological Magazine*, *155*(4), 841-864.

Kuhl, T., et al. (2021), Agile Sub-Ice Geological (ASIG) Drill development and Pirrit Hills field project, *Annals of Glaciology*, *62*(84), 53-66.

Kulessa, B., et al. (2006), Time-lapse imaging of subglacial drainage conditions using three-dimensional inversion of borehole electrical resistivity data, *Journal of Glaciology*, *52*(176), 49-57.

Kulessa, B. (2007), A Critical Review of the Low-Frequency Electrical Properties of Ice Sheets and Glaciers, *Journal of Environmental Engineering Geophysics*, *12*, 23-36.

Kulessa, B., et al. (2019), Heat and groundwater transport between the Antarctic Ice Sheet and subglacial sedimentary basins from electromagnetic geophysical measurements, in *SEG Technical Program Expanded Abstracts* edited by D. Bevc and O. Nedorub, pp. 4819-4823.

Kulhanek, D. K., et al. (2019), Revised chronostratigraphy of DSDP Site 270 and late Oligocene to early Miocene paleoecology of the Ross Sea sector of Antarctica, *Global and Planetary Change*, *178*, 46-64.

Kvas, A., et al. (2021), GOCO06s – a satellite-only global gravity field model, *Earth Syst. Sci. Data*, *13*(1), 99-118.

Lane, T. P., et al. (2015), Controls on bedrock bedform development beneath the Uummannaq Ice Stream onset zone, West Greenland, *Geomorphology*, *231*, 301-313.

Lawrence, J. F., et al. (2006), Rayleigh wave phase velocity analysis of the Ross Sea, Transantarctic Mountains, and East Antarctica from a temporary seismograph array, *Journal of Geophysical Research: Solid Earth*, *111*(B6).

Le Brocq, A. M., et al. (2013), Evidence from ice shelves for channelized meltwater flow beneath the Antarctic Ice Sheet, *Nature Geosci*, *6*(11), 945-948.

Leitchenkov, G. L., and G. A. Kudryavtzev (1997), Structure and Origin of the Earth's Crust in the Weddell Sea Embayment (beneath the Front of the Filchner and Ronne Ice Shelves) from Deep Seismic Sounding data, *Polarforschung*, *67*(3), 143-154.

Leitchenkov, G. L., et al. (2016), Geology and environments of subglacial Lake Vostok, *Philosophical Transactions of the Royal Society A: Mathematical, Physical and Engineering Sciences*, *374*(2059).

Levy, R., et al. (2016), Antarctic ice sheet sensitivity to atmospheric CO_2 variations in the early to mid-Miocene, *Proceedings of the National Academy of Sciences*, *113*(13), 3453-3458.

Li, L., et al. (2022), Sedimentary basins reduce stability of Antarctic ice streams through groundwater feedbacks, *Nature Geoscience*, *15*(8), 645-650.

Lin, F.-C., et al. (2012), Joint inversion of Rayleigh wave phase velocity and ellipticity using USArray: Constraining velocity and density structure in the upper crust, *Geophysical Research Letters*, *39*(12).

Lindeque, A., et al. (2013), Deep-sea pre-glacial to glacial sedimentation in the Weddell Sea and southern Scotia Sea from a cross-basin seismic transect, *Marine Geology*, *336*, 61-83.

Lindeque, A., et al. (2016a), Seismic stratigraphy along the Amundsen Sea to Ross Sea continental rise: A cross-regional record of pre-glacial to glacial processes of the West Antarctic margin, *Palaeogeography, Palaeoclimatology, Palaeoecology*, *443*, 183-202.

Lindeque, A., et al. (2016b), Preglacial to glacial sediment thickness grids for the Southern Pacific Margin of West Antarctica, *Geochemistry, Geophysics, Geosystems*, *17*(10), 4276-4285.

Lisker, F., et al. (2007), Thermal history of the Vestfold Hills (East Antarctica) between Lambert rifting and Gondwana break-up, evidence from apatite fission track data, *Antarctic Science*, *19*(1), 97-106.

Livingstone, S. J., et al. (2022), Subglacial lakes and their changing role in a warming climate, *Nature Reviews Earth & Environment*, *3*(2), 106-124.

Lloyd, A. J., et al. (2015), A seismic transect across West Antarctica: Evidence for mantle thermal anomalies beneath the Bentley Subglacial Trench and the Marie Byrd Land Dome, *Journal of Geophysical Research: Solid Earth*, *120*(12), 8439-8460.

Lloyd, A. J., et al. (2020), Seismic Structure of the Antarctic Upper Mantle Imaged with Adjoint Tomography, *Journal of Geophysical Research: Solid Earth*, *125*(3).

Lösing, M., and J. Ebbing (2021), Predicting Geothermal Heat Flow in Antarctica With a Machine Learning Approach, *Journal of Geophysical Research: Solid Earth*, *126*(6), e2020JB021499.

Lowry, D. P., et al. (2020), Geologic controls on ice sheet sensitivity to deglacial climate forcing in the Ross Embayment, Antarctica, *Quaternary Science Advances*, *1*, 100002.

Luyendyk, B. P., et al. (2001), Structural and tectonic evolution of the Ross Sea rift in the Cape Colbeck region, Eastern Ross Sea, Antarctica, *Tectonics*, *20*(6), 933-958.

Lythe, M. B., and D. G. Vaughan (2001), BEDMAP: A new ice thickness and subglacial topographic model of Antarctica, *Journal of Geophysical Research: Solid Earth*, *106*(B6), 11335-11351.

MacGregor, J. A., et al. (2021), The Scientific Legacy of NASA's Operation IceBridge, *Reviews of Geophysics*, *59*(2).

MacKie, E. J., et al. (2020), Antarctic Topographic Realizations and Geostatistical Modeling Used to Map Subglacial Lakes, *Journal of Geophysical Research: Earth Surface*, *125*(3), e2019JF005420.

MacKie, E. J., et al. (2021), Stochastic modeling of subglacial topography exposes uncertainty in water routing at Jakobshavn Glacier, *Journal of Glaciology*, *67*(261), 75-83.

Maggi, M., et al. (2016), Erosion by tectonic carving in the Concordia Subglacial Fault Zone, East Antarctica, *Earth and Planetary Science Letters*, *433*, 99-108.

Maldonado, A., et al. (1994), Forearc tectonic evolution of the South Shetland margin, Antarctic Peninsula, *Tectonics*, *13*(6), 1345-1370.

Maldonado, A., et al. (2006), Ocean basins near the Scotia-Antarctic plate boundary; influence of tectonics and paleoceanography on the Cenozoic deposits, *Marine Geophysical Researches*, *27*(2), 83-107.

Maritati, A., et al. (2016), The tectonic development and erosion of the Knox Subglacial Sedimentary Basin, East Antarctica, *Geophysical Research Letters*, *43*(20), 10,728-710,737.

Maritati, A., et al. (2019), Fingerprinting Proterozoic Bedrock in Interior Wilkes Land, East Antarctica, *Scientific Reports*, *9*(1).

Maritati, A., et al. (2020), Pangea Rifting Shaped the East Antarctic Landscape, *Tectonics*, *39*(8), e2020TC006180.

Maritati, A., et al. (2021), Provenance of Upper Jurassic–Lower Cretaceous strata in the Mentelle Basin, southwestern Australia, reveals a trans-Gondwanan fluvial pathway, *Gondwana Research*, *93*, 128-141.

Marschalek, J. W., et al. (2021), A large West Antarctic Ice Sheet explains early Neogene sea-level amplitude, *Nature*, *600*(7889), 450-455.

Marschall, H. R., et al. (2013), Mesoproterozoic subduction under the eastern edge of the Kalahari-Grunehogna Craton preceding Rodinia assembly: The Ritscherflya detrital zircon record, Ahlmannryggen (Dronning Maud Land, Antarctica), *Precambrian Research*, *236*, 31-45.

Matsuoka, K. (2011), Pitfalls in radar diagnosis of ice-sheet bed conditions: Lessons from englacial attenuation models, *Geophysical Research Letters*, *38*(5).

Mawson, D. (1928), Unsolved Problems of Antarctic Exploration and Research, *American Geographical Society Special Publication*, *7*, 253-266.

Mawson, D. (1940), Sedimentary Rocks, Australasian Antarctic Expedition, 1911-1914, Sci. Rept., Ser. A, Geol., vol. 4, pt.

11, pp. 347-367.

McCormack, F. S., et al. (2022), Fine-Scale Geothermal Heat Flow in Antarctica Can Increase Simulated Subglacial Melt Estimates, *Geophysical Research Letters*, *49*(15), e2022GL098539.

McKay, R., et al. (2012a), Antarctic and Southern Ocean influences on Late Pliocene global cooling, *Proceedings of the National Academy of Sciences of the United States of America*, *109*(17), 6423-6428.

McKay, R., et al. (2012b), Pleistocene variability of Antarctic Ice Sheet extent in the Ross Embayment, *Quaternary Science Reviews*, *34*, 93-112.

McKay, R. M., et al. (2016), Antarctic Cenozoic climate history from sedimentary records: ANDRILL and beyond, *Philosophical Transactions of the Royal Society A: Mathematical, Physical and Engineering Sciences*, *374*(2059).

McLean, M. A., et al. (2008), Three-dimensional inversion modelling of a Neoproterozoic basin in the southern Prince Charles Mountains, East Antarctica, *Tectonophysics*, *456*(3-4), 180-193.

McLean, M. A., et al. (2009), Basement interpretations from airborne magnetic and gravity data over the lambert rift region of east Antarctica, *Journal of Geophysical Research B: Solid Earth*, *114*(6).

McLoughlin, S., and A. N. Drinnan (1997), Revised stratigraphy of the Permian Bainmedart Coal Measures, northern Prince Charles Mountains, East Antarctica, *Geological Magazine*, *134*(3), 335-353.

McMahon, K. L., and M. A. Lackie (2006), Seismic reflection studies of the Amery Ice Shelf, East Antarctica: delineating meteoric and marine ice, *Geophysical Journal International*, *166*(2), 757-766.

Mieth, M., and W. Jokat (2014), New aeromagnetic view of the geological fabric of southern Dronning Maud Land and Coats Land, East Antarctica, *Gondwana Research*, *25*(1), 358-367.

Mikhalsky, E. V., et al. (2020), Low-grade Sandow Group metasediments of the Denman Glacier area (East Antarctica): Chemical composition, age and provenance from U–Pb detrital zircon data, with some palaeotectonic implications, *Polar Science*, *26*, 100587.

Mishra, D. C., et al. (1999), Crustal structure based on gravity-magnetic modelling constrained from seismic studies under Lambert Rift, Antarctica and Godavari and Mahanadi rifts, India and their interrelationship, *Earth and Planetary Science Letters*, *172*(3-4), 287-300.

Montelli, A., et al. (2019), Seismic stratigraphy of the Sabrina Coast shelf, East Antarctica: Early history of dynamic meltwater-rich glaciations, *GSA Bulletin*, *132*(3-4), 545-561.

Morlighem, M. (2020), MEaSUREs BedMachine Antarctica, Version 2, edited, NASA National Snow and Ice Data Center Distributed Active Archive Center, Boulder, Colorado USA.

Morlighem, M., et al. (2020), Deep glacial troughs and stabilizing ridges unveiled beneath the margins of the Antarctic ice sheet, *Nature Geoscience*, *13*(2), 132-137.

Mouginot, J., et al. (2019), Continent-Wide, Interferometric SAR Phase, Mapping of Antarctic Ice Velocity, *Geophysical Research Letters*, *46*(16), 9710-9718.

Mulder, J. A., et al. (2019), A Multiproxy provenance approach to uncovering the assembly of East Gondwana in Antarctica, *Geology*, *47*(7), 645-649.

Müller, R. D., et al. (2019), A Global Plate Model Including Lithospheric Deformation Along Major Rifts and Orogens Since the Triassic, *Tectonics*, *38*(6), 1884-1907.

Muto, A., et al. (2016), Subglacial bathymetry and sediment distribution beneath Pine Island Glacier ice shelf modeled using aerogravity and in situ geophysical data: New results, *Earth and Planetary Science Letters*, *433*, 63-75.

2512 Muto, A., et al. (2019a), Bed-type variability and till (dis)continuity beneath Thwaites Glacier, West
2513 Antarctica, *Annals of Glaciology*, *60*(80), 82-90.

2514 Muto, A., et al. (2019b), Relating bed character and subglacial morphology using seismic data from Thwaites
2515 Glacier, West Antarctica, *Earth and Planetary Science Letters*, *507*, 199-206.

2516 Naish, T., et al. (2009), Obliquity-paced Pliocene West Antarctic ice sheet oscillations, *Nature*, *458*(7236),
2517 322-328.

2518 Naylor, S., et al. (2008), The IGY and the ice sheet: surveying Antarctica, *Journal of Historical Geography*,
2519 *34*(4), 574-595.

2520 Noble, T. L., et al. (2020), The Sensitivity of the Antarctic Ice Sheet to a Changing Climate: Past, Present, and
2521 Future, *Reviews of Geophysics*, *58*(4), e2019RG000663.

2522 Olesen, A., et al. (2020), Processed line aerogravity data over the Recovery Lakes region and interior
2523 Dronning Maud Land, East Antarctica (2013) [Data set]. UK Polar Data Centre, Natural Environment Research
2524 Council, UK Research & Innovation., edited.

2525 Olierook, H. K. H., et al. (2016), Bunbury Basalt: Gondwana breakup products or earliest vestiges of the
2526 Kerguelen mantle plume?, *Earth and Planetary Science Letters*, *440*, 20-32.

2527 Paden, J., et al. (2010), Ice-sheet bed 3-D tomography, *Journal of Glaciology*, *56*(195), 3-11.

2528 Pappa, F., et al. (2019a), Moho Depths of Antarctica: Comparison of Seismic, Gravity, and Isostatic Results,
2529 *Geochemistry, Geophysics, Geosystems*, *20*(3), 1629-1645.

2530 Pappa, F., et al. (2019b), Modeling Satellite Gravity Gradient Data to Derive Density, Temperature, and
2531 Viscosity Structure of the Antarctic Lithosphere, *Journal of Geophysical Research: Solid Earth*, *124*(11),
2532 12053-12076.

2533 Paxman, G. J. G., et al. (2017), Uplift and tilting of the Shackleton Range in East Antarctica driven by glacial
2534 erosion and normal faulting, *Journal of Geophysical Research: Solid Earth*, *122*(3), 2390-2408.

2535 Paxman, G. J. G., et al. (2019a), Subglacial Geology and Geomorphology of the Pensacola-Pole Basin, East
2536 Antarctica, *Geochemistry, Geophysics, Geosystems*, *20*(6), 2786-2807.

2537 Paxman, G. J. G., et al. (2019b), Reconstructions of Antarctic topography since the Eocene–Oligocene
2538 boundary, *Palaeogeography, Palaeoclimatology, Palaeoecology*, *535*, 109346.

2539 Paxman, G. J. G., et al. (2020), Long-Term Increase in Antarctic Ice Sheet Vulnerability Driven by Bed
2540 Topography Evolution, *Geophysical Research Letters*, *47*(20), e2020GL090003.

2541 Pérez, L. F., et al. (2021), Early and middle Miocene ice sheet dynamics in the Ross Sea: Results from
2542 integrated core-log-seismic interpretation, *GSA Bulletin*, *134*(1-2), 348-370.

2543 Person, M., et al. (2007), Pleistocene hydrology of North America: The role of ice sheets in reorganizing
2544 groundwater flow systems, *Reviews of Geophysics*, *45*(3).

2545 Person, M., et al. (2012), Models of ice-sheet hydrogeologic interactions: A review, *Geofluids*, *12*(1), 58-78.

2546 Peters, L. E., et al. (2006), Subglacial sediments as a control on the onset and location of two Siple Coast ice
2547 streams, West Antarctica, *Journal of Geophysical Research: Solid Earth*, *111*(1).

2548 Peters, M. E., et al. (2007), Along-Track Focusing of Airborne Radar Sounding Data From West Antarctica for
2549 Improving Basal Reflection Analysis and Layer Detection, *IEEE Transactions on Geoscience and Remote
2550 Sensing*, *45*(9), 2725-2736.

2551 Phillips, G., and A. L. Läufer (2009), Brittle deformation relating to the Carboniferous–Cretaceous evolution
2552 of the Lambert Graben, East Antarctica: A precursor for Cenozoic relief development in an intraplate and
2553 glaciated region, *Tectonophysics*, *471*(3–4), 216-224.

Pollard, D., and R. M. DeConto (2020), Continuous simulations over the last 40 million years with a coupled Antarctic ice sheet-sediment model, *Palaeogeography, Palaeoclimatology, Palaeoecology*, *537*, 109374.

Pourpoint, M., et al. (2019), Constraints on shallow subglacial structure beneath Thwaites Glacier from joint inversion of receiver function and surface wave data. abstract #NS11B-0632, in *AGU Fall Meeting 2019 Abstracts* edited by AGU.

Pyle, M. L., et al. (2010), Crustal structure of the Transantarctic Mountains near the Ross Sea from ambient seismic noise tomography, *Journal of Geophysical Research: Solid Earth*, *115*(11).

Reid, A. B. (1980), Aeromagnetic survey design, *Geophysics*, *45*(5), 973-976.

Reid, A. B., et al. (1990), Magnetic interpretation in three dimensions using Euler deconvolution, *Geophysics*, *55*(1), 80-91.

Riedel, S., et al. (2012), Mapping tectonic provinces with airborne gravity and radar data in Dronning Maud Land, East Antarctica, *Geophysical Journal International*, *189*(1), 414-427.

Riedel, S., et al. (2013), Interpretation of new regional aeromagnetic data over Dronning Maud Land (East Antarctica), *Tectonophysics*, *585*, 161-171.

Riley, T. R., et al. (2012), Chrono- and lithostratigraphy of a Mesozoic-Tertiary fore- to intra-arc basin: Adelaide Island, Antarctic Peninsula, *Geological Magazine*, *149*(5), 768-782.

Riley, T. R., et al. (2020), Magmatism of the Weddell Sea rift system in Antarctica: Implications for the age and mechanism of rifting and early stage Gondwana breakup, *Gondwana Research*, *79*, 185-196.

Rippin, D. M., et al. (2014), Basal roughness of the Institute and Möller Ice Streams, West Antarctica: Process determination and landscape interpretation, *Geomorphology*, *214*, 139-147.

Robin, G. d. Q. (1958), Glaciology III: Seismic Shooting and Related Investigations, *Norwegian–British–Swedish Antarctic Expedition, 1949–52, Scientific Results*, *5*.

Rogenhagen, J., et al. (2004), Improved seismic stratigraphy of the Mesozoic Weddell Sea, *Marine Geophysical Research*, *25*(3-4), 265-282.

Rolland, Y., et al. (2019), Late Paleozoic Ice Age glaciers shaped East Antarctica landscape, *Earth and Planetary Science Letters*, *506*, 123-133.

Rosier, S. H. R., et al. (2018), A New Bathymetry for the Southeastern Filchner-Ronne Ice Shelf: Implications for Modern Oceanographic Processes and Glacial History, *Journal of Geophysical Research: Oceans*, *123*(7), 4610-4623.

Ruppel, A., et al. (2018), New geophysical data from a key region in East Antarctica: Estimates for the spatial extent of the Tonian Oceanic Arc Super Terrane (TOAST), *Gondwana Research*, *59*, 97-107.

Salvini, F., et al. (1997), Cenozoic geodynamics of the Ross Sea region, Antarctica: Crustal extension, intraplate strike-slip faulting, and tectonic inheritance, *Journal of Geophysical Research B: Solid Earth*, *102*(11), 24669-24696.

Sanchez, G., et al. (2021), PetroChron Antarctica: A Geological Database for Interdisciplinary Use, *Geochemistry, Geophysics, Geosystems*, *22*(12).

Sandwell, D. T., et al. (2014), New global marine gravity model from CryoSat-2 and Jason-1 reveals buried tectonic structure, *Science*, *346*(6205), 65-67.

Sauermilch, I., et al. (2019), Tectonic, Oceanographic, and Climatic Controls on the Cretaceous-Cenozoic Sedimentary Record of the Australian-Antarctic Basin, *Journal of Geophysical Research: Solid Earth*, *124*(8), 7699-7724.

Sauli, C., et al. (2021), Neogene Development of the Terror Rift, Western Ross Sea, Antarctica, *Geochemistry, Geophysics, Geosystems*, *22*(3).

Scambos, T. A., et al. (2017), How much, how fast?: A science review and outlook for research on the instability of Antarctica's Thwaites Glacier in the 21st century, *Global and Planetary Change*, *153*, 16-34.

Scanlan, K. M., et al. (2022), Polarimetric Airborne Radar Sounding as an Approach to Characterizing Subglacial Röthlisberger Channels, *IEEE Journal of Selected Topics in Applied Earth Observations and Remote Sensing*, *15*, 4455-4467.

Scheinert, M., et al. (2016), New Antarctic gravity anomaly grid for enhanced geodetic and geophysical studies in Antarctica, *Geophysical Research Letters*, *43*(2), 600-610.

Scher, H. D., and E. E. Martin (2006), Timing and climatic consequences of the opening of Drake Passage, *Science*, *312*(5772), 428-430.

Scher, H. D., et al. (2015), Onset of Antarctic Circumpolar Current 30 million years ago as Tasmanian Gateway aligned with westerlies, *Nature*, *523*(7562), 580-583.

Schoof, C. (2010), Ice-sheet acceleration driven by melt supply variability, *Nature*, *468*(7325), 803-806.

Schroeder, D. M., et al. (2013), Evidence for a water system transition beneath Thwaites Glacier, West Antarctica, *Proceedings of the National Academy of Sciences*, *110*(30), 12225-12228.

Schroeder, D. M., et al. (2015), Estimating Subglacial Water Geometry Using Radar Bed Echo Specularity: Application to Thwaites Glacier, West Antarctica, *IEEE Geoscience and Remote Sensing Letters*, *12*(3), 443-447.

Schroeder, D. M., et al. (2019), Multidecadal observations of the Antarctic ice sheet from restored analog radar records, *Proceedings of the National Academy of Sciences*, *116*(38), 18867-18873.

Schroeder, D. M., et al. (2020), Five decades of radioglaciology, *Annals of Glaciology*, *61*(81), 1-13.

Shen, W., et al. (2017), Seismic evidence for lithospheric foundering beneath the southern Transantarctic Mountains, Antarctica, *Geology*, *46*.

Shen, W., et al. (2018), The Crust and Upper Mantle Structure of Central and West Antarctica From Bayesian Inversion of Rayleigh Wave and Receiver Functions, *Journal of Geophysical Research: Solid Earth*, *123*(9), 7824-7849.

Siddoway, C. S., et al. (2004), Ross Sea mylonites and the timing of intracontinental extension within the West Antarctic rift system, *Geology*, *32*(1), 57-60.

Siddoway, C. S. (2008), Tectonics of the West Antarctic Rift System: new light on the history and dynamics of distributed intracontinental extension, *Antarctica: A keystone in a changing world*, 91-114.

Siegert, M., et al. (2011), Vostok Subglacial Lake: A Review of Geophysical Data Regarding Its Discovery and Topographic Setting, *Washington DC American Geophysical Union Geophysical Monograph Series*, *192*, 45-60.

Siegert, M. J., et al. (2005), Spectral roughness of subglacial topography and implications for former ice-sheet dynamics in East Antarctica, *Global and Planetary Change*, *45*(1), 249-263.

Siegert, M. J., et al. (2016), Subglacial controls on the flow of Institute Ice Stream, West Antarctica, *Annals of Glaciology*, *57*(73), 19-24.

Siegert, M. J., et al. (2018), Antarctic subglacial groundwater: A concept paper on its measurement and potential influence on ice flow, in *Geological Society Special Publication*, edited, pp. 197-213.

Smellie, J. L., and K. D. Collerson (2021), Chapter 5.5   Gaussberg: volcanology and petrology, in *Volcanism in Antarctica: 200 Million Years of Subduction, Rifting and Continental Break-up*, edited by J. L. Smellie, et al., p. 0, Geological Society of London.

Smith, A. M., et al. (2013), Influence of subglacial conditions on ice stream dynamics: Seismic and potential field data from Pine Island Glacier, West Antarctica, *Journal of Geophysical Research: Solid Earth*, *118*(4), 1471-1482.

Smith, C., et al. (2019a), New species from the Sabrina Flora: an early Paleogene pollen and spore assemblage from the Sabrina Coast, East Antarctica, *Palynology*, *43*(4), 650-659.

Smith, E. C., et al. (2020), Detailed Seismic Bathymetry Beneath Ekström Ice Shelf, Antarctica: Implications for Glacial History and Ice-Ocean Interaction, *Geophysical Research Letters*, *47*(10), e2019GL086187.

Smith, J. A., et al. (2019b), The marine geological imprint of Antarctic ice shelves, *Nature Communications*, *10*(1), 5635.

Song, T., and P. A. Cawood (2000), Structural styles in the Perth Basin associated with the Mesozoic break-up of Greater India and Australia, *Tectonophysics*, *317*(1-2), 55-72.

Stagg, H., et al. (2004), Geology of the Continental Margin of Enderby and Mac. Robertson Lands, East Antarctica: Insights from a Regional Data Set, *Marine Geophysical Researches*, *25*, 183-219.

Stål, T., et al. (2019), A Multivariate Approach for Mapping Lithospheric Domain Boundaries in East Antarctica, *Geophysical Research Letters*, *46*(17-18), 10404-10416.

Straume, E. O., et al. (2019), GlobSed: Updated Total Sediment Thickness in the World's Oceans, *Geochemistry, Geophysics, Geosystems*, *20*(4), 1756-1772.

Studinger, M., et al. (2001), Subglacial sediments: A regional geological template for iceflow in West Antarctica, *Geophysical Research Letters*, *28*(18), 3493-3496.

Studinger, M., et al. (2003), Geophysical models for the tectonic framework of the Lake Vostok region, East Antarctica, *Earth and Planetary Science Letters*, *216*(4), 663-677.

Studinger, M., et al. (2004), Sub-ice geology inland of the Transantarctic Mountains in light of new aerogeophysical data, *Earth and Planetary Science Letters*, *220*(3-4), 391-408.

Studinger, M., et al. (2008), Comparison of AIRGrav and GT-1A airborne gravimeters for research applications, *GEOPHYSICS*, *73*(6), I51-I61.

Swink, M., and C. Speier (1999), Presenting geographic information: effects of data aggregation, dispersion, and users' spatial orientation, *Decision sciences*, *30*(1), 169-195.

Tabacco, I. E., et al. (2006), Physiography and tectonic setting of the subglacial lake district between Vostok and Belgica subglacial highlands (Antarctica), *Geophysical Journal International*, *165*(3), 1029-1040.

Talalay, P., et al. (2021), Antarctic subglacial drilling rig: Part II. Ice and Bedrock Electromechanical Drill (IBED), *Annals of Glaciology*, *62*(84), 12-22.

Tankersley, M. D., et al. (2022), Basement topography and sediment thickness beneath Antarctica's Ross Ice Shelf imaged with airborne magnetic data, *Earth and Space Science Open Archive*, 17.

Teisberg, T. O., et al. (2022), Development of a Uav-Borne Pulsed ICE-Penetrating Radar System, paper presented at IGARSS 2022 - 2022 IEEE International Geoscience and Remote Sensing Symposium, 17-22 July 2022.

Thomson, S. N., et al. (2013), The contribution of glacial erosion to shaping the hidden landscape of East Antarctica, *Nature Geoscience*, *6*(3), 203-207.

Tinto, K. J., et al. (2019), Ross Ice Shelf response to climate driven by the tectonic imprint on seafloor bathymetry, *Nature Geoscience*, *12*(6), 441-449.

Tochilin, C. J., et al. (2012), Erosional history of the Prydz Bay sector of East Antarctica from detrital apatite and zircon geo-and thermochronology multidating, *Geochemistry, Geophysics, Geosystems*, *13*(11).

2680 Trey, H., et al. (1999), Transect across the West Antarctic rift system in the Ross Sea, Antarctica,
2681 *Tectonophysics*, *301*(1-2), 61-74.

2682 Tuckett, P. A., et al. (2019), Rapid accelerations of Antarctic Peninsula outlet glaciers driven by surface melt,
2683 *Nature Communications*, *10*(1).

2684 Tulaczyk, S. M., and N. T. Foley (2020), The role of electrical conductivity in radar wave reflection from
2685 glacier beds, *The Cryosphere*, *14*(12), 4495-4506.

2686 Turchetti, S., et al. (2008), Accidents and Opportunities: A History of the Radio Echo-Sounding of Antarctica,
2687 1958-79, *The British Journal for the History of Science*, *41*(3), 417-444.

2688 van de Lagemaat, S. H. A., et al. (2021), Subduction initiation in the Scotia Sea region and opening of the
2689 Drake Passage: When and why?, *Earth-Science Reviews*, *215*, 103551.

2690 Vaughan, D. G., et al. (2008), Flow-switching and water piracy between Rutford ice stream and Carlson inlet,
2691 West Antarctica, *Journal of Glaciology*, *54*(184), 41-48.

2692 Voigt, D. E., et al. (2013), 'Georods': the development of a four-element geophone for improved seismic
2693 imaging of glaciers and ice sheets, *Annals of Glaciology*, *54*(64), 142-148.

2694 Wannamaker, P., et al. (2017), Uplift of the central Transantarctic Mountains, *Nature Communications*, *8*(1),
2695 1588.

2696 Wannamaker, P. E., et al. (2004), Structure and thermal regime beneath the South Pole region, East
2697 Antarctica, from magnetotelluric measurements, *Geophysical Journal International*, *157*(1), 36-54.

2698 Wei, W., et al. (2020), Getz Ice Shelf melt enhanced by freshwater discharge from beneath the West
2699 Antarctic Ice Sheet, *The Cryosphere*, *14*(4), 1399-1408.

2700 Wenman, C. P., et al. (2020), Post Middle Miocene Tectonomagmatic and Stratigraphic Evolution of the
2701 Victoria Land Basin, West Antarctica, *Geochemistry, Geophysics, Geosystems*, *21*(3).

2702 Whitehead, J., et al. (2006), A review of the Cenozoic stratigraphy and glacial history of the Lambert
2703 Graben—Prydz Bay region, East Antarctica, *Antarctic Science*, *18*(1), 83-99.

2704 Willan, R. C. R. (2003), Provenance of Triassic-Cretaceous sandstones in the Antarctic Peninsula: Implications
2705 for terrane models during Gondwana breakup, *Journal of Sedimentary Research*, *73*(6), 1062-1077.

2706 Williams, S. E., et al. (2013), Early India-Australia spreading history revealed by newly detected Mesozoic
2707 magnetic anomalies in the Perth Abyssal Plain, *Journal of Geophysical Research: Solid Earth*, *118*(7), 3275-
2708 3284.

2709 Williams, S. E., et al. (2019), Australian-Antarctic breakup and seafloor spreading: Balancing geological and
2710 geophysical constraints, *Earth-Science Reviews*, *188*, 41-58.

2711 Wilson, C. G., et al. (2019), How can geologic decision-making under uncertainty be improved?, *Solid Earth*,
2712 *10*(5), 1469-1488.

2713 Wilson, D. S., and B. P. Luyendyk (2006), Bedrock platforms within the Ross Embayment, West Antarctica:
2714 Hypotheses for ice sheet history, wave erosion, Cenozoic extension, and thermal subsidence, *Geochemistry,*
2715 *Geophysics, Geosystems*, *7*(12).

2716 Wilson, D. S., et al. (2012), Antarctic topography at the Eocene-Oligocene boundary, *Palaeogeography,*
2717 *Palaeoclimatology, Palaeoecology*, *335-336*, 24-34.

2718 Wilson, G., et al. (2007), The geological evolution of southern McMurdo Sound - New evidence from a high-
2719 resolution aeromagnetic survey, *Geophysical Journal International*, *170*(1), 93-100.

2720 Wilson, T. J. (1999), Cenozoic structural segmentation of the Transantarctic Mountains rift flank in southern
2721 Victoria Land, *Global and Planetary Change*, *23*(1-4), 105-127.

2722   Wright, A. P., et al. (2008), High sensitivity of subglacial hydrological pathways in Antarctica to small ice-
2723   sheet changes, *Geophysical Research Letters*, *35*(17).

2724   Yakymchuk, C., et al. (2015), Paleozoic evolution of western Marie Byrd Land, Antarctica, *Bulletin of the
2725   Geological Society of America*, *127*(9-10), 1464-1484.

2726   Young, A., et al. (2019), Global kinematics of tectonic plates and subduction zones since the late Paleozoic
2727   Era, *Geoscience Frontiers*, *10*(3), 989-1013.

2728   Young, D. A., et al. (2016), The distribution of basal water between Antarctic subglacial lakes from radar
2729   sounding, *Philosophical Transactions of the Royal Society A: Mathematical, Physical and Engineering
2730   Sciences*, *374*(2059).

2731   Young, D. A., et al. (2017a), Gravity disturbance data over central Marie Byrd Land, West Antarctica
2732   (GIMBLE.GGCMG2) U.S. Antarctic Program (USAP) Data Center https://doi.org/10.15784/601003., edited.

2733   Young, D. A., et al. (2017b), Magnetic anomaly data over central Marie Byrd Land, West Antarctica
2734   (GIMBLE.GMGEO2) U.S. Antarctic Program (USAP) Data Center. doi: https://doi.org/10.15784/601002.,
2735   edited.

2736   Young, T. J., et al. (2018), Resolving the internal and basal geometry of ice masses using imaging phase-
2737   sensitive radar, *Journal of Glaciology*, *64*(246), 649-660.

2738   Zhang, Y., et al. (2018), Hydromechanical Impacts of Pleistocene Glaciations on Pore Fluid Pressure
2739   Evolution, Rock Failure, and Brine Migration Within Sedimentary Basins and the Crystalline Basement, *Water
2740   Resources Research*, *54*(10), 7577-7602.

2741   Zhou, Z., et al. (2022), Radial Anisotropy and Sediment Thickness of West and Central Antarctica Estimated
2742   From Rayleigh and Love Wave Velocities, *Journal of Geophysical Research: Solid Earth*, *127*(3),
2743   e2021JB022857.

2744